INFORMATION TO USERS

This manuscript has been reproduced from the microfilm master. UMI films the text directly from the original or copy submitted. Thus, some thesis and dissertation copies are in typewriter face, while others may be from any type of computer printer.

The quality of this reproduction is dependent upon the quality of the copy submitted. Broken or indistinct print, colored or poor quality illustrations and photographs, print bleedthrough, substandard margins, and improper alignment can adversely affect reproduction.

In the unlikely event that the author did not send UMI a complete manuscript and there are missing pages, these will be noted. Also, if unauthorized copyright material had to be removed, a note will indicate the deletion.

Oversize materials (e.g., maps, drawings, charts) are reproduced by sectioning the original, beginning at the upper left-hand corner and continuing from left to right in equal sections with small overlaps. Each original is also photographed in one exposure and is included in reduced form at the back of the book.

Photographs included in the original manuscript have been reproduced xerographically in this copy. Higher quality 6" x 9" black and white photographic prints are available for any photographs or illustrations appearing in this copy for an additional charge. Contact UMI directly to order.

UMI

A Bell & Howell Information Company
300 North Zeeb Road, Ann Arbor MI 48106-1346 USA
313/761-4700 800/521-0600

Vertebrate Detection of Polarized Light

by

Iñigo Novales Flamarique

BSc (Physics), McGill University, 1988

BSc (Biology), McGill University, 1990

MSc (Biology), University of Victoria, 1993

A Dissertation Submitted in Partial Fulfilment of the

Requirements for the Degree of

DOCTOR OF PHILOSOPHY

in the Department of Biology

We accept this dissertation as conforming

to the required standard

Dr. C.W. Hawryshyn, Supervisor (Department of Biology)

Dr. N. Sherwood, Department Member (Department of Biology)

Dr. L. Page, Department Member (Department of Biology)

Dr. J.P. van Netten, Associate Member (Royal Jubilee Hospital)

Dr. J.F.R. Gower, Outside Member (Institute of Ocean Sciences)

Dr. G.D. Bernard, Outside Member (Boeing Commercial Airplane Group)

Dr. T.W. Cronin, External Examiner (Department of Biological Sciences, University of Maryland Baltimore County)

Abstract

In addition to intensity and colour, the retinas of many invertebrates are capable of light detection based on its linear polarization (Wehner, 1983). The detection mechanism permitting this capability is based on the intrinsic dichroism of chromophores oriented along rhabdomeric microvilli. In vertebrates, however, except for anchovies (Fineran & Nicol, 1978), such axial dichroism is absent rendering vertebrate outer segments insensitive to the polarization of axially-incident light. Nonetheless, there is evidence for polarization sensitivity in a few species of fish (goldfish, rainbow trout and sunfish). But the findings for goldfish and rainbow trout appear contradictory to those for the green sunfish (Parkyn & Hawryshyn, 1993), and a detection mechanism that could explain polarization sensitivity for lower vertebrates in general is unknown.

This thesis was undertaken to try to solve some of these unknowns by investigating: 1) the neural polarization signal, at the level of the optic nerve, in fish species from four groups with distinct retinal cone mosaics (rainbow trout, green and pumpkinseed sunfishes, common white sucker, and northern anchovy), 2) the ultrastructure and light-transmission properties of different cone types (single, twin and double cones), and 3) the characteristics of the underwater polarized light field that could permit the

observed laboratory behaviours in nature. I measured compound action potential (CAP) responses from the optic nerve of live anaesthetized fish to evaluate the possibility that a fish could detect the orientation of the electric field of linearly polarized light (mathematically-designated as the E-vector). Results from these studies showed that rainbow trout and the northern anchovy were polarization-sensitive, but both species of sunfish and the common white sucker were not. In addition, CAP measurements conducted with rainbow trout exposed to light stimuli of varying polarization percentages showed, in conjunction with underwater polarized light measurements, that the use of polarized light in this animal was restricted to crepuscular time periods. To try to understand why some fish species were polarization-sensitive and others were not, I carried out microscopy studies of retinal cones. Optical measurements of transmitted polarized light through the length of cones showed: 1) small cone birefringence (retardance < 2nm), and 2) preferential transmission of polarized light that was parallel to the partition dividing twin and double cones (single cones were isotropic). In addition, histological studies showed that the partition in trout double cones was tilted with respect to the vertical while that of twin cones in sunfish was straight. We envisioned that the higher index of refraction of the partition with respect to the surrounding cell cytoplasm would make it behave as a mirror, reflecting and polarizing incident light. A large optical model was built

to test this idea consisting of two photodiodes evenly spaced on either side of a cover-slip "partition" upon which physiologically-relevant illumination was incident. Measurements using this model and theoretical calculations with refractive indices approaching those expected for double cone partitions and cytoplasm (Sidman, 1957) were consistent with the optical results obtained in situ. Thus the tilt in the partition of trout double cones relayed different amounts of light to each outer segment depending on the polarization of incident light, whereas a straight partition, as in sunfish, did not. Comparison of signals from orthogonally-arranged double cones and single cones in the centro-temporal retina of trout thus became the basis for a model neural network that could reproduce all the polarization sensitivity results known to date. To support the idea that an ordered (e.g. orthogonal) arrangement of double cones was a necessity for polarization detection, I showed that the common white sucker, a fish with double cones, had these arranged randomly in the centro-temporal retina (hence its lack of polarization sensitivity). Finally, the northern anchovy exhibited unique cones with lipid lamellae parallel to their lengths, forming a dichroic system for polarization detection somewhat analogous to that of cephalopods and decapod crustaceans.

Examiners:

Dr. C.W. Hawryshyn, Supervisor (Department of Biology)

Dr. N. Sherwood, Department Member (Department of Biology)

Dr. L. Page, Department Member (Department of Biology)

Dr. J.P. van Netten, Associate Member (Royal Jubilee Hospital)

Dr. J.F.R. Gower, Outside Member (Institute of Ocean Sciences)

Dr. G.D. Bernard, Outside Member (Boeing Commercial Airplane Group)

Dr. T.W. Cronin, External Examiner (Department of Biological Sciences, University of Maryland Baltimore County)

Table of Contents

List of Tables

List of Figures

Acknowledgements

There are many persons that contributed to this dissertation. I would like to thank my supervisor, Dr. Craig W. Hawryshyn, for allowing me the freedom to explore my own ideas and for funding and contributing to this research. I was very lucky to have Dr. Gary Bernard to discuss research ideas and to look over my manuscripts; Dr. Bernard was the first scientist to suggest back in the 1970's that the double cones of fishes may act as polarization-sensitive waveguides (see Forward et al., 1972). I would also like to thank the rest of my committee members, fellow graduate students Luc Beaudet, Craig McDonald and Daryl Parkyn, and many journal editors and anonymous reviewers that interacted with me over the past years and greatly improved the quality of my work.

The biophysical mechanism for polarization detection in fishes presented in this thesis was conceptualized with Dr. Ferenc I. Hárosi of the Marine Biological Laboratory (Woods Hole, Mass., USA). Working with Dr. Hárosi and Dr. Oldenbourg and interacting with other scientists at the MBL was the highlight of my PhD program. I thank Dr. Hárosi for all his past help and his continuous scientific guidance, and the Grass Foundation for sponsoring my research in Dr. Hárosi's laboratory as a Grass Fellow during the summer of 1995.

The optic nerve recording technique used in this thesis was developed by Luc Beaudet. I thank him for teaching me the technique and the constant scientific interaction and

friendship. Karen Barry, Dr. Dave Coughlin and Jim Austin were sufficiently adventurous to dive with me for the light measurements, while Lisa Grebinsky and Luc Beaudet volunteered to operate the computer. The Canadian West Coast Lifeguard allowed my research team to dive inside Ogden Point Breakwater and provided a rowboat for which I am very thankful. Mr. Gordon Davies built the column and spectroradiometer accessories necessary for the underwater light measurements, and Dr. Roberto Racca was invaluable in developing software and discussing optical set-ups for my electrophysiology experiments. I thank them both greatly. Mr. and Mrs. Cormoran of West Seafood Exchange Ltd. were very kind in donating the anchovies, and Dr. Eric Desmers provided the common white suckers. Finally, I would like to thank Luc Beaudet and Lisa Grebinsky for all their research-related chauffeur services since a bum like me can only pedal a bike.

A little while ago, my little brother Julian sent me this drawing for my birthday. I think it captures the essence of my personality. This dissertation is dedicated to him and to the rest of my family for putting up with me all these years!

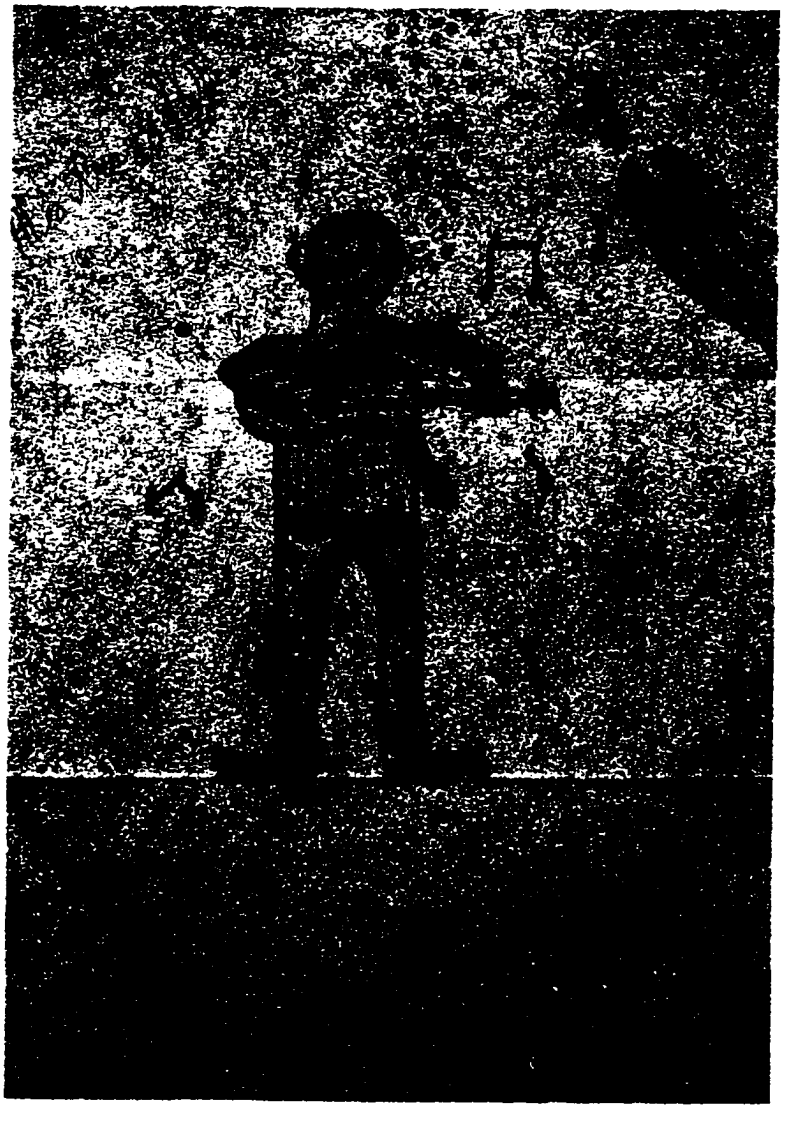

Chapter 1: General Introduction

The study of animal polarization visual systems has always incorporated research from many fields of science including optics, physiology, neuroanatomy and behaviour (e.g. Menzel & Snyder, 1975). This thesis follows such a multi-facetted, comparative approach to construct an overall picture of vertebrate polarization sensitivity and the possible biophysical mechanisms behind this sensory capability. The goals of this introduction are: 1) to familiarize the reader with basic concepts in the physics of light, 2) to present the general structure of the vertebrate and invertebrate retinas (since polarization sensitivity is primarily an invertebrate capability and some detection principles appear to be common between invertebrates and fishes), 3) to give a general overview of the history of the field for both invertebrates and vertebrates, and 4) to state the purpose of the thesis.

1.1 Basic concepts in the physics of light

The basic unit of light is a massless elementary particle called the photon. Because of its quantum nature, the behaviour of light can only be understood by two complementary theories: the quantum (particle) theory and the wave theory. One way to think about this duality is to imagine the photon as a wave that carries a certain momentum (ρ) and energy (E). Mathematically, $E=h\nu=\rho^2/(2m)=mc^2$, where h is Planck's constant, m is the moving mass and ν is the photon's frequency. The

energy of the wave can interact with matter and be quantified, hence its particle attribute. In the following, we will derive the basic mathematical formulation of the wave equation, introduce the concept of a harmonic wave and present some equations describing different sorts of polarized light. The concepts introduced here were adapted from various optic textbooks, in particular from Hecht & Zajac (1974), Jenkins & White (1976), Grant & Phillips (1984) and Inoué (1989). The reader may wish to refer to these and other optic textbooks for further details.

1.1.1 The one-dimensional wave equation

Figure 1.1 shows a wave disturbance ψ travelling at speed v along the positive x axis. Y-x defines the coordinate system at time t=0, when the wave is stationary. Y′-x′ is the coordinate system that travels with the moving wave at t>0. It should be apparent from the figure that, for a wave that does not change its shape, the wave at any position $x_{t>0}$ is equal to that at $x_{t=0}$ but for the lateral displacement during time t. Mathematically,

$$\psi(x,t)=f(x-vt) \qquad (1)$$

Equation 1 represents the generalized form of the one-dimensional wave function travelling in the positive x direction (f(x+vt) defines the same wave travelling in the opposite sense).

Figure 1.1 Wave disturbance travelling with speed v in the positive x direction.

Fig. 1.1

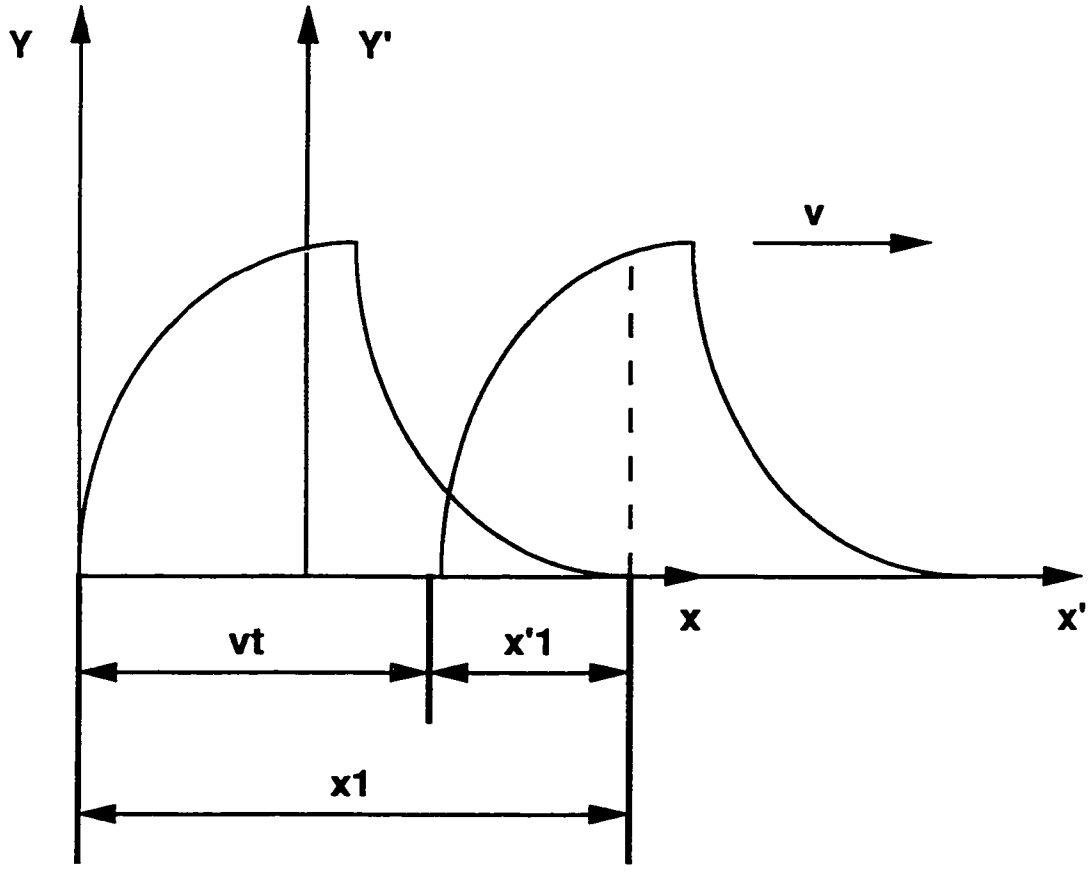

1.1.2 The harmonic wave

Harmonic waves are commonly known as sinusoidal waves. Using (1), we can formulate a simple harmonic cosine wave of amplitude E propagating at speed v in the positive x direction (Fig. 1.2):

$$\psi(x,t)=E\cos k(x-vt) \qquad (2)$$

Holding x or t constant in (2) results in an undulating wave that is periodic in space and time. The wave repeats itself every wavelength (λ), hence we can write:

$$E\cos k[x-vt]=E\cos k[(x\pm\lambda)-vt]=E\cos[k(x-vt)\pm 2\pi]$$

from which $k=2\pi/\lambda$ (k is known as the propagation number) (3)

We now perform a similar analysis with respect to time to give:

$$E\cos k[x-vt]=E\cos k[x-v(t\pm\tau)]=E\cos[k(x-vt)\pm 2\pi]$$

from which $kv\tau=2\pi$, and using (3), we arrive at an expression for the period (τ): $\tau=\lambda/v$ (4)

The frequency is defined as the reciprocal of the period, so that $v=\lambda\nu$, where ν is the frequency of the wave. The angular frequency (ω) is another quantity commonly used in the optics literature, $\omega=2\pi\nu$ (5)

To describe wave motion and polarization state of light, we need one remaining physical quantity called the phase of the wave, φ. The phase is given by the entire argument within the cosine function, i.e. $\varphi=(kx-wt)$. To differentiate between phases at t=0, we introduce the initial phase or epoch angle ε, and write a generalized form for the cosine harmonic wave

Figure 1.2 Harmonic wave moving in the positive x direction seen at different times.

Fig. 1.2

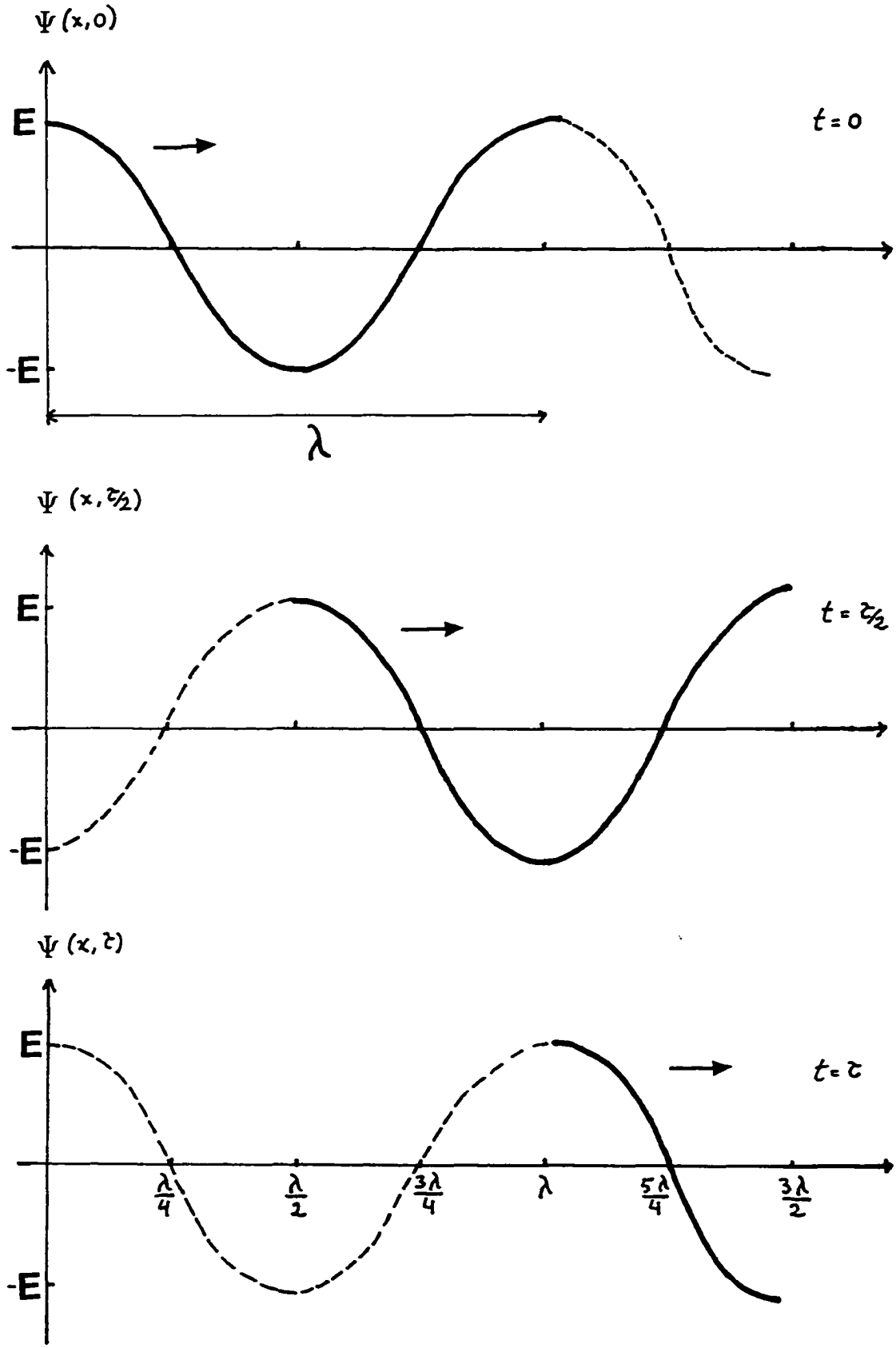

as:

$$\Psi(x,t)=E\cos[kx-\omega t+\varepsilon] \quad (6)$$

1.1.3 The concept of polarized light

As previously mentioned, light is made of electromagnetic waves called photons. Each photon is composed of two harmonic waves that are perpendicular and in phase with each other; these are the electric and magnetic field components (**E** and **H**). If the photons comprising a light beam share the same electric field orientation (the same E-vector), the light is said to be linearly polarized in the E-vector plane. The amplitude of the light at any point in time will be a function of the relative phase differences between photons. If, however, the photons differ in their electric field orientations, then the resultant may or not be linearly polarized depending on the relative phases between photons. In the following, we will consider different types of polarization created by superimposing perpendicular electric field waves.

1.1.3.1 *Linearly polarized light*

Using the previous general form for a cosine harmonic wave (6), we will postulate a light beam composed of two perpendicular electric fields ($\mathbf{E}_x$ and $\mathbf{E}_y$) with phase difference ε between them:

$$\mathbf{E}_x(z,t)=E_0\cos(kz-\omega t)\,\mathbf{i} \qquad (7)$$

$$\mathbf{E}_y(z,t)=E_1\cos(kz-\omega t+\varepsilon)\,\mathbf{j} \qquad (8)$$

($\mathbf{i}$ and $\mathbf{j}$ are unit vectors along the x and y axis)

The sum of both waves [(7) and (8)] is a linearly polarized wave if $\varepsilon=2n\pi$ (i.e. a multiple of 2π, n is an integer) (Fig. 1.3). If $\varepsilon=n\pi$, then the resultant wave is rotated by 90° (if $E_0=E_1$) but it still remains linearly polarized.

1.1.3.2 *Circularly polarized light*

If waves (7) and (8) differ by $\varepsilon=-\pi/2 + 2n\pi$, then the electric field expressions become:

$$\mathbf{E}_x(z,t)=E_0\cos(kz-\omega t)\,\mathbf{i} \qquad (9)$$

$$\mathbf{E}_y(z,t)=E_1\sin(kz-\omega t)\,\mathbf{j} \qquad (10)$$

(one should note that, for any angle α, $\cos(\alpha-\pi/2)=\sin(\alpha)$)

The sum of (9) and (10) gives the resultant field (for $E_0=E_1=E$):

$$\mathbf{E}(z,t)=E[\cos(kz-\omega t)\,\mathbf{i} + \sin(kz-\omega t)\,\mathbf{j}] \qquad (11)$$

This equation represents a wave that is rotating clockwise with angular frequency ω (Fig. 1.4). The E-vector makes one rotation every time the wave advances by one wavelength. Similarly, one can obtain circularly polarized light rotating anti-clockwise by imposing the condition $\varepsilon=\pi/2$. In this case $\cos(\alpha+\pi/2)=-\sin(\alpha)$, for any angle α, and we end up with the resultant field:

$$\mathbf{E}(z,t)=E[\cos(kz-\omega t)\,\mathbf{i} - \sin(kz-\omega t)\,\mathbf{j}] \qquad (12)$$

It is interesting to note that the addition of (11) to (12)

Figures 1.3-4 (3) Decomposition of linearly polarized light with electric field (**E**) tilted 45° from the vertical, into two orthogonal components (this illustrates the vectorial nature of light which is a very useful tool in computations). **(4)** Right circularly polarized light. The electric field assumes opposite values every half wavelength. Adapted from Hecht & Zajac (1974).

Fig. 1.3

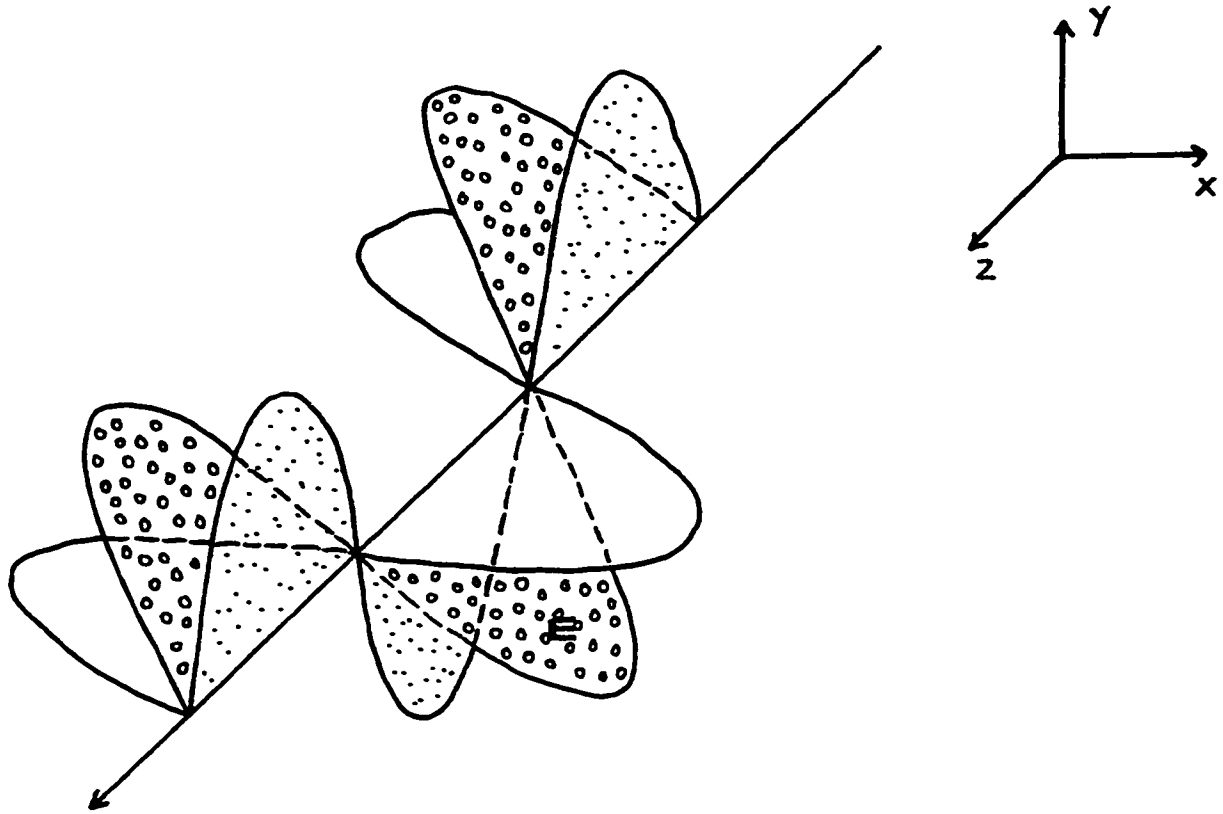

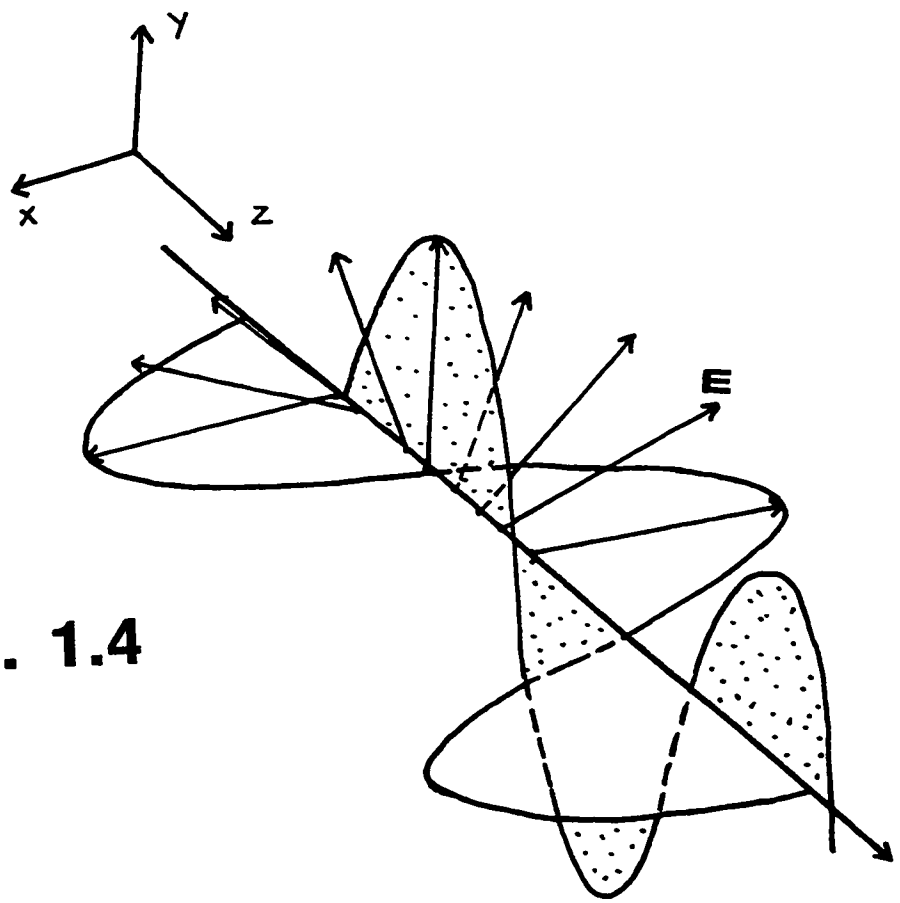

Fig. 1.4

leads to $\mathbf{E}(z,t)=2E\cos(kz-\omega t)\mathbf{i}$, which is linearly polarized light.

1.1.3.3 *Elliptically polarized light*

Most of the polarized light in nature is elliptically polarized, i.e. the resultant electric field will change both in magnitude and direction. In fact, both linearly polarized and circularly polarized light are special cases of elliptically polarized light. We can see this by the following derivation.

First we expand the cosine argument in (8) and divide by the electric field amplitude to give the scalar:

$$E_y/E_1=\cos(kz-\omega t)\cos\varepsilon-\sin(kz-\omega t)\sin\varepsilon \qquad (13)$$

[note: for any angles α and β, $\cos(\alpha+\beta)=\cos\alpha\cos\beta-\sin\alpha\sin\beta$]

We now introduce $E_x/E_0=\cos(kz-\omega t)$ (from (7)) and note, also from (7), that $\sin(kz-\omega t)=[1-\cos(kz-\omega t)]^{1/2}=[1-(E_x/E_0)]^{1/2}$, to give:

$$[(E_y/E_1)-(E_x/E_0)\cos\varepsilon]^2 = [1-(E_x/E_0)^2]\sin^2\varepsilon$$

This equation can be expanded resulting in:

$$(E_y/E_1)^2 + (E_x/E_0)^2 - 2(E_x/E_0)(E_y/E_1)\cos\varepsilon = \sin^2\varepsilon \qquad (14)$$

which is the formula for an ellipse making an angle α with the E_x-E_y coordinate system (Fig. 1.5), such that:

$$\tan(2\alpha) = 2E_0E_1\cos\varepsilon/(E_0^2-E_1^2) \qquad (15)$$

If $\alpha=0$, then $\cos\varepsilon=0$ from (15), and $\varepsilon=n\pi/2$ (where $n=\pm1,\pm3,\pm5\ldots$); equation (14) then becomes:

$(E_y/E_1)^2 + (E_x/E_0)^2 = 1$, which is the simplified equation

Figure 1.5 Elliptically polarized light is characterized by the resultant electric field tracing the contour of an ellipse. As seen in the series of diagrams in the lower half of the figure, linear and circular polarizations are special cases of elliptical polarization. Adapted from Hecht & Zajac (1974).

Fig. 1.5

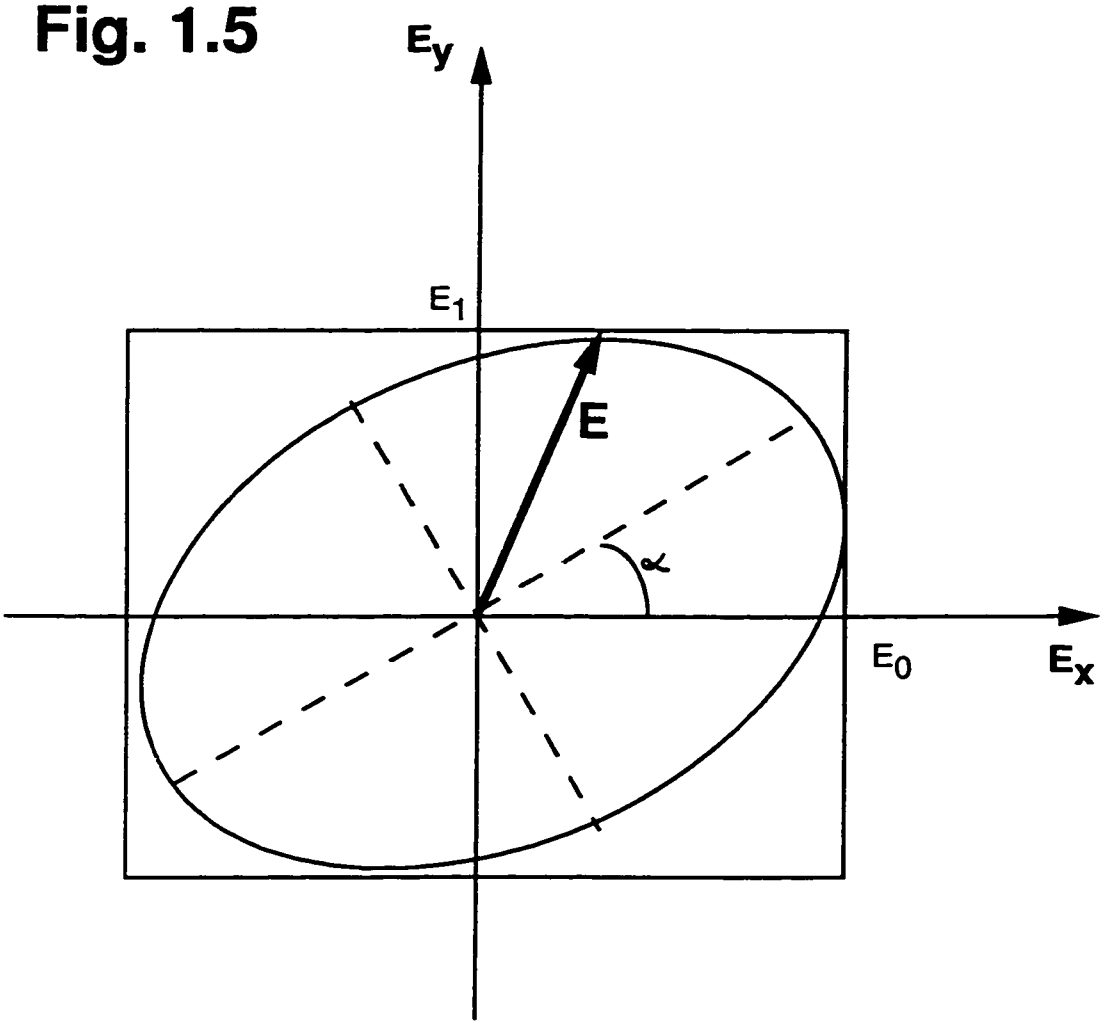

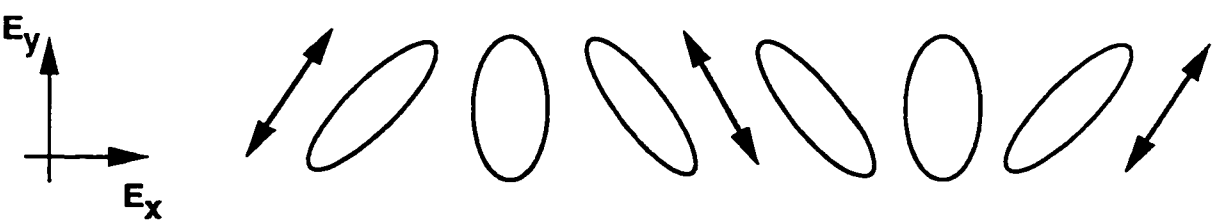

ε	0	π/4	π/2	3π/4	π	5π/4	3π/2	7π/4	2π

for the ellipse with major and minor axes along the E_x and E_y axes. In addition, if $E_1=E_0=E$, the previous equation reduces to: $E_y^2+E_x^2=E_0^2$, which is a circle centred at the origin, defining circularly polarized light. This equation can also be obtained by squaring (9) and (10) above, and adding both expressions.

If ε is a multiple of π, equation (14) reduces to:

$E_y=(E_1/E_0)E_x$ (for even multiples), or

$E_y=-(E_1/E_0)E_x$ (for odd multiples)

Both these equations are straight lines passing by the origin, and correspond to linearly polarized light. They are easily obtained dividing (8) by (7) for the cases when $\varepsilon=2n\pi$ and $\varepsilon=n\pi$ (multiples of 2π and π as previously stated).

1.1.3.4 *Randomly polarized light*

Diffuse light sources such as the sun emit light that is randomly polarized. As opposed to the previous polarization scenarios in which the resultant E-vector changes in amplitude and direction in a periodic and predictable fashion, randomly polarized light consists of polarized light waves with random, incoherent, phase changes between them. The resultant E-vector is unpredictable. Randomly polarized light is rendered partially polarized by a variety of ways in nature.

1.1.3.5 *Polarization of light in nature*

Unpolarized light can be rendered partially polarized

through various mechanisms including molecular and particle scattering (Figs. 1.6-1.9), surface reflection (Fig. 1.10), absorption-based dichroism (Fig. 1.11), birefringence (Fig. 1.11), waveguiding, and multiple scattering in anisotropic media. All these mechanisms occur in nature and give rise to polarization cues, and/or are the basis for structural features in the eyes of animals to detect the orientation of linearly polarized light.

Scattering by small molecules and particles (i.e. of dimensions 1/10th of the incident wavelength) was first described by Lord Rayleigh (Rayleigh, 1889). His scattering formula indicates a λ^{-4} and $\cos(\theta)$ intensity dependence (Figs. 1.6-1.9), which means that shorter wavelengths will be scattered most, and maximum scattering will occur at 90° to the incident light source. The molecule doing the scattering becomes an oscillating dipole under the action of the photon's electric field, and emits photons with E-vector directions predicted by antenna theory (Grant & Phillips, 1984). The E-vector of a scattered photon under perfect Rayleigh conditions is generally perpendicular to the plane comprising the observer, the light source, and the dipole (exceptions are the locations of the four neutral points close to the sun and antisun directions; Timofeeva, 1974). Rayleigh scattering gives rise to a polarization map of the sky where the E-vectors change predictably with elevation and azimuth from the sun (Fig. 1.9; Craig, 1984). Theoretical calculations and

Figure 1.6-9. **(6)** Formation of a particle dipole upon interaction with an electric field. **(7-8)** A particle dipole will re-emit light in all directions except along the dipole axis. **(9)** Randomly-polarized light is scattered by the dipole creating 100% linearly polarized light at right angles to the dipole (this is Rayleigh scattering). Percent polarization is a measure of the proportion of photons that are linearly polarized in a given plane with respect to the total number of photons. Percent polarization = $100(I_{Emax}-I_{Emin})/(I_{Emax}+I_{Emin})$; where E_{max} is the plane containing the highest number of polarized photons and E_{min} is the plane perpendicular to E_{max} (I is the intensity of light in a given plane). Adapted from Hecht & Zajac (1974).

Fig. 1.6

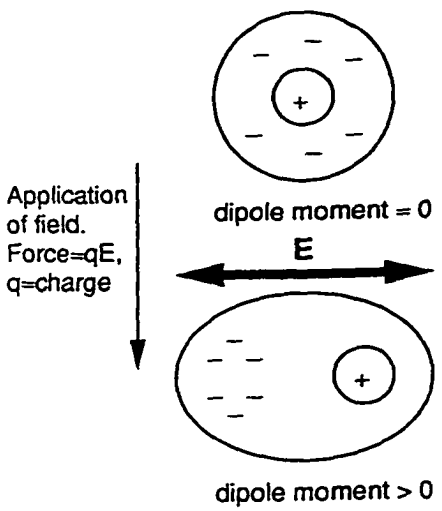

Fig. 1.7

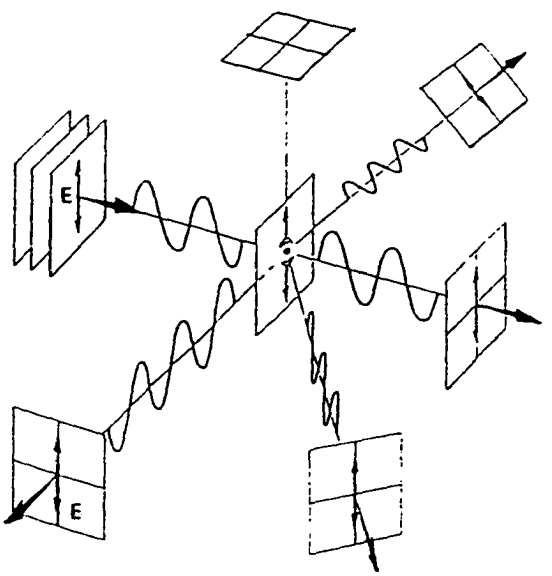

Fig. 1.8

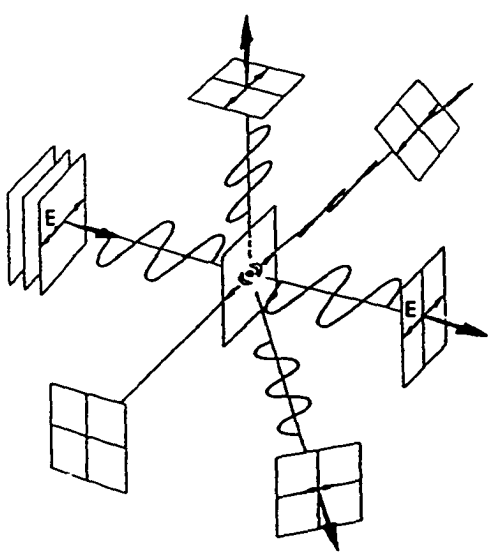

Fig. 1.9

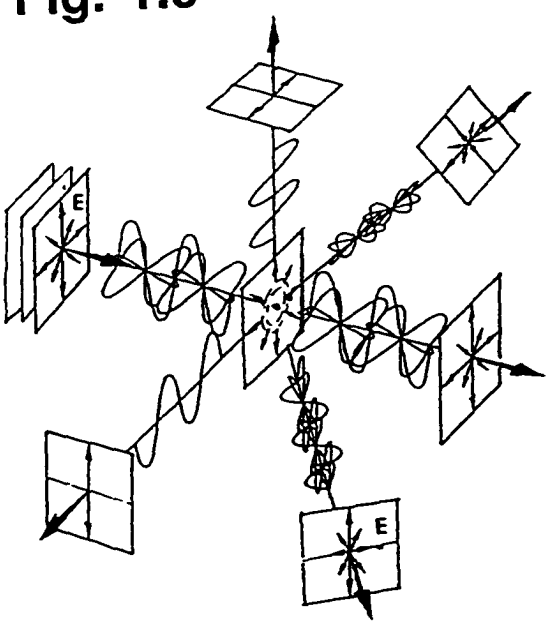

radiometric measurements for UV and green wavelengths show that maximum skylight polarization varies around 70-73% under hazeless conditions (Brines & Gould, 1982).

Another way to polarize light involves surface reflection. Polarization by reflection can be very high (>50%) for shiny dielectrics like glass (Land, 1987; Reali, 1992; Wolff, 1987, 1994a,b), and for liquids like water (Horvàth & Varjú, 1995). The amplitude and polarization state of reflected and refracted rays at the interface can be calculated from Fresnel's equations (Reali, 1992; Horvàth & Varjú, 1995); percent polarization is maximum for Brewster's angle where $\theta_r + \theta_t = 90°$ (Fig. 1.10; De Smet, 1994).

Dichroic absorption refers to the selective absorption of one of the two orthogonal polarization components of an incident unpolarized beam (Fig. 1.11; note that the resultant E-vector of a light beam at any given time can be mathematically dissected into two orthogonal polarization components, equations (7) and (8)). Some naturally-occurring minerals like tourmaline and herapathite are inherently dichroic in that polarization components perpendicular to the "optical axis" of these crystals are strongly absorbed (a property of the direction of maximum absorption of the atomic bonds). The principle of dichroic absorption is the basis for invertebrate polarization sensitivity which relies on a combination of absorption and restricted orientation of chromophores along microvillar membranes (Goldsmith & Wehner,

Figure 1.10 Creation of partial polarization by reflection of unpolarized light at a dielectric interface. The intensity and polarization direction of the reflected and refracted rays can be computed from Fresnel's equations (see, for instance, Jenkins & White, 1976).

Fig. 1.10

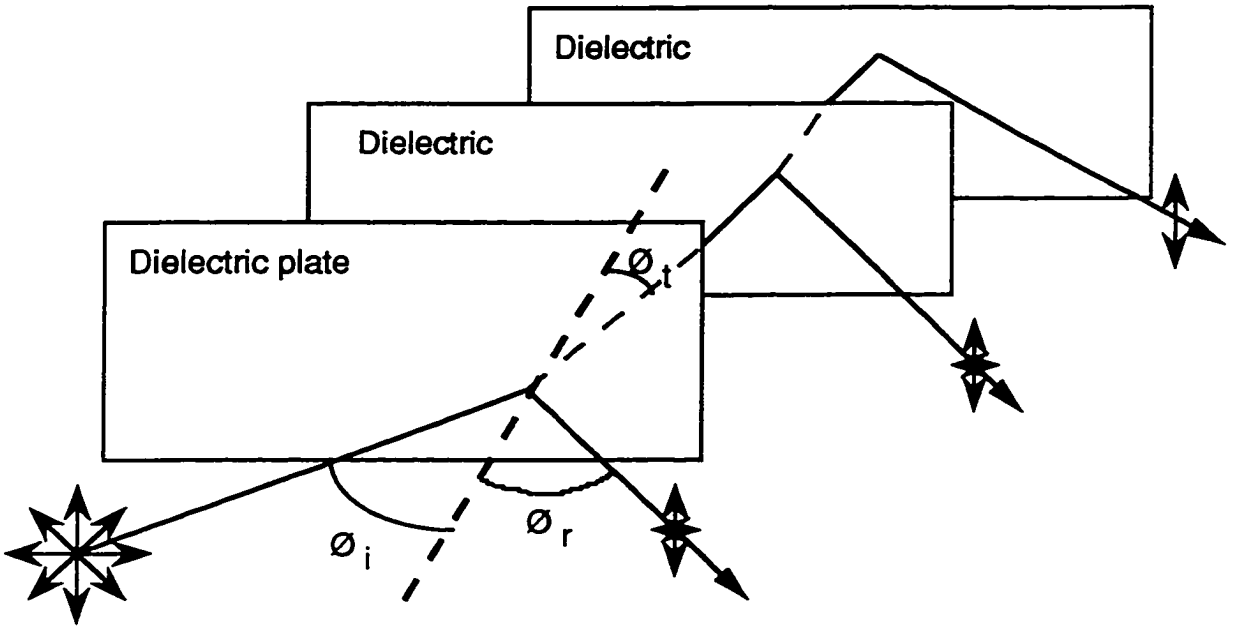

Figure 1.11 Unpolarized light incident on a polarizer will be polarized along the transmission axis of the polarizer (T, shown as a line on the figure). This is the phenomenon of dichroic absorption; only photons with electric field parallel to the transmission axis will pass through. If the polarized light then traverses a birefringent object, depending on the angle made by the incident electric field (OP) and the optic axis of the object, the light will split into two components. The ray along the fast axis of the birefringent body will travel faster than the one along the slow axis, so that the slow ray will be retarded with respect to the fast one. This creates elliptical polarization (a change in phase between rays and therefore a change in orientation and amplitude of the resultant electric field, see section 1.1.3.3). Hence, some light will pass through a polarizer with transmission axis oriented perpendicular to the first, as shown in the figure.

Fig. 1.11

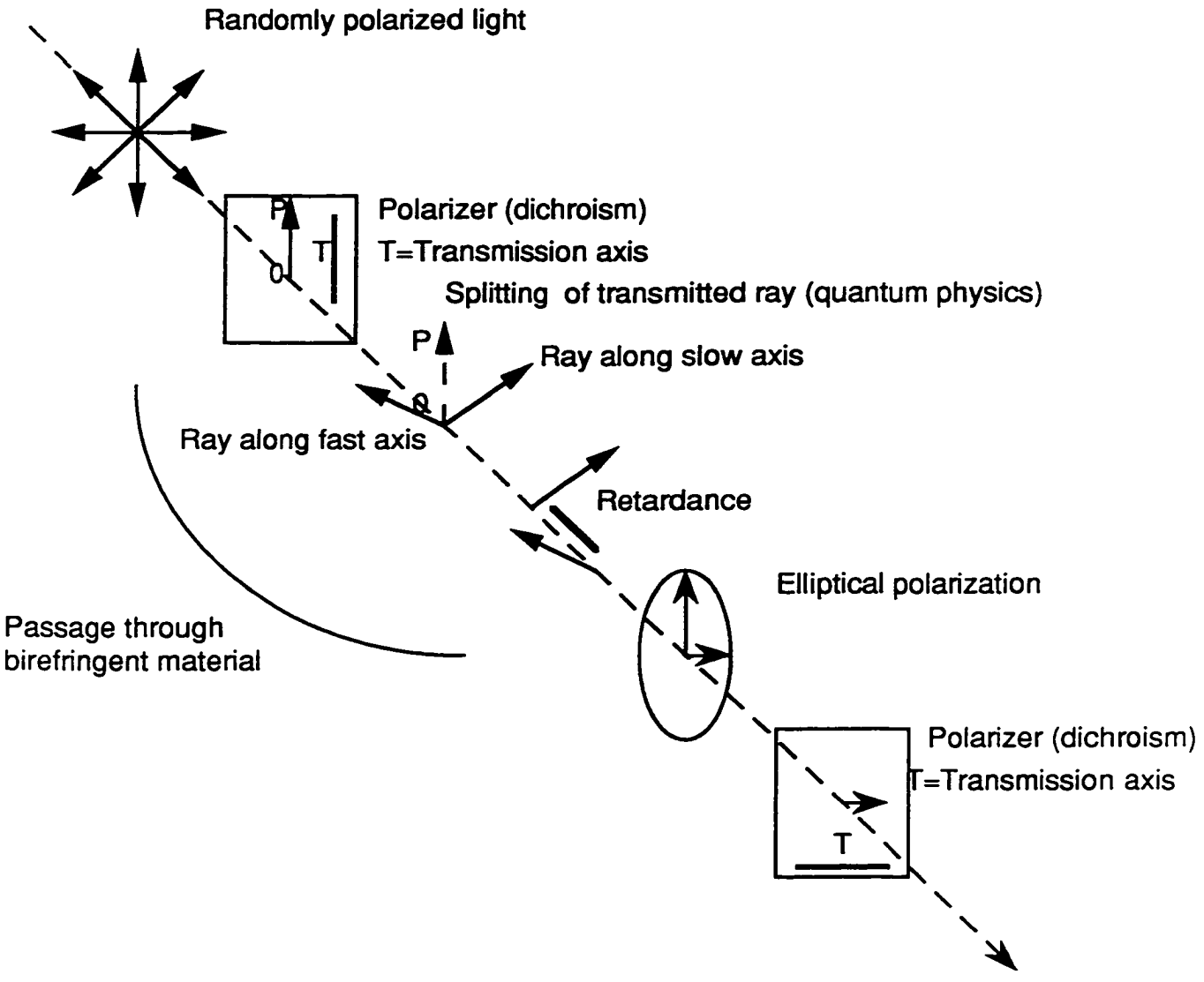
Randomly polarized light
P
T
Polarizer (dichroism)
T=Transmission axis
Splitting of transmitted ray (quantum physics)
P
Ray along slow axis
Ray along fast axis
Retardance
Elliptical polarization
Passage through
birefringent material
Polarizer (dichroism)
T=Transmission axis
T

1977).

Birefringent materials are optically anisotropic structures and different polarization components will travel at different speeds through them (Fig. 1.11). This phenomenon is due to differences in the atomic coupling between electron oscillators and the direction of the incident electric field. As such, orthogonal polarization components will experience different indices of refraction resulting in a retardance (slowing down) of one of the components with respect to the other. This will in turn lead to the creation of elliptically polarized light (Fig. 1.11, see section 1.1.3.3). Low birefringence is a desired property for high polarization sensitivity in twisted fused rhabdoms of insects (Wehner et al., 1975).

Waveguiding is yet another method that can lead to polarization of light. In vision, waveguiding plays a major role in the propagation and polarization of light through invertebrate rhabdoms (Snyder, 1973a,b; Snyder & Pask, 1973; Bernard, 1975; Wehner et al., 1975) and in modal propagation through vertebrate rods and foveal cones (Enoch, 1961; Tannenbaum, 1975; Goyal et al., 1977) due to their small diameters. The properties of a waveguide depend on the refractive index difference between the inside of the waveguide (higher for dielectric waveguides) and the outside medium (lower), the cross-section dimensions of the waveguide, and the angle of incidence of the light ray entering the

waveguide (Menzel & Snyder, 1975). Solutions of Maxwell's equations for a given set of initial parameters result in Transverse Electric (TE), Transverse Magnetic (TM) or Transverse Electric and Magnetic (TEM) modes propagating through the waveguide. The number of modes carried by the guide is frequency (or wavelength) dependent (Grant & Phillips, 1984; Midwinter, 1979). For waveguides of cross section approaching wavelengths in the visible spectrum, more modes will be carried in the lower wavelengths and polarization should be higher when the maximum frequency is approached. However, for waveguides with cross sections much bigger than wavelengths in the visible spectrum, only the longer wavelengths can be polarized as they may reach the maximum frequency limit at which the guide's effects are operative (e.g. Rowe et al., 1994).

Another phenomenon that may take place in nature is multiple scattering reflection from anisotropic dielectric-like objects. In the case where the reflection takes place at an occluding point (i.e. a position on the object where the surface normal is almost parallel to the viewing angle), Wolff (1987, 1994b) has shown that polarized light from diffuse reflection is perpendicular to that from specular reflection. Since these two types of polarization appear as a combined state of partially polarized light to the viewer, this effect can contribute to the detection of edges and other surface abnormalities in nature.

1.2 Anatomy of invertebrate and vertebrate retinas

1.2.1 Invertebrates

There are two major groups of invertebrates for which polarization sensitivity appears to be a widespread capability. These are the terrestrial arthropods (Wehner, 1983; Nilsson et al., 1987) and the marine invertebrates, specifically, the cephalopods and decapod crustaceans (Waterman, 1981; Goddard & Forward, 1991). Figure 1.12A shows the basic organization of the invertebrate retina as described for the octopus (Moody & Parriss, 1961). The major difference between this retina and that of some insects (e.g. the ant) is the distribution of microvilli within the rhabdom. In marine cephalopods and decapod crustaceans, the retinular microvilli make orthogonal stacks down the length of the fused rhabdom (or photoreceptor), while in terrestrial arthropods, each retinula cell expands the length of the rhabdom and stacking of orthogonal microvilli is absent (Fig. 1.12B; Waterman, 1981). In addition, the retinas of terrestrial arthropods may exhibit rhabdoms that are either twisted or not about their lengths (Fig. 1.12C; Wehner, 1983). Non-twisting rhabdoms form a fan along the upper rim of the compound eye and are specialized for polarization detection (Fig. 1.12C; Labhart, 1980; Wehner, 1983).

The biophysical mechanism for polarization detection in invertebrates relies on the orientation of photopigment chromophores along the membrane of the microvilli (the

Figure 1.12 (A) Basic plan of the octopus retina, a model retina for many cephalopods and decapod crustaceans. Note that the rhabdoms of adjacent cells from different levels form crossed perpendicular columns (top insert; crab rhabdom). **(B)** typical photoreceptor (containing various retinula cells) of terrestrial arthropods. The retinula cells may or may not twist about the vertical axis, but the rhabdoms do not form stacked crossed bundles as in the octopus. **(C)** View of the eye of the desert ant and the different specialized rhabdoms (viewed tangentially) in three areas of the retina (Wehner, 1983). The POL area comprises photoreceptors with rhabdoms that do not twist; these form a fan across the upper hemisphere of the eye (black band in the figure) that matches the electric field distribution of a clear crepuscular sky (Wehner, 1989). Abbreviations: RL, Receptor Layer (contains the retinula cells and their rhabdoms which are the microvilli projections that house the visual pigment molecules (G-proteins and attached chromophores); the ensemble of adjacent rhabdoms form a rhabdomere). BPL, Basal Pigment Layer; Bcn, basal cell nuclei layer; PS, Proximal Segment layer; PL, Plexiform Layer; olm, outer limiting membrane; pg, pigment granule; rc retinula cell; rh, rhabdom; bc, basal cell; psn, proximal segment nucleus; pl, plexus; c, cornea; rco, refractile core; dpc, distal pigment cells; rcp, retinular cell processes; rcn, retinular cell nucleus; bm, basal membrane; rca, retinular cell axons; E depicts incident light; ilm, inner limiting membrane; onf, optic nerve fibres.

Fig. 1.12

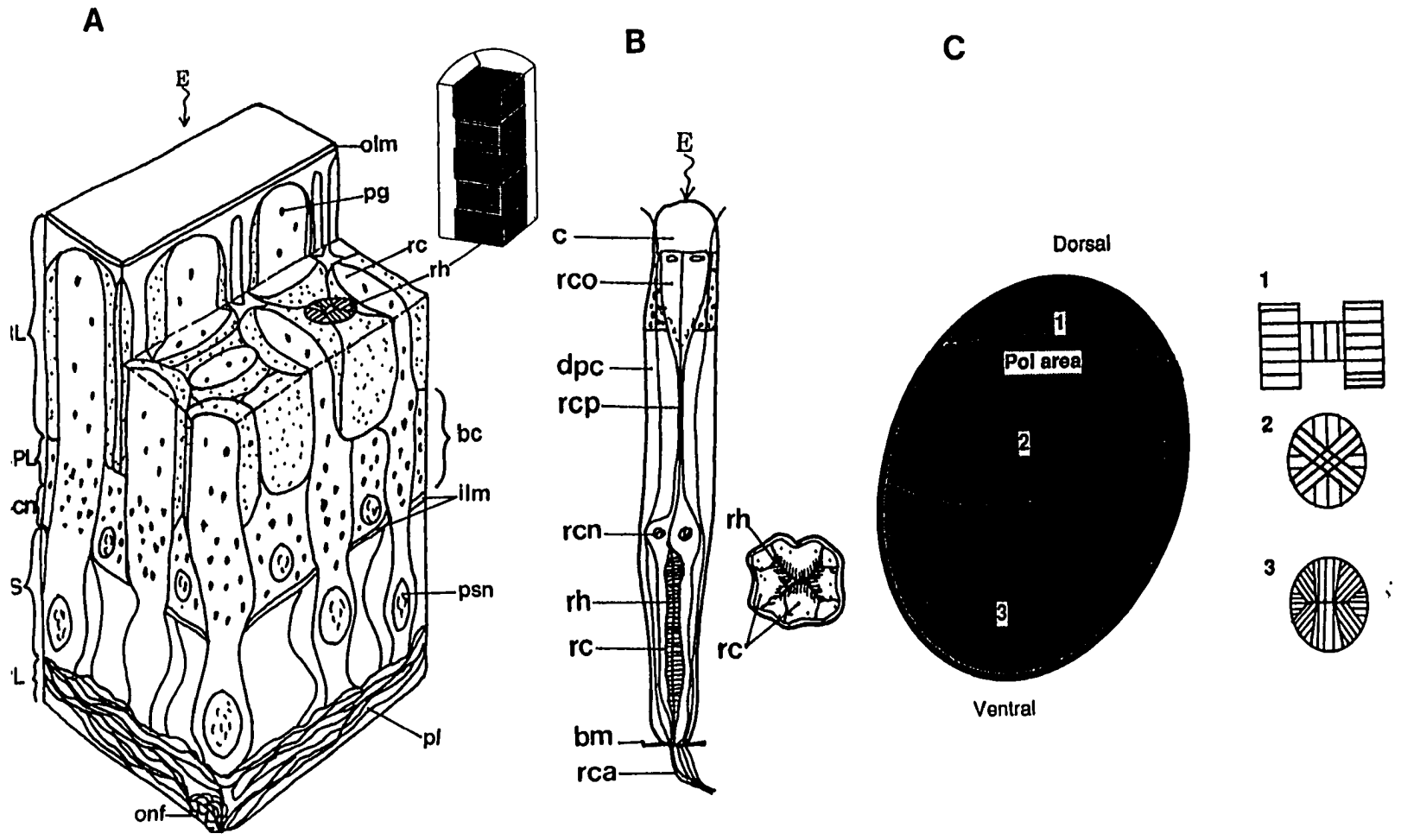
A
E
olm
pg
rc
rh
iL
PL
cn
S
L
bc
ilm
psn
pl
onf
B
E
c
rco
dpc
rcp
rcn
rh
rc
bm
rca
rh
rc
C
Dorsal
1
Pol area
2
3
Ventral
1
2
3

chromophore group that is linked to the visual protein absorbs preferentially electric fields that are parallel to its length; Goldsmith & Wehner, 1977; see also Fein & Szuts, 1982). This dichroic property of the microvilli and their orthogonal disposition in the rhabdom make for a two-axis system to detect polarization direction (Wehner, 1983). The polarization sensitivity (PS) of retinula cells in insect retinas is highest for cells in the POL area (Labhart, 1980), but PS is even higher in crustacean rhabdoms due to their stacking arrangement (Snyder, 1973b; Fig. 1.13A). Mathematically, PS = P_{par}/P_{perp}, where P_{par} and P_{perp} are the amounts of light absorbed by the rhabdomere for polarized light with E-vector parallel and perpendicular to the microvilli. The absorption loss per unit length in the microvillar medium (Δ), a quantity that depends only on E-vector direction, is given by $\Delta = \gamma_{par}/\gamma_{perp}$. Both quantities are related by: PS = $[(1-e^{-\gamma l})/(1-e^{-\gamma l/\Delta})]$, where γ is the absorption coefficient of the medium within the rhabdomere for an electric field either parallel (par) or perpendicular (perp) to the microvilli and l is the rhabdomere's length. In the case of the cephalopod or decapod crustacean rhabdom, PS = Δ because $\gamma_{par}=\gamma_{perp}$ for these animals (see Snyder, 1973b).

1.2.2 Vertebrates

The basic structure of the vertebrate retina can be illustrated by that of a young salmonid eye (Fig. 1.13). Light

Figure 1.13 (A) Radial section from a 5-week-old sockeye salmon retina (alevin stage); a retina that is similar to that of rainbow trout and other salmonids. **(B)** Radial section of the optic nerve head showing the nerve fibre layer (NFL). Arrowhead points to ganglion cell layer (GCL) bodies, also shown in (A). The NFL is thickest where axons accumulate near the optic nerve head. Scale bar, 10 μm. acoc, accessory corner cone; am, amacrine cell; bi, bipolar cell; cc, central cone; dc, double cone; ell, ellipsoid (of inner segment); gc, ganglion cell; hc, horizontal cell; M, Mueller cell; my, myoid (of inner segment); ON, optic nerve; os, outer segment; Scl, Sclera. Retinal layers: RPE, Retinal Pigment Epithelium; VCL, Visual Cell Layer; elm, external limiting membrane; ONL, Outer Nuclear Layer; OPL, Outer Plexiform Layer; INL, Inner Nuclear Layer; IPL, Inner Plexiform Layer; GCL, Ganglion Cell Layer, NFL, Nerve Fibre Layer; E depicts incident light.

Fig. 1.13

travels from the ganglion cell layer to the photoreceptors where photons are absorbed by the photopigments, and the phototransduction cascade begins. The photopigments in vertebrates are located in stacked lipid bilayers in the outer segments of rods and cones (Fig. 1.14), with the population of chromophores freely rotating on the surface of the bilayer (Cone, 1972; Liebman & Entine, 1974). Hence, at any given time, photoreceptor outer segments show random distribution of chromophores and are therefore insensitive to the direction of axially polarized illumination. Nonetheless, they are dichroic to transverse illumination (i.e. incident on the sides of the lipid bilayers; e.g. Hárosi, 1975; Hárosi & MacNichol, 1974).

1.3 Animal sensitivity to polarized light

1.3.1 Invertebrates

von Frisch (1949) was the first to suggest that honeybees used sky polarized light cues, in addition to the sun's position, for orientation (see also Stockhammer, 1956). By the early 1970's, various workers had found polarization sensitivity in several terrestrial and aquatic invertebrates (Moody & Parriss, 1961; Tomita, 1968; Eguchi & Waterman, 1968; Kirshfeld, 1969; Snyder, 1973a). Shaw (1969) recorded intracellularly from single retinula cells of crabs and crayfish showing a 180° periodicity in the polarization sensitivity response. He also inferred a polarization detection mechanism based on preferential absorption along

Figure 1.14 Basic morphology of rods and cones in the vertebrate retina. In addition to single cones, lower vertebrates and marsupials also possess paired cones which look like two single cones squeezed together sharing a double membrane partition in between. The inserts in the upper part of the figure represent views of the pigment molecules within the lamellar lipid bilayers. Note that the pigment molecules are free to rotate and diffuse along the lamellar plane, but their pitch movement is restricted to about 11° from the horizontal (Chabre, 1985). In this figure: os, outer segment; is, inner segment; nu, nucleus; st, synaptic terminal; mt, microtubule; mf, microfilament; ser, smooth endoplasmic reticulum; mi, mitochondria; ch, chromophore; ell, ellipsoid; my, myoid; $\vec{E}$ depicts incident light.

Fig. 1.14

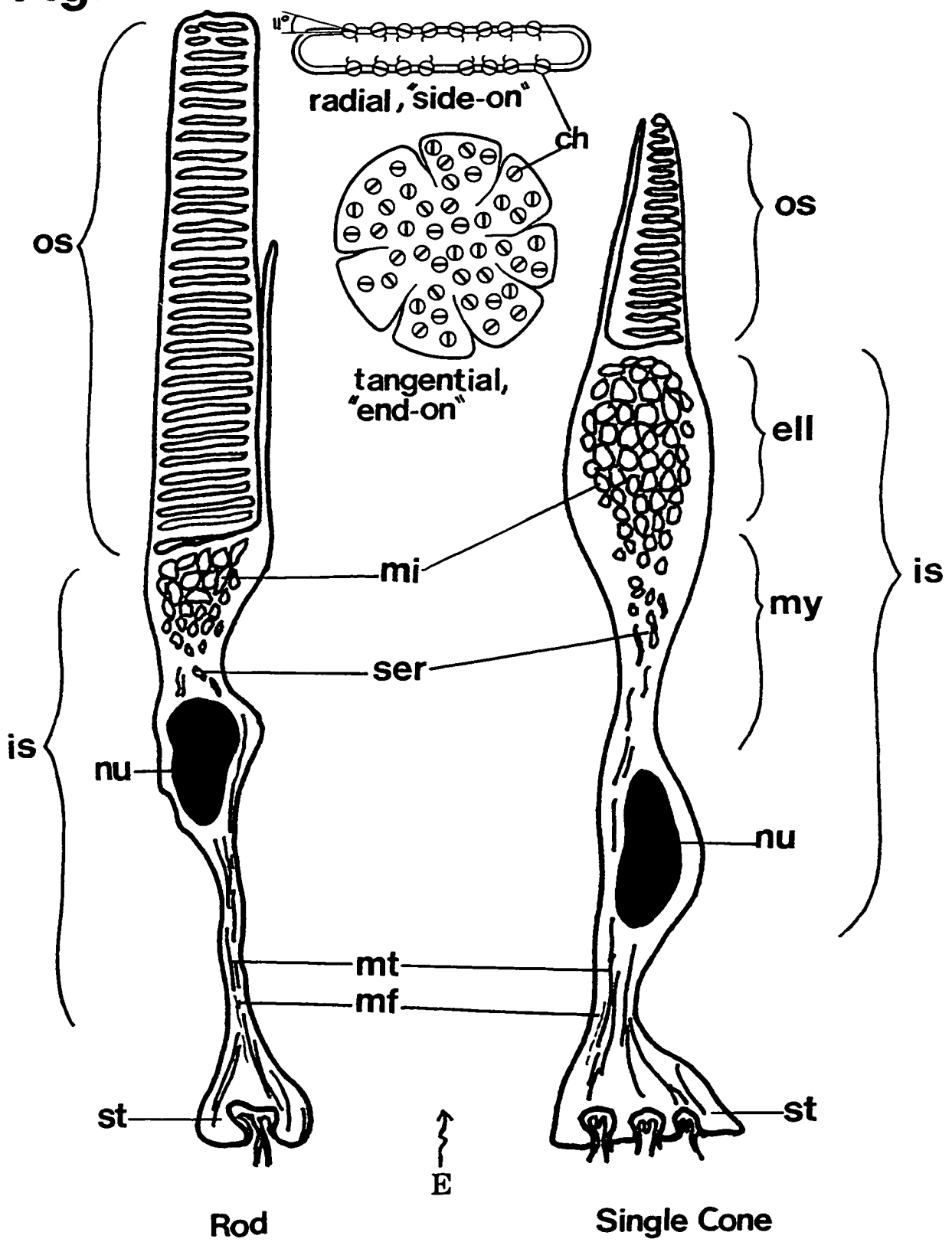
radial, "side-on"
ch
tangential, "end-on"
os
os
ell
is
mi
my
ser
is
nu
nu
mt
mf
st
st
E
Rod
Single Cone

rhabdomeric microvilli, and measured large polarization sensitivity (PS) values of 9 for the crab *Arcinus* and the lobster *Homarus americanus*. By comparison, cephalopods (squid) were shown to exhibit PS up to 6 (Hagins & Liebman, 1963), *Diptera* (flies) around 3 to 5 (Snyder, 1973b), and bees and ants (with fused rhabdom) from 2 to 7 approximately (Snyder, 1973b). These physiological findings were subsequently attributed to differences in size and structure of rhabdoms, waveguiding properties, microvillar orientations and superposition of cells' microvilli (Snyder, 1973a,b; Snyder & Pask, 1973; Snyder et al., 1973; Bernard, 1975). In particular, some general conclusions drawn from this research (that can also be modified to understand vertebrate polarization systems) were: 1) the longer a dipteran (fly) rhabdom or the greater the concentration of photopigment within it, the lower the PS of the retinula cell and the broader the spectral sensitivity curve (this relationship was later used to localize spectral receptors in the butterfly from polarization measurements alone, Bandai et al., 1992), 2) due to waveguide effects, the smaller the diameter of the rhabdom the greater the PS, 3) the small diameter and cross sectional area of cells 7 and 8 in the fly, and cell 9 in the honeybee rhabdom (all sensitive to UV light, Hamdorf et al., 1971) rendered them high PS, 4) the layered rhabdom of crustaceans with one single visual pigment satisfied the condition PS = ∞; this resulted in very high PS values (see

also Shaw, 1969), 5) electrical coupling in the fused rhabdom diminished PS (at least for the dragonfly); the fused rhabdom was therefore an adaptation for maximizing absolute sensitivity, 6) the bee's rhabdomeres acted as lateral absorption filters and due to this optical coupling between cells, the shape of the spectral sensitivity of each retinula cell was approximately independent of the rhabdomere's length and photopigment concentration [which was the opposite of 1) for the fly eye].

Contemporary to these physiological and biophysical analyses of polarization sensitivity, behavioural experiments showed that ultraviolet light was sufficient for orientation of the desert ant (Duelli & Wehner, 1973). UV sensitive cell 9 of the bee's rhabdom thus became the focus for various models to explain the detection of polarized light in invertebrates based on combinations of polarization and luminosity detectors (Kirschfeld, 1973; Bernard & Wehner, 1977). One model involved two 9th cells of different twist and a luminance detector (cells in the central retina of insects twist about the rhabdom's length axis; Wehner et al., 1975; Smola & Wunderer, 1981). The consequences for polarization sensitivity of twisted and non-twisted rhabdoms were quantified in this model resulting in decreased PS with minima every 180° of twist (Wehner et al., 1975; McIntyre & Snyder, 1978). Another model (Ribi, 1980) involved three 9th cells of different orientation located in the dorsal retina of the bee

as the necessary functional unit for polarization discrimination. Although both these detection models were valid, later research showed that it is the dorsal rim of the bee, the ant, and the cricket compound eye that is specialized for polarization sensitivity (this is the so-called POL area of insects; Labhart, 1980; Wehner, 1983; Labhart, 1988, 1996; Nilsson et al. 1987). The rhabdoms in this area do not twist; pairs of UV-sensitive (bee, ant) or blue-sensitive (cricket) retinular rhabdomeres are oriented perpendicular to each other in the rhabdom, and average PS for these cells in the bee is 6.6, as opposed to 2 for the rest of the eye (Labhart, 1980). Such retinular disposition corresponded to a 3-dimensional system of E-vector discrimination based on two detectors (with perpendicular microvilli) and a green luminance detector (Labhart, 1980; Bernard & Wehner, 1977). Subsequent to these findings, intracellular recordings from the cricket's dorsal eye rim have shown polarization sensitive interneurons with 180° periodicity (Labhart, 1988, 1996). These results can be modeled by assuming a subtractive interaction between rhabdomere outputs, and such an interaction is presumed to enhance the neural polarization signal (Wehner, 1983). Further anatomical specializations may also improve the process of detection. In the fly, for instance, polarization interneurons from cells 7 and 8 project to the dorsal posterior medulla, defining a specialized marginal zone of this optic lobe for processing polarized light information (Fortini & Rubin,

1991).

Behavioural studies have shown that the rhabdoms of the POL area in the eye of the ant, the bee and the cricket are distributed so that sensitivity is maximized to the E-vector pattern of a crepuscular sky (Wehner, 1982, 1983, 1989; Rossel & Wehner, 1986). The ant orients by matching its receptors as closely as possible to this "ideal" hard wired E-vector pattern (Wehner, 1989). Present research in this field focuses on the study of 3-dimensional representation of space by the ant (Wehner, 1994), as well as on the use of polarization cues and mechanisms of detection for other invertebrates (e.g. Goddard & Forward, 1991).

1.3.2 Vertebrates

Unlike the well-studied field of invertebrate polarization sensitivity, the vertebrate counterpart is poorly understood.

The first studies documenting behavioural responses to polarized light were obtained with fish (Groot, 1965; Waterman & Forward, 1970; Dill, 1971; Forward et al., 1972), amphibians (Taylor & Adler, 1973), lizards (Adler & Phillips, 1985) and migratory birds (Able, 1982; Moore, 1987). During these early experiments, polarotactic responses of the animals were recorded as the polarization direction of the ambient light was altered using polarizers. Following these behavioral observations, single unit electrophysiological recordings and heart rate conditioning protocols were used to obtain

polarization sensitivity curves in fish (rainbow trout, Kawamura et al., 1981; goldfish, Waterman & Hashimoto, 1974, Waterman & Aoki, 1974; cichlids, Davitz & MacKaye, 1978, Kawamura et al., 1981). However, the results obtained did not exhibit discernable patterns, and have not been reproduced. Similarly, the latest electrophysiological findings with birds question their capability to detect the polarization of light (Coemans et al., 1990; Vos Hzn et al., 1995).

More recent research with fish using behavioural heart rate recordings and extracellular CNS recordings suggest that goldfish (Hawryshyn & McFarland, 1987) and rainbow trout (Parkyn & Hawryshyn, 1993; Coughlin & Hawryshyn, 1995) exhibit two polarization sensitivity mechanisms with opposite sensitivity maxima based on different cone types (the single corner or UV cone and the double cone, Fig. 1.15A). In contrast to this, evidence has been presented for a single type of polarization sensitivity function based on the action of one cone type (the twin cone) in green sunfish (Fig. 1.15B; Cameron & Pugh, 1991). A mathematical model for polarization detection based on birefringent waveguide properties of twin cones has also been proposed for the green sunfish (Rowe et al., 1994), but this model does not explain results for ultraviolet sensitive fishes.

1.4 Goals of this thesis

It should be apparent from the discussion above that the

Figure 1.15 (A) Idealized polarization sensitivity functions for fishes with full square mosaics containing ultraviolet (UV) cones (the cone mosaic changes to a row with double cone partitions arranged in a square pattern in the central retina of salmonids). Chromatic isolation of either double cone outer segment members [green (G) or red (R)] results in polarization sensitivity curves that are roughly opposite to those obtained from isolation of the UV cones. When double and UV cones are both active, the resulting function comprises three local maxima. The blue cone (B) and the rods are insensitive to the orientation of the electric field of polarized light (Hawryshyn & McFarland, 1987; Parkyn & Hawryshyn, 1993; Coughlin & Hawryshyn, 1995). **(B)** Polarization sensitivity curve published for green sunfish and attributed to the action of the equal twin cone (Cameron & Pugh, 1991). Notice that the retinal mosaic in post-larval sunfish lacks corner (UV) cones.

Fig. 1.15

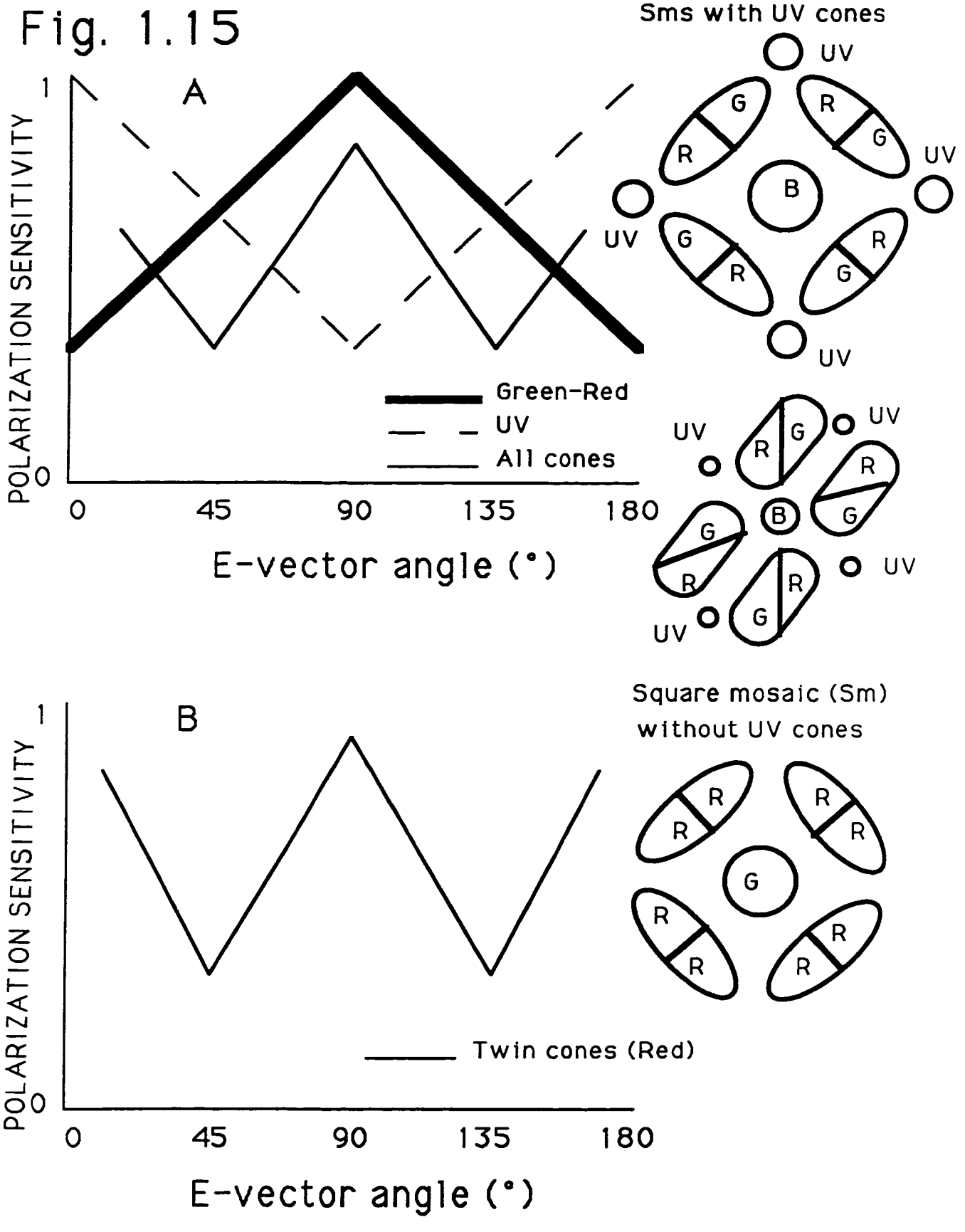
A
1
0
POLARIZATION SENSITIVITY
0
45
90
135
180
E-vector angle (°)
Green-Red
UV
All cones
Sms with UV cones
UV
G
R
B
Square mosaic (Sm)
without UV cones
B
Twin cones (Red)

field of vertebrate polarization sensitivity contains many unknowns and inconsistencies. In particular, two major areas appeared critical to the development of this field that became the goals of this thesis. One was the formulation of detection and neural-processing mechanisms that could explain cohesively the various polarization responses observed to date. The other was to find out, for aquatic vertebrates, whether the polarization signals used in laboratory experiments were also present in nature. This research was essential because polarization measurements ranging the entire visual spectrum (340-760nm) were lacking for aquatic environments and, among the vertebrates, polarization sensitivity has only been shown for some species of fish and only in the laboratory. For this reason and their local availability, fish were used as model vertebrates in this thesis. Nonetheless, the similarity in retinal structure and higher visual centres between some fish, birds, amphibians, reptiles, and even marsupials (Tovée, 1995; Ahnelt et al., 1995) suggests applicability of the findings presented to species of birds, lower vertebrates and marsupials that exhibit similar polarotactic responses.

To answer whether the necessary polarization signals were present in nature, light measurements were taken underwater in lakes and coastal waters inhabited by species for which polarization sensitivity has been reported. Electrophysiological experiments varying the intensity and percent polarization of the incident light were carried out in

the laboratory to determine the spatial and temporal restrictions of polarized light utilization by rainbow trout. These results were then extrapolated to percomorph fish in general, given our knowledge of polarization sensitivity in other fish species and previous measurements of polarized light in oligotrophic waters.

The formulation of one or various models for detection and processing of polarized light information in fish (and vertebrates with similar visual systems) required comparative physiological and anatomical studies. The basic questions to be answered were: 1) are all fish polarization-sensitive? If not, what differences in retinal structure can account for the presence or lack of polarization sensitivity?, 2) what is the biophysical mechanism for polarization detection, i.e. is there an optical anisotropy within photoreceptors that would render them capable of detecting the orientation of linearly polarized light?, and 3) can a neural model be constructed that would incorporate and explain all the polarization sensitivity results obtained for vertebrates to date? In the following chapters, I present physiological and ultrastructural results from different species of fish, chosen for their retinal peculiarities, to attempt answers to these questions. In particular, a general mechanism for polarization detection in fish is presented which, in addition to a previous one formulated for birds (Young & Martin, 1984), may cover the majority of possibilities used by vertebrates to

detect the electric field orientation of polarized light. I also show a simple neural model, analogous to that proposed for invertebrates (Wehner, 1983), that explains all the polarization sensitivity results obtained for vertebrates to date.

Chapter 2: Distribution of polarized light underwater and its implications for polarization sensitivity in rainbow trout, *Oncorhynchus mykiss*.

2.1 Introduction

Sunlight reaching the Earth's atmosphere is unpolarized, i.e. there is no preferential plane in which the electric field of most photons oscillates. However, when individual photons interact with various components of the atmosphere and water column, a scattering phenomenon takes place first described by Lord Rayleigh (Rayleigh, 1889, see chapter 1). In the water, Rayleigh scattering is caused by molecular and particle scattering. In the sky, Rayleigh scattering arises from minute density fluctuations in the atmosphere caused by changes in temperature. These fluctuations create microirregularities in refractive index of the medium through which the light travels. If the physical scale of the irregularities is smaller than about 1/10th of the wavelength of the incident light, the resulting radiation pattern is a toroid around the scattering dipole (chapter 1). Rayleigh scattering produces scattered light which is 100% polarized at right angles to the incident unpolarized beam. It is this, as well as other natural phenomena leading to polarization of sunlight (see chapter 1), that are exploited by animals capable of differentiating between individual planes of light. Such animals are sensitive to the amplitude and direction of

the Electric field (E-vector) of polarized light.

Polarization sensitivity was first documented for the honeybee in the late forties (von Frisch, 1949). Since this early pioneering work, other invertebrates, terrestrial and aquatic, as well as fishes, amphibians, reptiles and birds have been shown to exhibit at least polarotactic responses (for reviews see Waterman, 1981, 1984). Nevertheless, it is only for the desert ant (*Cataglyphis bicolor*), the honey bee (*Apis apis*), and the cricket (*Grillus campestris*) that thorough descriptions linking the anatomical features and neurophysiological mechanisms underlying the animal's use of polarized light are well documented (Wehner, 1983, 1989; Labhart, 1988, 1996). Work with vertebrates, by comparison, is at an early stage (see chapter 1).

Most polarized light investigations with vertebrates have used fish as study subjects (Waterman, 1981; Cameron & Pugh, 1991; Parkyn & Hawryshyn, 1993). This choice, although satisfactory due to the potential for visual diversity from the richness of photic environments that fish inhabit, nonetheless makes implications for the behaviour and life strategies of the animal hard to discern. Indeed, it is difficult to follow a fish in its natural habitat and to isolate the effect that a particular variable, such as polarized light, has on its behaviour. As a consequence our knowledge of polarized light sensitivity in vertebrates is restricted to responses under laboratory settings, which may

not be representative of the natural environment of the animal. This restricted knowledge also applies to the characterization of the natural underwater polarized light field that would permit the observed laboratory behaviours in nature.

Since the first observations of polarized light in the ocean (Waterman, 1954), a magnificent body of experimental work has been carried out by various researchers to characterize the underwater polarized light field and to determine the biological and physical factors controlling it (see Ivanoff, 1974; Loew & McFarland, 1990). The most complete description of underwater polarization combining laboratory and field measurements was given by Timofeeva (Timofeeva, 1961, 1962, 1969, 1974). In accordance with this author's work (Timofeeva, 1974), I describe the present results using previous notation (Fig. 2.1, Table 2.1).

The physical parameters controlling the degree and E-max orientation of polarized light arising from underwater scattering were investigated by Timofeeva in the laboratory using "milky" solutions (Timofeeva, 1961, 1969, 1974; the E-max plane of a light source is the oscillation plane for the majority of electric fields from photons comprising the light source, it is the plane of maximum polarization). Timofeeva concluded that percent polarization was highest for solutions with the biggest absorption and lowest dispersion coefficients, regardless of the source's azimuth

Figure 2.1 Geometrical definitions of variables used in the text (modified from Timofeeva, 1974). See also Table 1.

Fig. 2.1

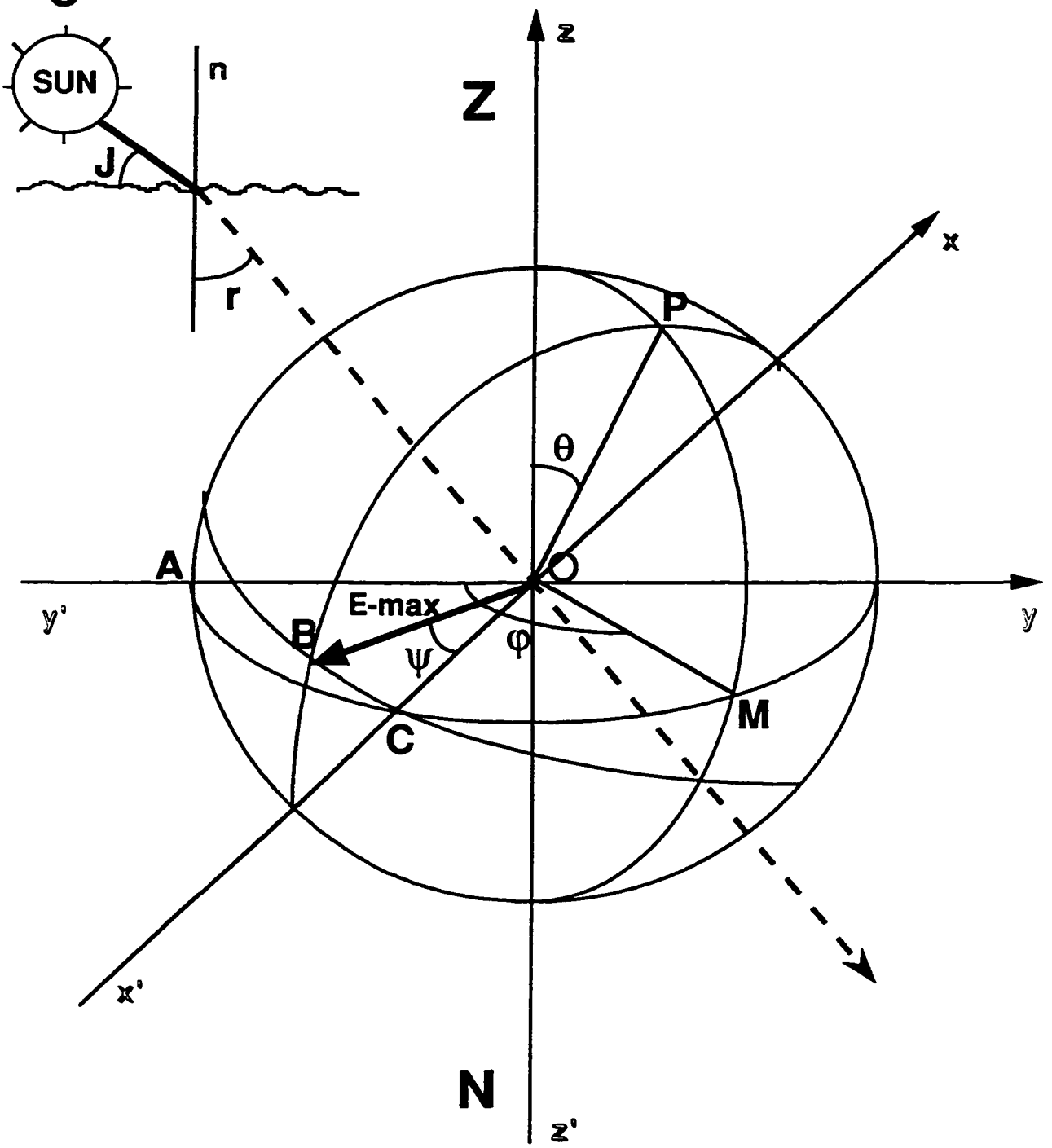

Table 2.1 Definitions of variables shown in Figure 2.1.

J= elevation of the sun ($0° \leq J \leq 90°$)

n= normal to a calm water surface

N= Nadir (straight down on zy plane)

OB= E-max vector

OC= reference line (0° or 180°) on spectroradiometer radiance cone collector

OP= long axis of spectroradiometer, the plane containing the light ray and OP is the scattering plane

r= angle of refraction (on zy plane)

Z= Zenith (straight up on zy plane),

ψ= E-max angle (angle between the reference line OC and the E-max vector ($0° \leq \psi \leq 180°$), E-min= E-max + 90°

φ= azimuth angle (angle between the vertical plane through the light source and the vertical plane through OP containing the point in space viewed, angle AOM is in the xy plane)

θ= zenith angle, angle from Zenith direction ($\angle$ZOP)

percent (%) polarization=

100(rad(E-max)-rad(E-min))/(rad(E-max)+rad(E-min))

where rad= radiance.

---

direction (Timofeeva, 1961). In accordance with these observations, the regions of the spectrum least absorbed in laboratory solutions and in the ocean were also the least polarized (Timofeeva, 1962; Ivanoff & Waterman, 1958). Timofeeva also studied the dependence of the degree of polarization and direction of E-max on azimuth angle of the light source and direction of observation (Timofeeva, 1969, 1974). Results from these studies proved the existence of submarine neutral points in the plane of the sun (Timofeeva, 1974), and explained E-max and percent polarization trends observed for all azimuth planes (Timofeeva, 1962; Ivanoff & Waterman, 1958; Waterman & Westell, 1956). Further work by this and other authors also revealed a negative relationship between percent polarization and increasing depth (Timofeeva, 1974; Ivanoff & Waterman, 1958; Waterman & Westell, 1956; Waterman, 1955).

Although the underwater polarized light field has been thoroughly studied in the past, the application of these findings to animal visual systems requires further measurements. In particular, previous studies did not describe the polarized light field in the UV range (wavelengths<400 nm) (Ivanoff & Waterman, 1958; Timofeeva, 1962), yet the UV photoreceptor in many invertebrates and most fish (Hawryshyn & McFarland, 1987; Parkyn & Hawryshyn, 1993) is involved in polarized light sensitivity. Published measurements were also for individual wavelengths, or for the integrated spectrum

from 400 to 700 nm without showing the spectral distribution of the energy. Yet, activation of individual photoreceptors is a wavelength dependent process dictated by the absorption properties of the photopigments (Govardovskii, 1976). Hence, the measurements presented in this study improve on previous ones by incorporating the spectrum from 300 to 400 nm and by showing the energy distribution for the expanded spectrum from 300 to 850 nm. As well, these measurements show the dependence of the polarized light field on additional variables such as the time of day and different atmospheric and water conditions. In particular, I provide the first polarized light measurements in a lake, an important set of data since most polarized light sensitive fish species documented are fresh water (Hawryshyn & McFarland, 1987; Cameron & Pugh, 1991; Parkyn & Hawryshyn, 1993; Coughlin & Hawryshyn, 1995).

The purpose of this study was therefore twofold. First, the study describes the spectral and polarized light fields in mesoeutrophic waters inhabited by polarized light sensitive fish species such as rainbow trout (*Oncorhyncus mykiss*), and assesses whether the light cues required for the observed laboratory behaviours (Hawryshyn et al., 1990; Hawryshyn & Bolger, 1990; Cameron & Pugh, 1991; Parkyn & Hawryshyn, 1993) are present in nature. Second, the study reproduces the natural spectral background conditions in laboratory experiments to test the visual capabilities of the animal in nearly natural light settings. Although the data are

interpreted in relation to the visual system of young rainbow trout, the characteristics of the light field can be used to assess the broader possibility of polarized light utilization by other aquatic organisms.

2.2 Materials and Methods

2.2.1 Measuring the polarized light field

The equipment used for the light measurements consisted of two major components: an LI-800 underwater spectroradiometer (Biggs, 1984) and a rotatable column (Figs. 2.2A-D). The column was made of 3 m pieces of plastic ABS pipe linked together with T connections by means of screws (Figs. 2.2C,D). By releasing and re-tightening the top T screws at a certain depth of water, the length of column above it could be rotated through 360° in the x-y plane (Fig. 2.1). The spectroradiometer was fastened to the middle part of the T, and in the same fashion, it too could be rotated through 360° in the y-z plane. Combining these two axes permitted a scan to be taken in any direction within the allowed depths by the column (every 3 meters). The column was secured by a heavy cement block at the bottom of the lake/ocean, and extended up to 1 meter from the surface where a partially submerged buoy provided a surface fix for the column (Fig. 2.2D). These attachments at both ends maintained the column upright and stable even under powerful ocean swells. The column once installed was maintained on the spot for the duration of the

Figure 2.2 (A) Spectroradiometer (Spec) and associated equipment to measure the light field underwater. Lev: level, Comp: compass, Pro: protractor, E-vf: E-vector finder (polarization axis finder), Rc: radiance cone collector, Coc: Column connector, Col: column. **(B)** view of spectroradiometer 1.5 meters below the ocean surface. Notice the multitude of speckles on the photograph indicating high numbers of particles in mesoeutrophic waters. **(C)** diver searching for E-max; arrows indicate rotational joints and the planes of rotation on spectroradiometer-column system. **(D)** view of column with spectroradiometer attached.

Fig. 2.2

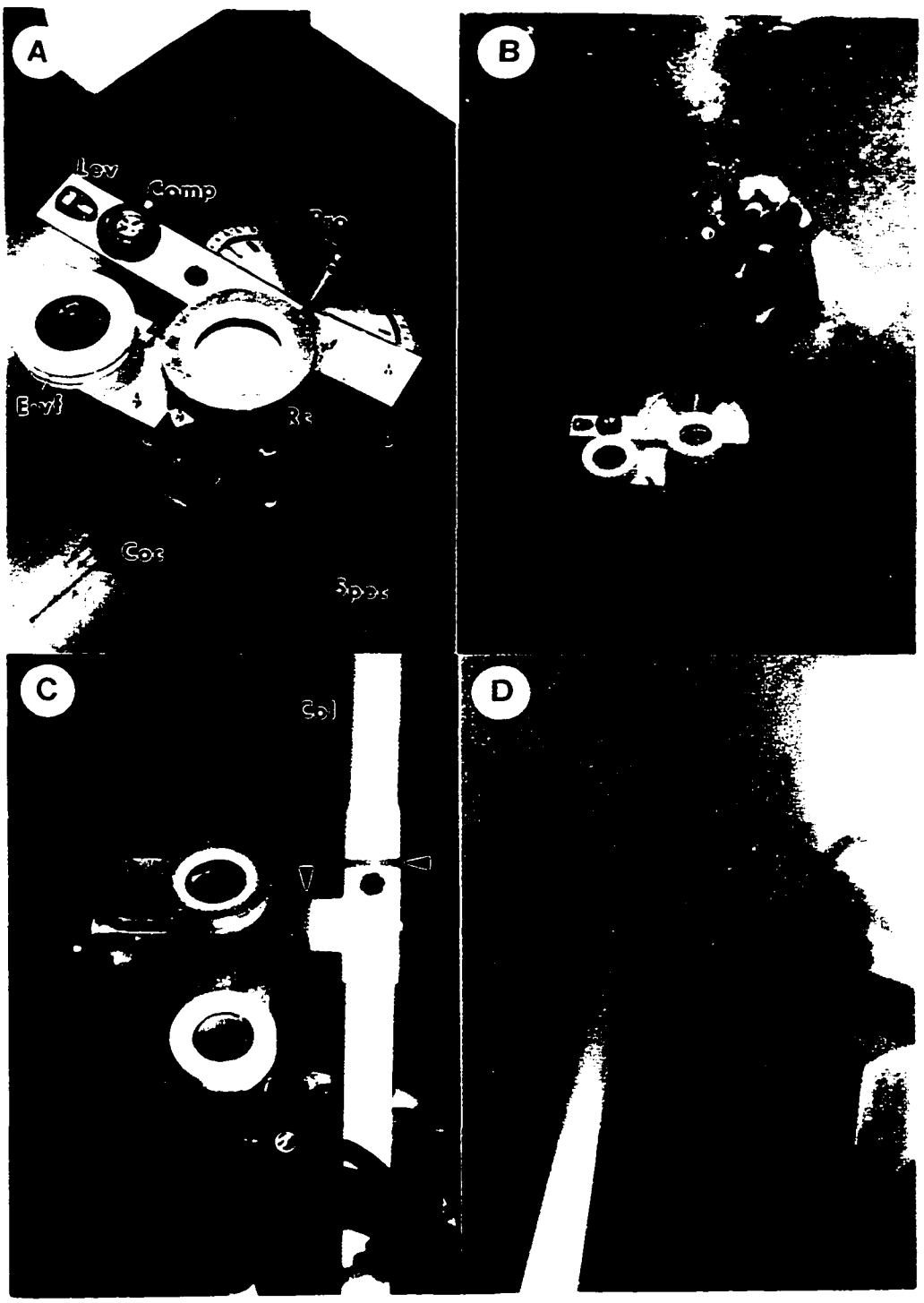

study. Only when a different water body was studied was the column re-positioned.

The spectroradiometer apparatus could be modified for different types of light measurements by addition of various accessories (Fig. 2.2A, Table 2.1). To control the zenith angle θ, a metal protractor with 1° delineations was fastened on top of the spectroradiometer. By rotating the arm of the protractor, a specific angle (corresponding to θ) could be selected (the protractor arm holds the level and compass in Figure 2.2A; it rotates from 0° to 180° in the y-z plane irrespective of spectroradiometer rotation). The angle θ could then be set by rotating the spectroradiometer until the level built onto the rotatable arm indicated evenness in the x-y plane. A compass, located on the rotatable arm specified the azimuth angle φ. Without any other accessory, the spectroradiometer was ready to take spectral irradiance readings. To measure radiance, a solid cone holding a 30° angle aperture was placed over the cosine collector. This aperture was chosen because it is within the range of numerical apertures (30-45°) measured for parr rainbow trout eyes (Novales Flamarique, 1993). The cone was painted in black externally so that no stray light could reach the cosine collector. If polarized light readings were to be taken, a UV-grade linear polarizer transmissive from 300-850 nm (Polaroid HPN'B) was inserted into the top part of the cone. This polarizer could rotate over 180°, the delineations for which

were engraved on the side of the cone in 1° intervals. To select the plane of maximum polarization (E-max), the diver looked through a polarization axis finder (Edmund Scientific) and transferred the angle read to the polarizer on the cone (Fig. 2.2C). Both polarization axis finder and cone polarizer were sandwiched between two UV transmissive acrylite sheets (OP-4, Cyro Canada) and the degree delineations and directions of observation were the same for the cone and the polarization axis finder holder. All the parameters read were transferred to the boat-tender researcher using a two-way diver-to-boat communication system (Ocean Technology). The spectroradiometer was connected to a computer on the boat. Scans from 300 to 850 nm, every 5 nm, were taken upon diver signal. The time to complete a scan was approximately 35 seconds. Scans were taken at different times of the day in various azimuth planes at depths from 10 meters to 1 meter below the surface. Parallel studies were conducted in Lake Cowichan and Ogden Point Breakwater (Vancouver Island, British Columbia, Canada). Both of these types of waters exhibit similar spectral irradiance characteristics (Novales Flamarique et al., 1992; Novales Flamarique & Hawryshyn, 1993).

2.2.2 Mathematical treatment of light measurements

To make the data meaningful in terms of salmonid vision the loss of light before the rays encounter the fish retina as well as the wavelength-dependent absorption of the four types

of cone pigments found in young rainbow trout (UV, short (blue), middle (green) and long (red)-sensitive) had to be considered (Novales Flamarique & Hawryshyn, 1993). Thus the raw data were multiplied by transmission coefficients giving the percentage of light that would traverse the lens, cornea and vitreous fluid of the eye (Hawryshyn et al., 1989), and by the absorptance values of the cone photoreceptors examined. To obtain the absorptance values (Fig. 2.3), the pigment absorbance spectra, derived from an eighth order polynomial template for vertebrate cone absorption (Bernard, 1987) using MSP-obtained wavelength maxima, were first multiplied by the specific absorbance (0,0124/μm; Hárosi, 1975) and then by the average photoreceptor outer segment length in retinas of 12g rainbow trout (~10 μm). Absorptance values were then calculated using the equation:

$$\text{Absorptance} = 1-10^{(-\text{absorbance})}$$

Integrating the products of the absorptance values for each cone photoreceptor type and irradiance values throughout any part of the spectrum thus indicated how much light was available to stimulate each cone type in that part of the spectrum. These results could then be compared to average irradiance values that elicit fish responses in laboratory experiments (transformed similarly) to judge whether polarized light vision, in terms of required intensity, could occur in nature. The second requirement is that the degree of polarization be sufficiently high for the animal to

Figure 2.3 Absorptance spectra for the different cone photoreceptor mechanisms in rainbow trout. The ranges used for integrations correspond to the α peaks of the different cone absorbance spectra: 300-450 nm (UV), 340-520 nm (short or blue), 400-640 nm (middle or green) and 440-700 nm (long, or red, wavelength mechanism). Integration values were also computed for the β bands of the middle (300-400 nm) and long (320-420) wavelength mechanisms. β band integrations are useful for comparison with laboratory results involving only UV light in the stimulus. In nature, the animal likely uses mostly green and red light for visual processes involving double cones (which are green and red sensitive), and UV light for UV cones, whether the light is polarized or not.

Fig. 2.3

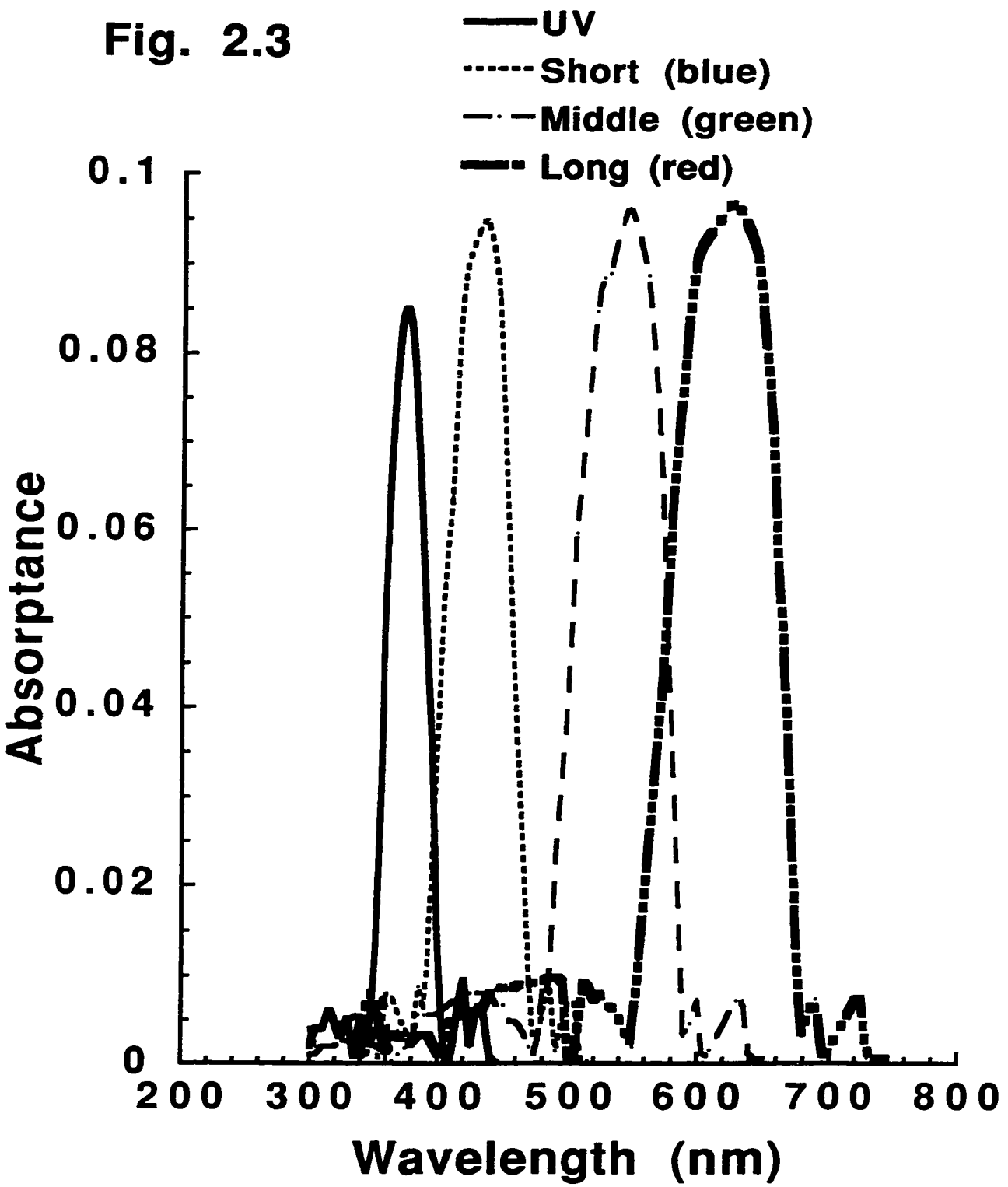
UV
Short (blue)
Middle (green)
Long (red)
0.1
0.08
0.06
0.04
0.02
0
Absorptance
200
300
400
500
600
700
800
Wavelength (nm)

distinguish E-max from unpolarized light, or light polarized in a different orientation (any other E-vector). To calculate degree of polarization (percent (%) polarization), two scans in the E-max and E-min planes were conducted for each direction of observation (the E-min plane is the plane of least polarization, and is oriented perpendicular to the E-max plane, Table 2.1).

As an index to classify the waters studied, I measured chlorophyll concentrations in triplicated samples (Jeffrey & Humphrey, 1975; Table 2.2). All mathematical analyses in this section used Li-Cor software and the Statistical Analysis System (SAS, version 5).

2.2.3 The visual system of young rainbow trout

Once the properties of the light field in mesoeutrophic waters had been described, the next endeavour was to determine the visual characteristics of the animal under natural light settings. To do this I mimicked the spectral backgrounds found in nature in the laboratory and measured electrophysiologically (as described below) the responses of the animal to spectral stimuli that were either polarized or unpolarized. These experiments permitted me to determine the polarization and spectral sensitivities of the animal for particular spectral background radiances (Fig. 2.4).

Table 2.2 Representative chlorophyll concentrations for May and June 1993 in Lake Cowichan and Ogden Point Breakwater. LC: Lake Cowichan, OPG: Ogden Point Breakwater. Chla,b,c: Chlorophyll a,b,c, Phaeo: Phaeopigment (in mg/ml), n=3 replicates, all standard errors <30% of value. Oligotrophic waters are characterized by 0.3 mg/ml< [Chla] <3 mg/ml and appear blue, mesotrophic waters are greener and have typically 2 mg/ml< [Chla] <15mg/ml, eutrophic waters are dark green and show 10mg/ml< [Chla] <500 mg/ml. At either end of this spectrum are ultra-oligotrophic and hypereutrophic waters exhibiting extremely low and high Chla concentrations respectively.

Depth (m)	LC (May 15, 1993)				OPG (May 23, 1993)			
	Chla	Chlb	Chlc	Phaeo	Chla	Chlb	Chlc	Phaeo
1	4.53	1.17	1.34	0.076	5.71	1.12	3.21	0.082
4	6.23	1.12	1.73	0.124	4.93	1.24	2.45	0.344
7	3.94	0.523	1.41	0.231	3.03	0.927	1.96	0.171
			LC (June 20, 1993)			OPG (June 28, 1993)		
1	2.21	1.02	1.29	0.607	5.02	1.65	2.94	0.122
4	2.94	1.31	1.03	0.128	2.38	1.09	1.67	0.138
7	6.34	1.42	1.96	0.342	2.26	0.847	1.13	0.067

Figure 2.4 Light backgrounds used during electrophysiology experiments. Except for the middle-wavelength isolation background, all others mimic natural conditions in mesotrophic waters for the various time periods specified in the figure.

Fig. 2.4

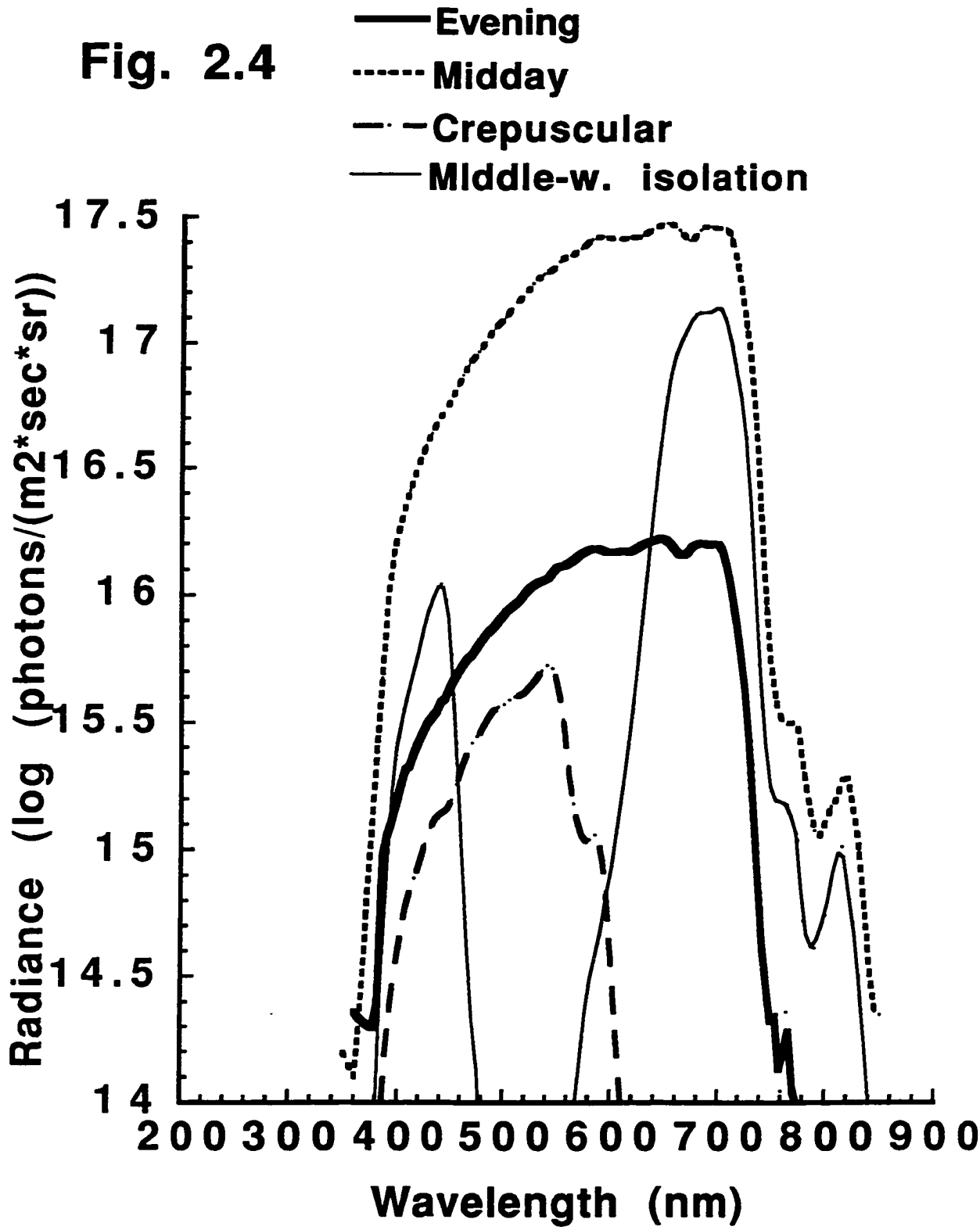
Evening
Midday
Crepuscular
Middle-w. isolation
17.5
17
16.5
16
15.5
15
14.5
14
Radiance (log (photons/(m2*sec*sr))
200 300 400 500 600 700 800 900
Wavelength (nm)

2.2.4 Electrophysiological experiments and treatment of data

Animals were anaesthetized by immersion in MS-222 (0.1g/l) and paralysed by Pavulon injection (pancuronium bromide, 0.038mg/g body mass). The fish were irrigated with MS-222 solution (0.005%) during surgery to expose the optic tectum. A local anaesthetic (tetracaine, 0.5%) was applied to the surgical area.

A Teflon-coated silver wire electrode (0.34 mm in diameter) was inserted rostro-ventrally through the optic tectum into the optic nerve. This electrode monitored compound action potentials from the optic nerve while a reference electrode was inserted into one of the nares of the fish and its signal subtracted from that of the recording electrode. The resulting difference signal was amplified using a Grass preamplifier (P50 series) with bandpass between 0.3 Hz and 0.1 kHz, and was displayed on an oscilloscope while simultaneously received and processed by computer.

The optical system used in this study consisted of a stimulus channel (with a 300 W xenon light source, Oriel) and two background channels (using 250 W tungsten-halogen sources, EJH Spectro) (Fig. 2.5A). The stimulus energy and spectral output were controlled by an Inconel neutral density wedge and a monochromator. Using Corion interference filters, four types of background lighting conditions were produced, three that mimicked natural levels of illumination at different times of the day, and one that isolated the action of the middle cone

mechanism (Fig. 2.4).

During spectral sensitivity experiments, the output from the three optical channels converged onto a diffuser placed in front of the fish's eye. This ensured an even illumination from all the channels across the entire retina. In the case of polarization sensitivity measurements, each channel had its own diffuser, and a rotatable polarizer was placed immediately following the diffuser in the stimulus channel. The channels were positioned so that the stimulus polarized light was incident on the central retina, where background radiances overlapped as much as possible (nonetheless, adaptation in this set-up was probably due mostly to overlapping horizontal cell dendritic fields in the retina). Light from the background channels did not cross the polarizer.

To measure percent polarization levels of the light source required for detection by rainbow trout, the optical set up described above was altered (Fig. 2.5B). The stimulus light was now split into two components using a variable density beam splitter (Edmund Scientific). The reflected component bounced off a front surface mirror and passed through a rotatable polarizer before reaching the fish's eye. The transmitted component went directly to the fish's eye. Both rays were positioned to overlap as closely as possible the central region of the eye (retina). The ratio of transmitted to reflected energies was altered by changing the position along the length of the beam splitter upon which the light

Figure 2.5 (A) Electrophysiology rig, S: light source, C: condenser lens, M: monochrometer, Nd: Neutral density wedge, Fl: field lens, d: diaphragm, Pl: projection lens, es: electronic shutter, Ft: filter tray, Lg: light guide, Pol: HNP'B polarizer (light passes through a diffuser just prior to the polarizer), FC: Faraday cage, Rec: recording electrode, Ref: reference electrode, Rfw: respiration flow-through water system, Cnr: common noise rejection unit, Amp: amplifier, Osc: oscilloscope, BCh1, BCh2: Background light channels 1 and 2. Stch: Stimulus channel, Computer shows a typical amplitude response vs. radiance curve, **(B)** Percent Pol measurements addition: VBS: variable density beam splitter, FSM: front surface mirror.

Fig. 2.5

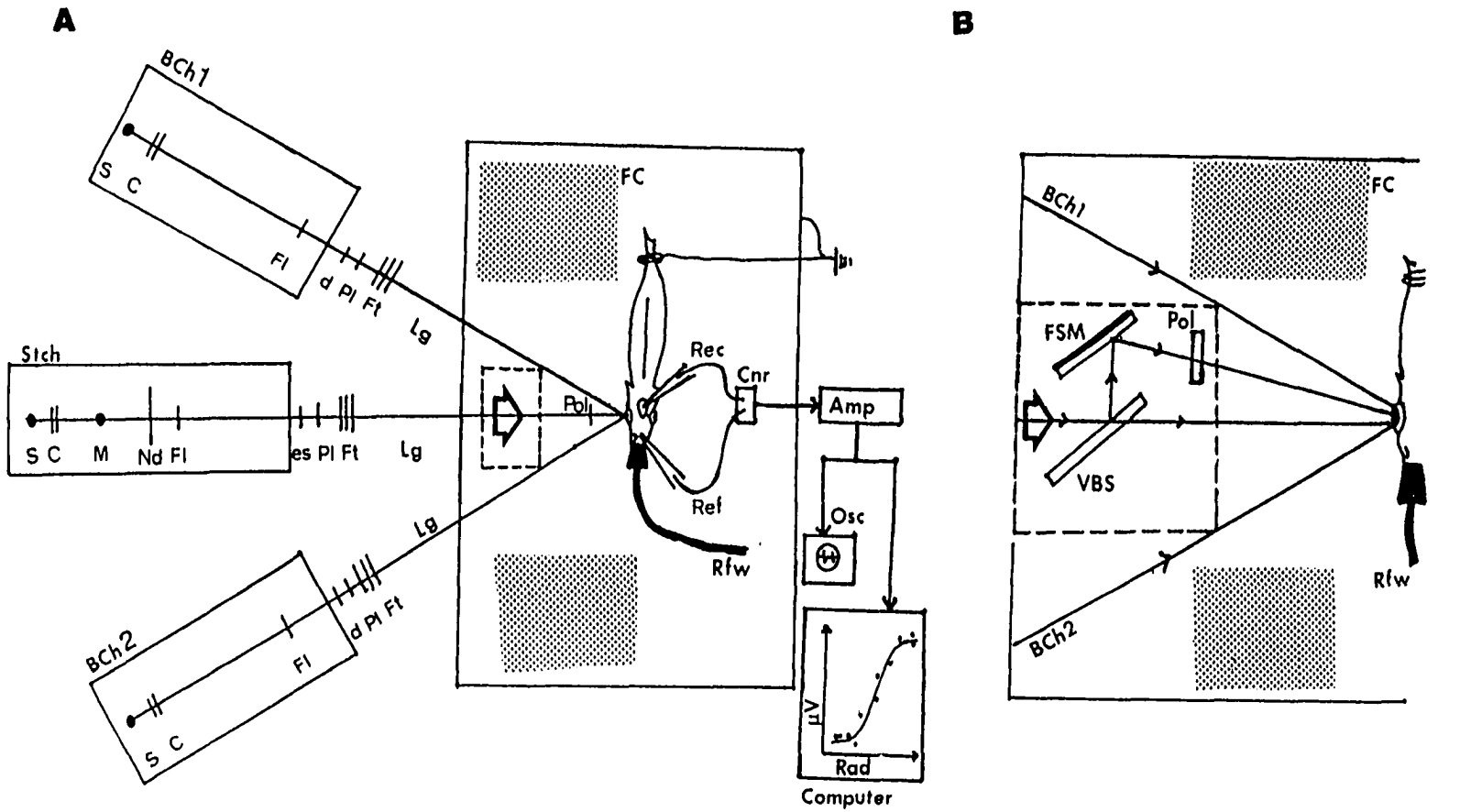
A
BCh1
S C
Fl
d Pl Ft
Lg
Stch
S C
M
Nd Fl
es Pl Ft
Lg
BCh2
S C
Fl
d Pl Ft
Lg
FC
Pol
Rec
Cnr
Ref
Rfw
Amp
Osc
mV
Rad
Computer
B
BCh1
FC
FSM
Pol
VBS
Rfw
BCh2

from the source was incident. Because polarized light is produced by reflection from dielectric surfaces (see chapter 1; Hecht & Zajac, 1974), the percentage of polarized light for the two polarizer angles tested in this experiment (0° and 90°) was calculated from combined measurements from the two components of the stimulus channel. Following measurements of E-max and E-min for the two optical paths individually at the level of the fish's eye, the total % polarization was calculated as:

$$(E\text{-}max_{mir}+E\text{-}max_{bs}-E\text{-}min_{bs})/(E\text{-}max_{mir}+E\text{-}max_{bs}+E\text{-}min_{bs}).$$

In this expression "bs" refers to light coming from the beam splitter, while "mir" is light reflected from the front-surface mirror. The difference in percent polarization for the two polarizer angles tested was less than 6% for total polarization values above 52%. Continuous readings from the two optical paths for a given beam splitter position did not reveal differences in energy for the polarization components with time.

Prior to commencement of recordings, the fish was adapted to a particular background light for 1 h. Then stimulus wavelengths ranging from 350 to 660 nm were presented to the fish in an order that precluded the adaptation of any particular cone mechanism. The stimulus duration was 750 ms. Each wavelength was presented in an increasing series of 0.2 log unit intensities. The time between stimuli in each series was 30 s. This procedure was slightly different for

polarization sensitivity measurements. In this case, one wavelength was chosen for the entire experiment and the polarizer was rotated from 0° to 180° in 45° increments.

Compound action potentials (CAPs) were observed at the onset and at the end of the light stimulus (ON and OFF signals, Fig. 2.6A). For each wavelength, the voltage amplitude of these responses was plotted against increasing radiance (Figure 2.6B). A third-order polynomial function was fitted to the data points and the radiance required to elicit a 20 μV response was chosen as the threshold response. This signal level was chosen for two reasons: (1) it was very close to the absolute response threshold for all wavelengths tested (below which no response was obtained), and (2) it was in the linear part of the response curve (ensuring a regular and predictable response). Further details on the procedure may be obtained from other studies (Beaudet et al., 1993; Novales Flamarique & Hawryshyn, 1996).

We conducted three types of experiments on rainbow trout to determine the visual performance of this species under natural light settings. First, we measured the spectral sensitivities of the animal under midday, evening and crepuscular illumination (Fig. 2.4). In these experiments, the simplex algorithm (Caceci & Cacheris, 1984) was used to fit template-derived pigment absorption values (Fig. 2.3; Bernard, 1987) according to the general pseudopigment equation:

$R=(\Sigma k_i A^p_i(\lambda))^{1/p}$ (Sirovich & Abramov, 1977),

Figure 2.6 (A) First nine compound action potential ON-OFF trace signals giving rise to values in (B), the stimulus intensity was increased by 0.2 log units between traces. **(B)** Response amplitude as a function of stimulus intensity and third order polynomial fit. The response curve could also shift towards higher radiances (1-2 log units) depending on the state of adaptation of each mechanism, and the intrinsic physiology of the fish.

Fig.2.6

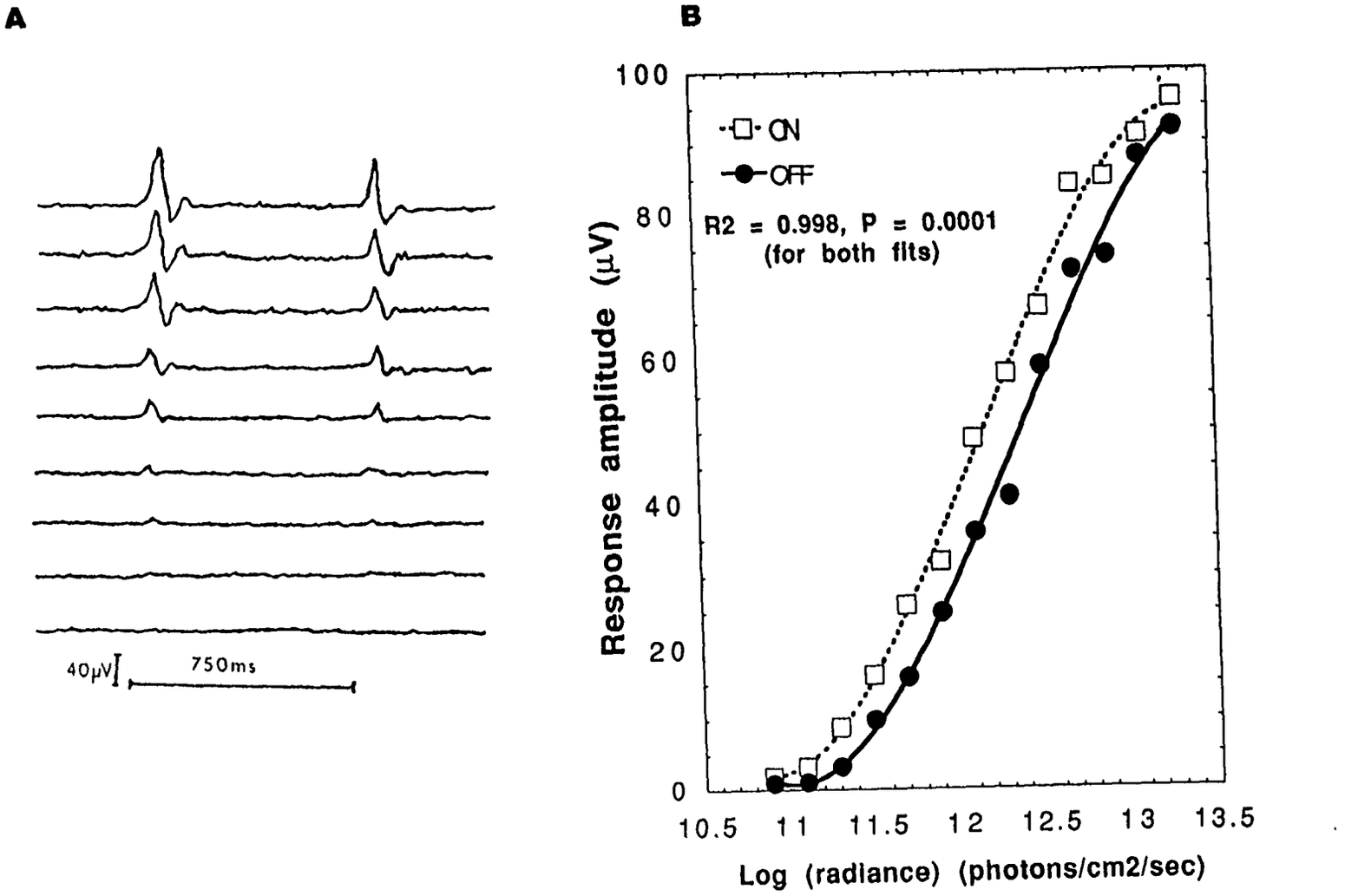
A
40μV
750ms
B
100
80
60
40
20
0
ON
OFF
R2 = 0.998, P = 0.0001
(for both fits)
Response amplitude (μV)
10.5
11
11.5
12
12.5
13
13.5
Log (radiance) (photons/cm2/sec)

where R is the response curve amplitude at a given wavelength λ, $A_i(\lambda)$ is the absorbance of pigment i at light of wavelength λ, k_i are the coupling constants derived from the fit to the data, and p is an exponent resulting from the mathematical requirement that the function describing the spectral sensitivity curve be differentiable at the origin (Sirovich & Abramov, 1977). The k_i parameters obtained indicate which photoreceptor mechanisms are most active at different times of the day. The λ-max values for generating the pigment absorption spectra from the nomogram had been obtained microspectrophotometrically for rainbow trout (Hawryshyn & Hárosi, 1994). These are 365 nm (UV), 434 nm (short), 531 nm (middle) and 576 nm (long wavelength mechanism). I then generated polarization sensitivity curves under crepuscular conditions since it is at these times of the day that % polarization was highest in nature (see results later, Fig. 2.8), and fish activity seems to be at its peak (Johnson & Groot, 1963). Lastly I changed the % polarization of a 520 nm light stimulus to determine the minimum polarization levels required by the fish to detect E-max. I chose 520 nm for these experiments because it approaches the maximum wavelength penetration in meso-eutrophic waters (Novales Flamarique & Hawryshyn, 1993), and is within the absorption spectrum of the short, middle and long wavelength cone mechanisms of rainbow trout. Lack of energy from the Xenon lamp source at 400 nm (after optical reflections) did not permit me to do

experiments within the UV cone photoreceptor absorption range. However, behavioral, electrophysiological and psychophysical experiments suggest that the minimum % polarization values should be similar for all the mechanisms, and lowest for the middle wavelength one (Hawryshyn & Bolger, 1990; Hawryshyn, 1991; Parkyn & Hawryshyn, 1993) so I was studying the best case scenario. Furthermore, under white light backgrounds of moderate intensity, the "W"-function visual response obtained spans a similar sensitivity range to the isolated responses from either middle or long wavelength mechanisms (Parkyn & Hawryshyn, 1993; Coughlin & Hawryshyn, 1995). This does not suggest higher sensitivities to % polarization (i.e. lower detection thresholds) when more than one cone mechanism is acting, as is the case in nature.

All handling and use of animals was in accordance with the guidelines set by the Canadian Council for Animal Care.

2.3 Results and Discussion

2.3.1 General features of the underwater polarized light field

To describe the polarized light field at a specific depth, time of day and for a specific set of atmospheric and water conditions, one must answer how E-max, total energy and percent polarization vary with direction of observation. We will deal with these questions by studying the polarized light field at 4 meters depth under cloudless skies. Then we shall investigate the effects of depth and different atmospheric

conditions. For comparison, I will also present spectral radiance measurements under the same light regimes.

In general, the ratio of total radiance on sunny days to light intensities in either the E-max or E-min planes is at least 1.5 (Fig. 2.7). The distribution of energy across the spectrum changes during the course of the day with proportionately more short-wavelength photons contributing to the total spectrum during crepuscular periods (Novales Flamarique et al., 1992; Loew & McFarland, 1990). This in turn changes the shape of the E-max and E-min functions in a similar fashion (Fig. 2.8).

The percent of polarized light in the plane of E-max is a function of the direction of propagation of the incident sunlight and the direction of observation of the spectroradiometer sensor (see also Timofeeva, 1962, 1974). The direction of sunlight is mostly dependent on the elevation of the sun, while the direction of observation depends both on the azimuth angle φ and the zenith angle θ. The percentage of polarized light changes with azimuth reaching the two highest maxima at θs near 90° and 270° in the plane perpendicular to that of the sun (Fig. 2.9A). The appearance of these maxima can also be observed by scanning all azimuths in a horizontal plane (Fig. 2.9B; Ivanoff & Waterman, 1958; Timofeeva, 1974).

Assuming perfect Rayleigh scattering, it can be geometrically derived that the highest % polarization for any direction of observation is given by:

Figure 2.7 Spectral characteristics of the polarized light field at 4 m depth in **(A)** Lake Cowichan (J=60°42′, $\%Pol_{tot}$= 29.2) and **(B)** Ogden Point Breakwater (J=56°28′, $\%Pol_{tot}$= 26.4). Highest %Pol in the UV part of the spectrum (32% and 35% respectively). The zenith angle for each scan is between brackets, and E-max is always the highest curve for any given pair of zenith polarization scans.

Fig. 2.7

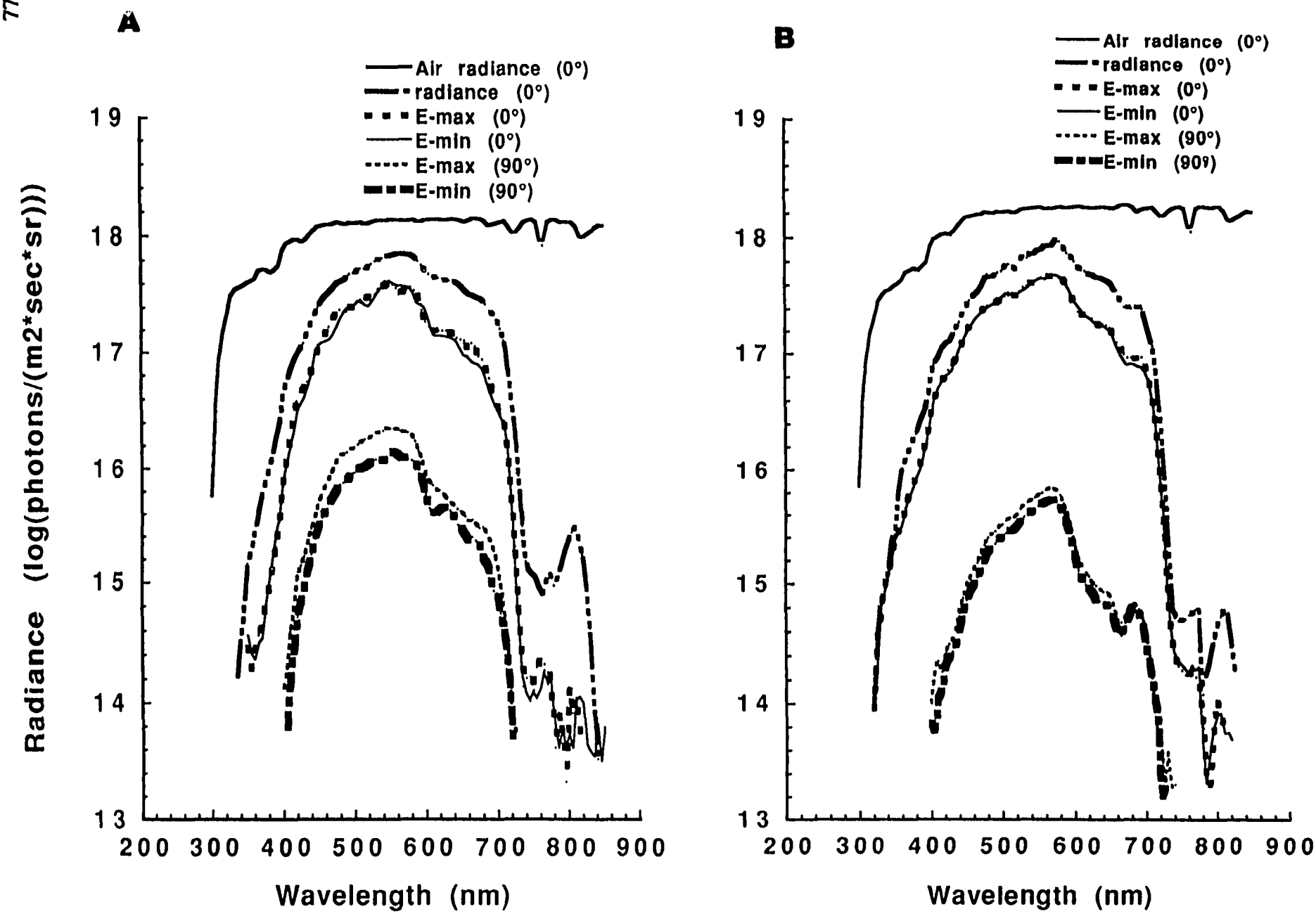
A
B
Air radiance (0°)
radiance (0°)
E-max (0°)
E-min (0°)
E-max (90°)
E-min (90°)
Radiance (log(photons/(m2*sec*sr)))
19
18
17
16
15
14
13
200 300 400 500 600 700 800 900
Wavelength (nm)

Figure 2.8 Spectral characteristics of the radiance and polarized light fields during dusk in **(A)** Lake Cowichan (sun just above the horizon) **(B)** Ogden Point Breakwater (sun just below the horizon, sunset at 21:02 hrs Pacific Standard Time). Scans were taken in the zenith direction. Percent Pol_{tot} are 74.2% (air), 65.4% (1 m), 63% (4 m), 52.3% (7 m) (Lake Cowichan), 72.7% (air), 67.2% (1 m), 65.4% (4 m) (Ogden Point Breakwater). Radiance is always the highest in air and diminishes with depth. E-max, E-min curves for a given depth have the same trace but E-max is always the highest. For clarity, one log unit was added to all air and 1 m scans in (A), and 0.5 log unit was added to the 4 m scans. In (B), 0.5 log unit was added to the air and 1 m scans.

Fig. 2.8

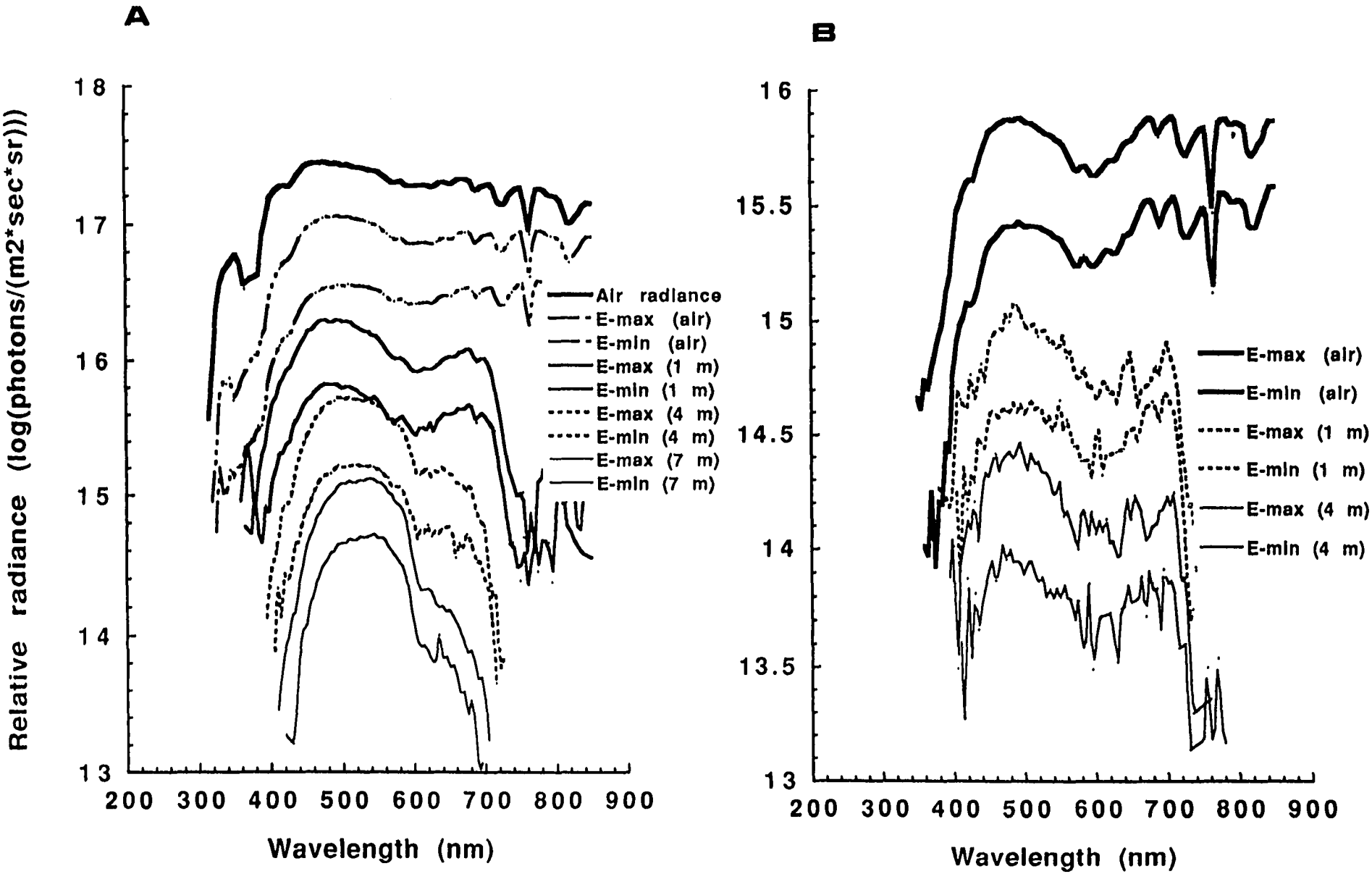
A
B
Relative radiance (log(photons/(m2*sec*sr)))
Wavelength (nm)
Air radiance
E-max (air)
E-min (air)
E-max (1 m)
E-min (1 m)
E-max (4 m)
E-min (4 m)
E-max (7 m)
E-min (7 m)
18
17
16
15
14
13
16
15.5
15
14.5
14
13.5
200 300 400 500 600 700 800 900

Figure 2.9 (A) Percent Pol_{tot} as a function of azimuth and zenith angle in Ogden Point Breakwater (4 m depth, J=43°32′). Arrows indicate approximate position of submarine neutral points (A=Arago, B=Brewster, Ba=Babinet, Cn= "close to Nadir"), **(B)** Percent Pol_{tot} in the plane perpendicular to the sun and as a function of azimuth in Lake Cowichan (J=56°33′).

Fig. 2.9

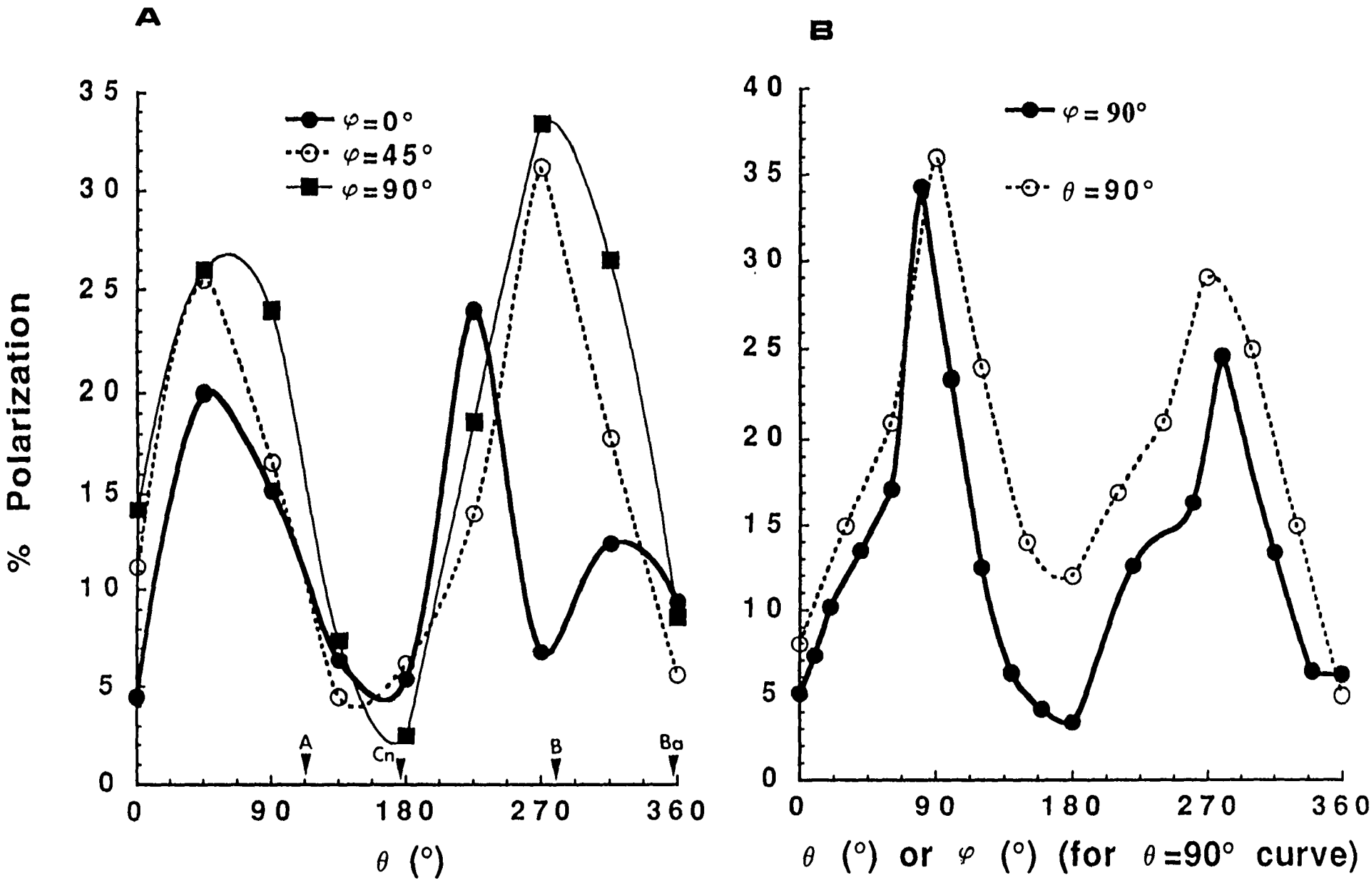

$\tan(\theta) = -\text{cotan}(r)/\cos(\varphi)$ (Appendix 1),

where r is the angle of refraction at the air-water interface. The slight disagreement between angles predicted by this formula and those observed in the field demonstrates that Rayleigh's formula is only an approximation (although a good one) of the scattering taking place in mesoeutrophic waters. Timofeeva (1974) derived the following empirical formula based on laboratory observations to predict the same polarization maxima: $\cos\theta(\max) = -\sin 98° * \sin J * \cos\varphi + \cos 98° * \cos J$, where J is the sun's elevation. More precise equations than those derived using Rayleigh's theory or empirical curve fittings would require the application of Mie's scattering theory to light impinging on an ensemble of particles possessing the range of geometries, sizes and indices of refraction representative of the waters studied (e.g. Zaneveld et al., 1974). Furthermore, the effect of anisotropy and multiple scattering would have to be accounted for (Plass et al., 1975; Marshall & Smith, 1990). Such analyses however are more complicated (Van de Hulst, 1957) and do not provide significant additional insight into distributions of light important for visual processes (Wehner, 1983).

As may be inferred by the dispersion and absorption coefficients of light, wavelengths that penetrate most through the media are also the least polarized (% polarization increases with increasing absorption and decreasing dispersion; Timofeeva, 1961). Accordingly, middle wavelength

light, which penetrates most in the waters examined, exhibits the lowest degree of polarization, while UV and short wavelengths show the highest percentages (Fig. 2.10). During the day the highest % polarizations could reach 35%, while during crepuscular periods these values were significantly higher (Fig. 2.8 legend). These increases during dawn and dusk and the spectral changes observed are primarily due to enhanced scattering but also to airglow phenomena. Indeed, the crepuscular (or twilight) sky is characterized by electronic transitions of atoms and molecules resulting in emission bands at various visible wavelengths (Craig, 1965). Oxygen atoms emit a dual "line" in the red part of the spectrum at 630 and 636.4 nm contributing to the observed "red" sunsets. However, the strongest emission bands are the product of N^{2+} transitions and occur in the UV-A (λ = 391.4 nm) and in the blue (λ = 427.8 nm) parts of the spectrum (Craig, 1965), which would contribute to the shifts towards shorter wavelengths during twilight. The observed increases in underwater polarization at these times likely result from sky polarization. However, changes in the water column (biotic and chemical) may also influence polarization levels by secondary scattering of sky polarized light.

Two peculiarities were observed in % polarization throughout the study period. The first occurred during measurements in directions near that of the sun's refracted rays and in the antisun direction. At these angles the diver

Figure 2.10 Percent Pol for different parts of the spectrum as a function of zenith angle (Lake Cowichan, J=64°24′, July 7th, 1993). Results are similar for Ogden Point Breakwater location.

Fig. 2.10

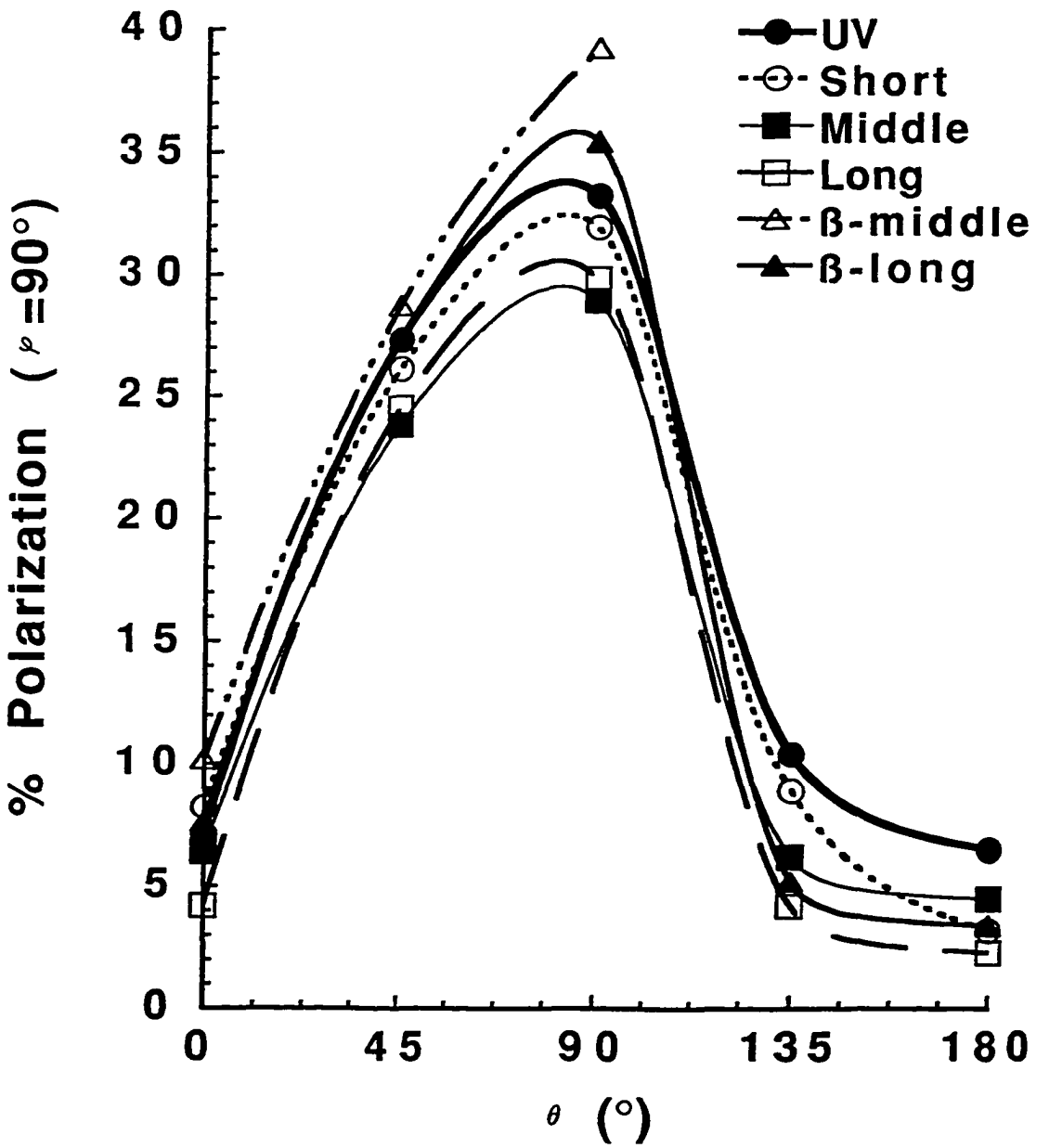
40
35
30
25
20
15
10
5
0
% Polarization (φ=90°)
0
45
90
135
180
θ (°)
UV
Short
Middle
Long
ß-middle
ß-long

could not detect a clear E-max. Results in these directions are therefore best approximations based on trends followed by nearby points. Previous studies have shown that the E-max vector in these directions can lie in any plane (even in the scattering plane, from which the term "negative zones of polarization" occurring between neutral points where % polarization is zero; Timofeeva, 1969, 1974). Secondly, a few measurements showed 25% polarization levels when scanning reflected light from the silty ocean/lake floor. Such levels of polarization have also been observed using dark sandy substrates in laboratory studies (Chen & Nagaraja Rao, 1968). The values increased further if turbidity was created by re-suspending the very fine particles that constituted the bottom.

The plane of maximum polarization (E-max) also varies with θ and φ (Fig. 2.11). Except for directions near the sun and antisun points, E-max can be approximated to be perpendicular to the plane comprising the direction of the incident light, the observer (spectroradiometer sensor) and the point of observation. In the case of crepuscular measurements (the sun being just below the horizon), the E-max angle Ψ (measured with respect to the horizontal, Fig. 2.1) is always close to 0° and % polarization is maximum at $\theta = 0°$. This follows from the fact that the incident light on the ocean is already partially polarized and that subsequent secondary polarization by Rayleigh-type particles in the ocean should not alter the

Figure 2.11 Angle of E-max as a function of azimuth and zenith angle. The E-max value for $\theta = 360°$ must in reality correspond to a zenith angle slightly smaller than 360° (Ψ at $\theta = 360°$ should be equal to Ψ at $\theta = 0°$).

Fig. 2.11

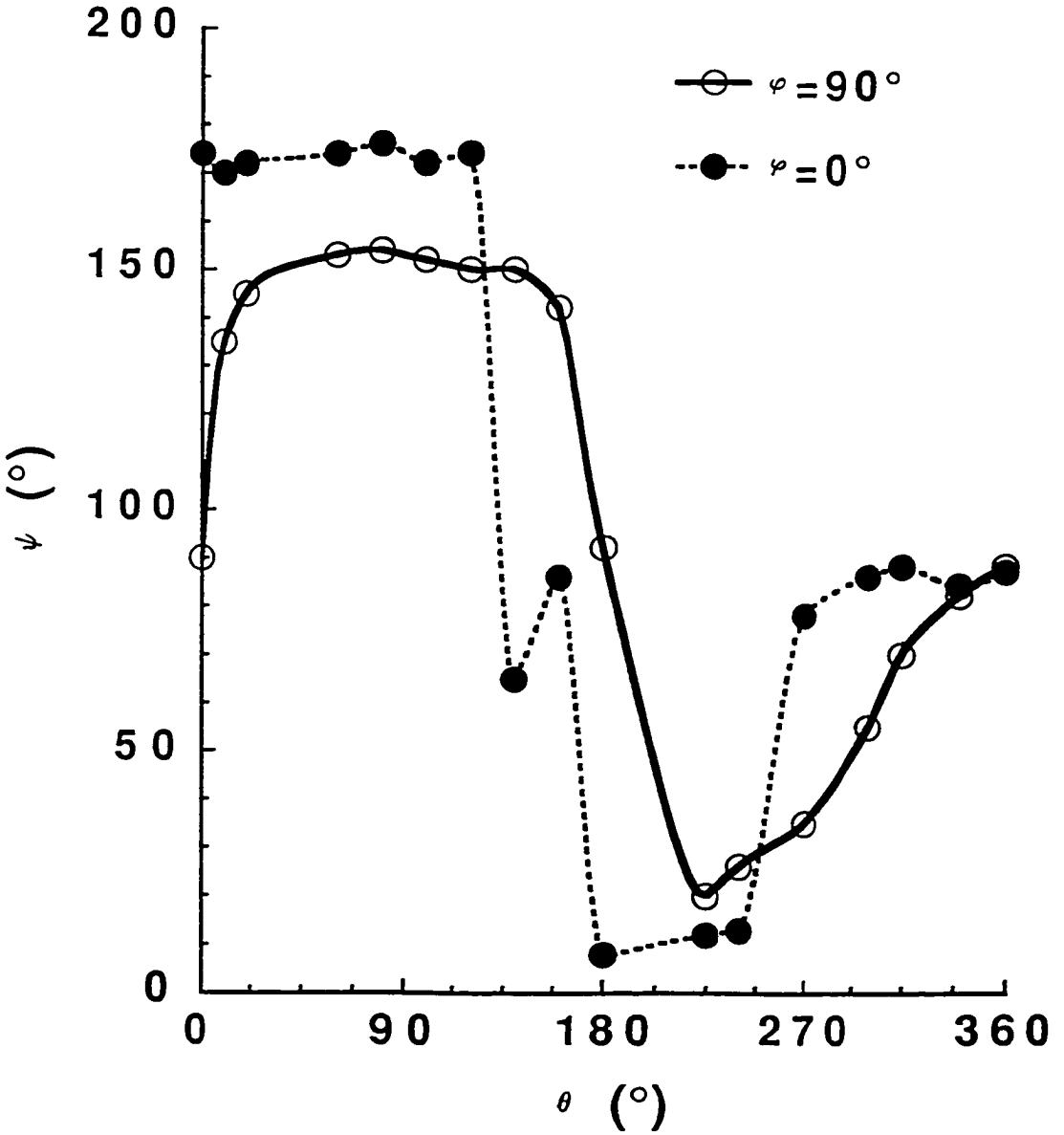

maximum E-vector direction (see scattering diagrams in chapter 1, Hecht & Zajac, 1974). It is worth noticing that by being able to detect these variations in Ψ, an observer is able to tell, regardless of the radiance distribution, the azimuth and elevation of the sun. An expression to predict Ψ from other angles in Figure 2.1 was given by Timofeeva (1969). Another way to predict the position of the sun would be to be sensitive to variations in spatial % polarization.

2.3.2 Changes in polarization with depth and overcast skies

Previous studies have shown that the degree of polarization decreases with depth, and reaches a constant maximum at θ = 90° when the radiance distribution no longer varies with direction of observation (Ivanoff & Waterman, 1958; Timofeeva, 1969). The depth at which this asymptotic radiance distribution occurs is a function of the optical properties of the medium (Timofeeva, 1969) and has been shown to vary from 40-50 m (Ivanoff & Waterman, 1958) to 200 m (Waterman, 1955) in very clear waters. My measurements by comparison were carried out at shallower depths; however they also show decreases in photon flux, and % polarization with depth in some directions (Fig. 2.12A, θ = 90°, see also Novales Flamarique & Hawryshyn, 1993). Percent polarizations vary slightly with maxima tending to be found at higher zenith angles with depth (Timofeeva, 1962). E-max distributions also vary as downwelling incident light gradually loses its

directionality (becoming more vertical) and multiple scattering increases (Fig. 2.12B). Perhaps the most important effect in terms of energy is the rapid attenuation of wavelengths below 400 nm and above 700 nm, and the presence of a peak in middle wavelengths as depth increases (Fig. 2.7; Novales Flamarique & Hawryshyn, 1993).

Although spectral irradiance measurements have indicated differences in intensity with direction of observation under slight cloud cover (Novales Flamarique & Hawryshyn, 1993), polarized light measurements near the surface under similar conditions show very small polarization levels (Fig. 2.13A). It would appear that the intensity of light that maintains its directionality through the cloud layer is insufficient to create high levels of polarization near the ocean surface. The traces of sun directionality still detectable under light cloud cover are lost under heavy overcast, but the distribution of polarized light still peaks near the horizontal (Fig. 2.13B). In this case multiple Mie-scattering by water droplets in the atmosphere could be diffusing the light reaching the ocean resulting in mostly vertical downwelling light at the water surface.

2.3.3 Visual responses of rainbow trout under natural light settings

Although the model fit was not always very accurate (possibly due to inaccuracy of the polynomial template,

Figure 2.12 (A) Percent Pol as a function of depth under cloudless skies in Lake Cowichan (J=56°44′). Reflected light from the lake's bottom may have caused the higher than expected % polarizations at higher zenith angles. **(B)** Angle of E-max as a function of depth for two zenith angles.

Fig. 2.12

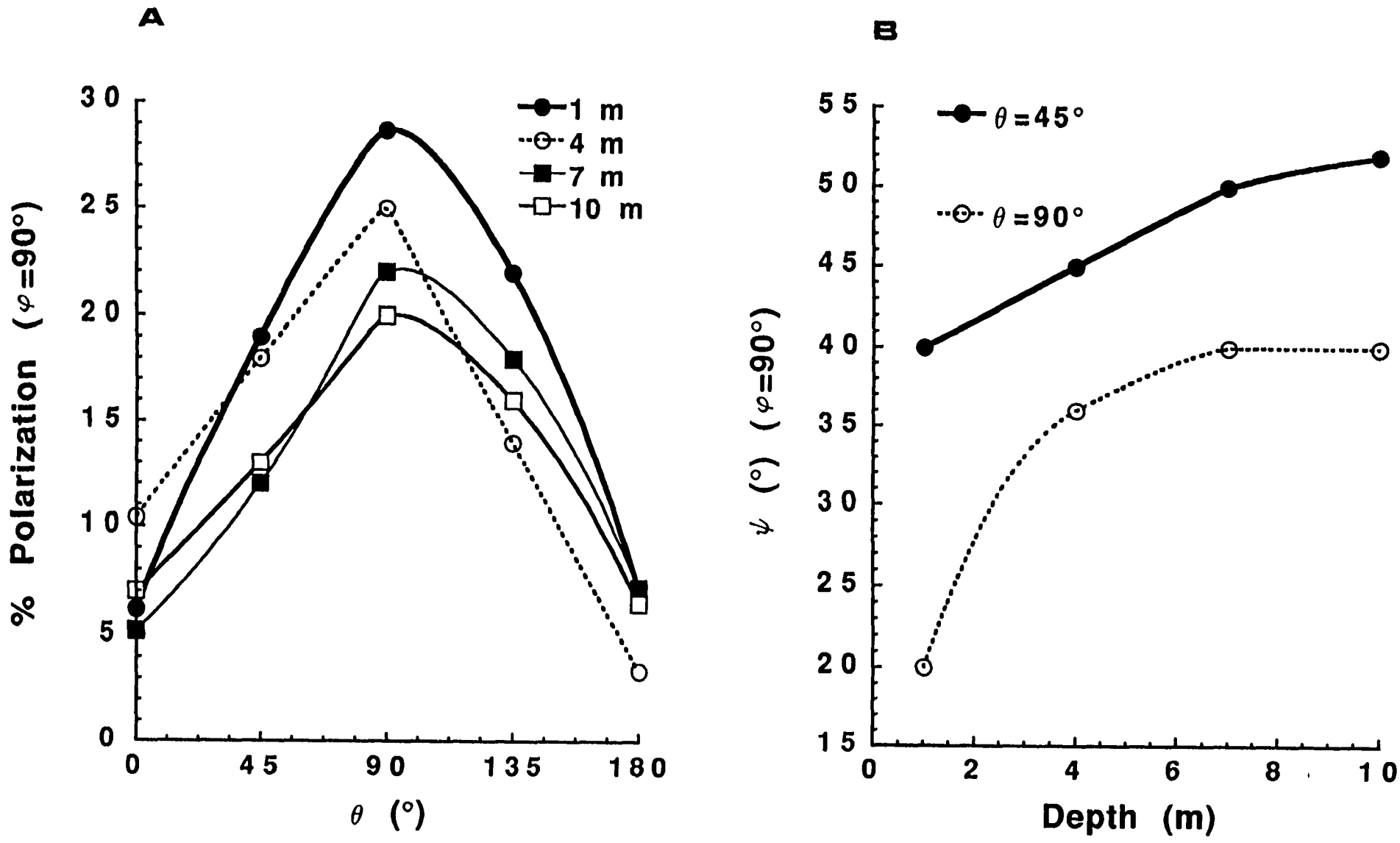
A
% Polarization (φ=90°)
θ (°)
1 m
4 m
7 m
10 m
0
5
10
15
20
25
30
0
45
90
135
180
B
ψ (°) (φ=90°)
Depth (m)
θ=45°
θ=90°
15
20
25
30
35
40
45
50
55
0
2
4
6
8
10

Figure 2.13 (A) Percent Pol under slight changing overcast (cirrus clouds) and **(B)** under heavy overcast (grey cumulus clouds), in Ogden Point Breakwater. Scans taken between 11:30-12:52 hrs, Pacific Local Time in May 1994.

Fig. 2.13

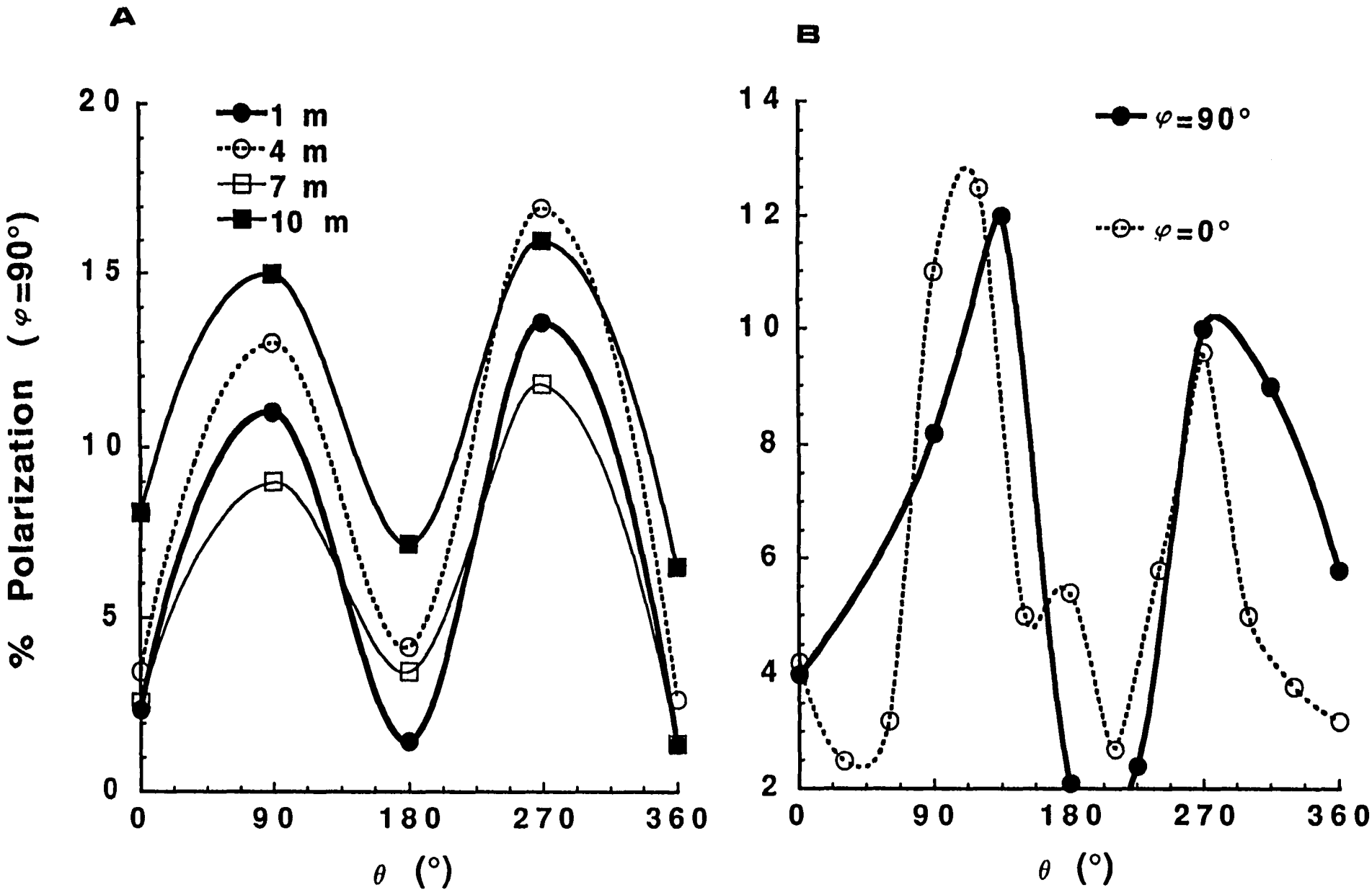
A
B
1 m
4 m
7 m
10 m
φ=90°
φ=0°
% Polarization (φ=90°)
θ (°)
θ (°)
0
5
10
15
20
2
4
6
8
10
12
14
0
90
180
270
360

especially in the β band absorbing regions), the fits show a progression of increased activation of the UV cone mechanism towards crepuscular periods for the ON response pathway (Fig. 2.14, Table 2.3). During bright light conditions (Fig. 2.14A), the ON response is dominated by the short and long wavelength mechanisms, with a prominent OFF response in the middle to long wavelengths. The OFF response is dominated by the middle wavelength mechanism under moderate light levels (Fig. 2.14B), but the ON-response is now a combination of all the cone mechanisms. In particular, the UV peak starts being noticeable and a middle wavelength mechanism is also present. As the levels of background light diminish towards the crepuscular condition, only the UV and long wavelength mechanisms are major components of the ON response (Fig. 2.14C). The OFF response is still dominated by middle wavelength mechanism input, but a smaller contribution now arises from the long wavelength mechanism.

Under crepuscular background conditions, rainbow trout exhibits a so called "W"-shaped polarization sensitivity function with local maxima at 0°, 90° and 180° using a 400 nm stimulus (Fig. 2.15A). When the middle wavelength mechanism is isolated, the response to polarized light changes to a one-peak maximum at 90° (Fig. 2.15A, see also Parkyn & Hawryshyn, 1993). If the fish is then tested for differences in the responses between the 0° and 90° E-vector conditions while varying the degree of incident polarized light, no significant

Figure 2.14 Compound Action Potential (CAP) responses from the optic nerve of rainbow trout with the animal adapted to different light intensity backgrounds: **(A)** midday, **(B)** evening, **(C)** crepuscular. Each data point was divided by the inverse of the values at λ-max and the data normalized to obtain the curves shown. The λ-max values (in nm) and associated radiance thresholds in log (cm^2*sec*sr/photons) are as follows: Midday-ON (600nm, -13.46), Midday-OFF (540, -13.8), Evening-ON (420, -12.81), Evening-OFF (540, -12.87), Crepuscular-ON (380, -12.4), Crepuscular-OFF (500, -13.52). See Table 3 for simplex parameters. N=4 for each curve, bars represent standard errors of the mean.

Fig. 2.14

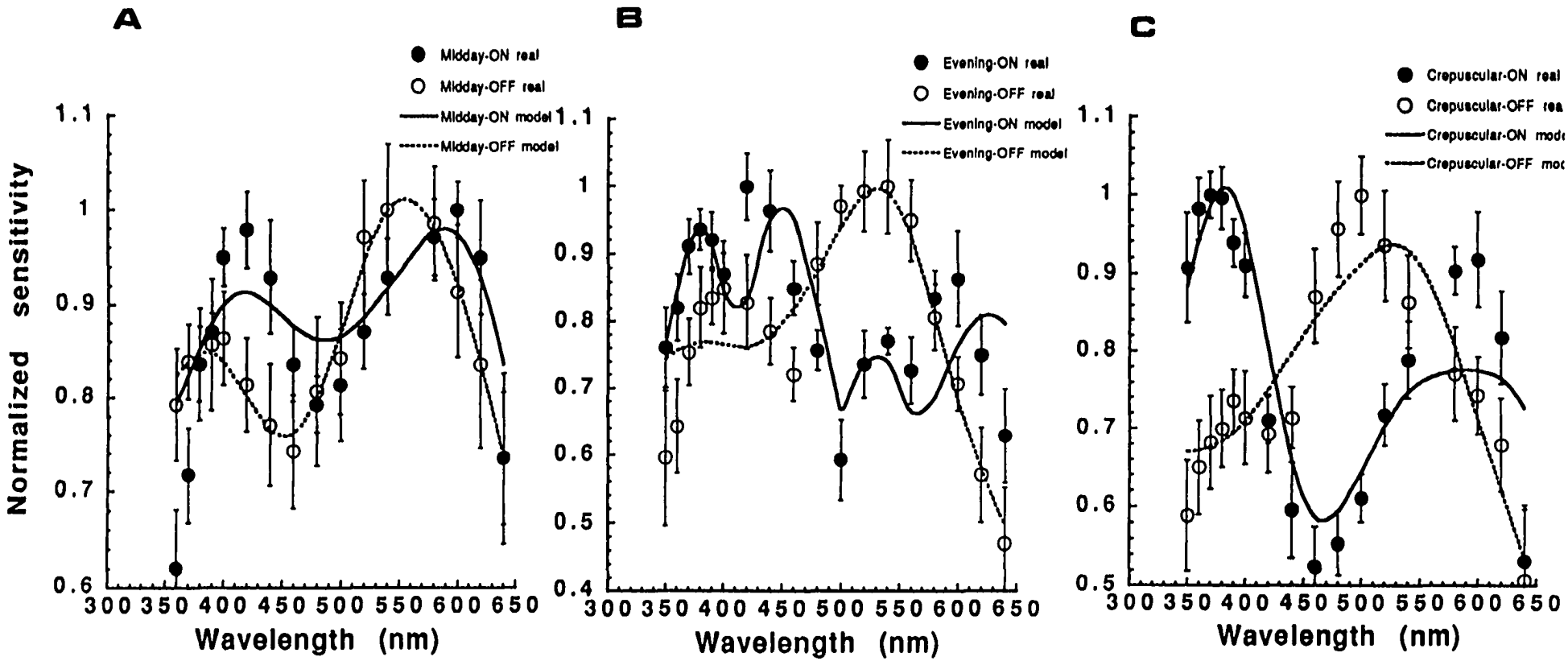
A
Midday-ON real
Midday-OFF real
Midday-ON model
Midday-OFF model
Normalized sensitivity
Wavelength (nm)
B
Evening-ON real
Evening-OFF real
Evening-ON model
Evening-OFF model
Wavelength (nm)
C
Crepuscular-ON real
Crepuscular-OFF rea
Crepuscular-ON mod
Crepuscular-OFF mo
Wavelength (nm)

Table 2.3 Simplex parameters for best fits to CAP recordings, SS: sum of squares from the best fit to the data.

Response	K(UV)	K(short)	K(middle)	K(long)	p	SS
MIdday-ON	0.002	0.161	0.118	0.844	0.187	0.064
Midday-OFF	0.147	0.008	0.547	0.657	0.814	0.004
Evening-ON	0.067	0.271	0.004	0.009	40.65	0.118
Evening-OFF	0.156	0.197	0.826	0.304	1.47	0.066
Crepuscular-ON	0.626	0.004	0.34	0.611	1.429	0.105
Crepuscular-OFF	0	0.243	0.638	0.457	1.103	0.044

Figure 2.15 (A) Polarization responses under crepuscular, and middle wavelength isolating backgrounds. The 0° E-vector angle (polarizer position) corresponds to light vibrating in the plane vertical to the long axis of the fish. One fish did not exhibit polarization sensitivity, perhaps due to the placement of the electrode (i.e. not all optic nerve fibres may carry polarization information). This fish was discarded from the analysis. **(B)** Difference response from the 90° and 0° polarizer positions under middle wavelength isolation conditions. N=4 for each curve, bars are standard errors of the mean.

100

Fig. 2.15

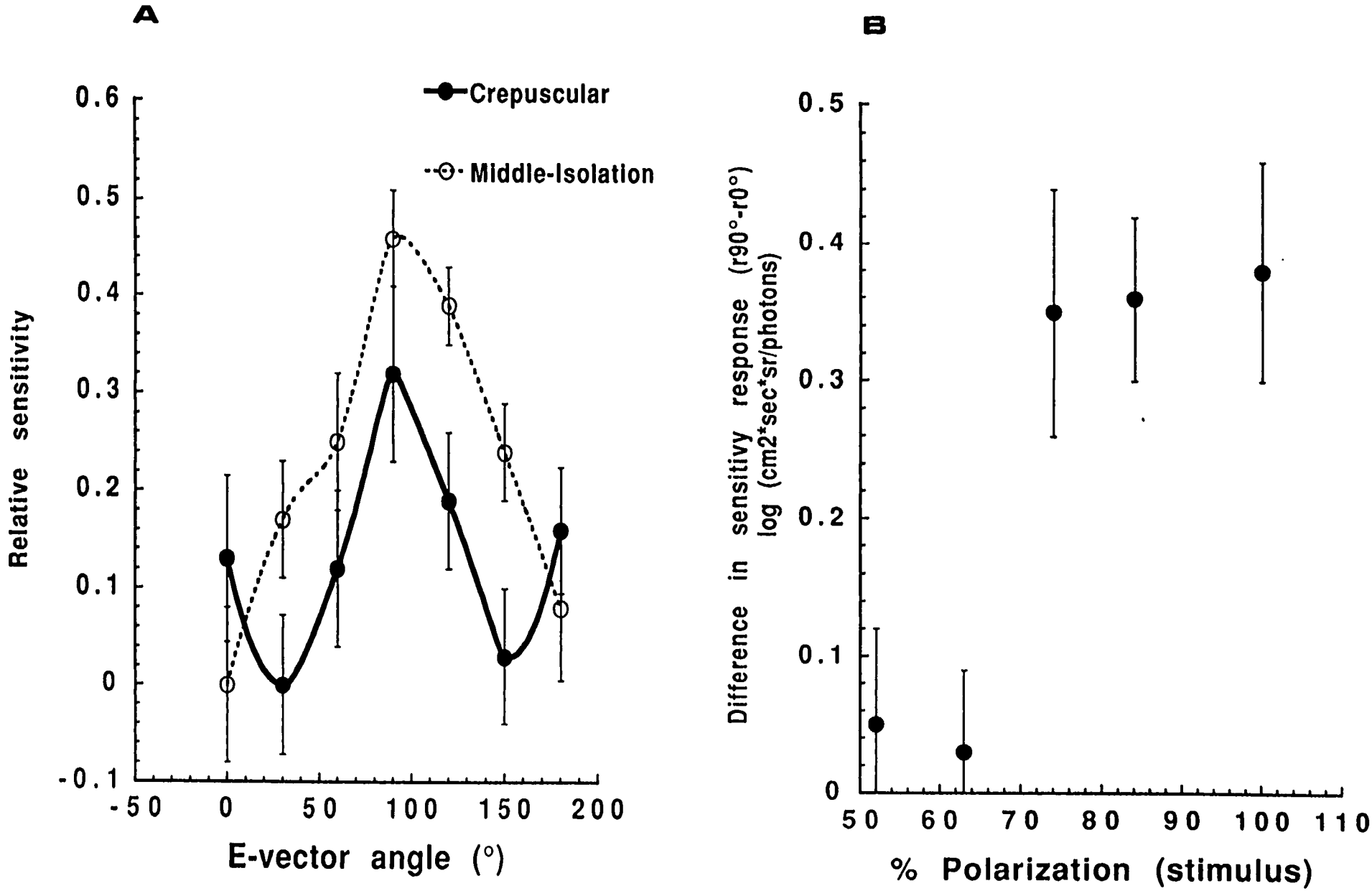
A
Crepuscular
Middle-Isolation
Relative sensitivity
0.6
0.5
0.4
0.3
0.2
0.1
0
-0.1
-50
0
50
100
150
200
E-vector angle (°)
B
Difference in sensitivy response (r90°-r0°)
log (cm2*sec*sr/photons)
0.5
0.4
0.3
0.2
0.1
0
50
60
70
80
90
100
110
% Polarization (stimulus)

difference is found below 72% (Fig. 2.15B). Polarization sensitivity is therefore lost somewhere between 63% and 72%.

2.3.4 Conclusion: Can underwater polarized-light mediated vision occur in nature?

To answer this question, we must go back to the polarized light measurements and search for time periods when the levels of radiance and % polarization are sufficient to stimulate fish polarization detectors. The measurements point towards crepuscular time periods and only near the water surface (<7m, Fig. 2.8). Only during these light conditions can the % polarization attain 67%, and the polarized light energy in the E-max plane be sufficient to stimulate the cone photoreceptors (many regressions showed the onset of the response to start between -14 and -15 $\log(m^2/(photons*sec*sr))$; Fig. 2.6B).

Although the method used to determine polarization perception thresholds was based on optic nerve recordings, other studies using different protocols also support our results. For instance, Heart Rate Associated (HRA) experiments which evaluate the response of the entire animal by monitoring changes in heart rate (Hawryshyn & McFarland, 1987; Cameron & Pugh, 1991) show maximum sensitivities around -13 log $(m^2/(sec*photons*sr))$(unpublished data). Such sensitivities are at most one log unit above those observed electrophysiologically. In terms of intensity, this would only change the threshold depth for polarized light perception by

a few meters in the waters studied. However, because the amount of polarization at 7 meters is below the threshold value for perception in terms of % polarized light (see Fig. 2.8), the conclusions reached here would be unaltered. Behavioral studies also support our results. Orientation experiments in tanks using rainbow trout suggest that the animal is unable to orient to the E-max of polarized light when the light is 65% polarized or less (Hawryshyn & Bolger, 1990). As well, orientation experiments with sockeye salmon performed at different times of the day in tanks with view of the sky show major orientation changes only at dusk. Only during this time period (as opposed to midday and afternoon), do the fish change their swimming orientation with respect to the position of a polarizer filter covering the tank (Groot, 1965). Observations during migratory periods (times when the fish could be using polarized light cues for orientation) show peaks in activity at dawn and dusk (Johnson & Groot, 1963). Furthermore, the fish are found near the surface during these time periods (Scarsbrook et al., 1978; Groot, 1965).

It is noteworthy that Horvàth and Varjú's (1995) model of the refraction-polarization pattern of skylight at the air-water interface also shows high % polarization values at crepuscular periods. There are two observations that explain this agreement: 1) polarization measurements during crepuscular periods are dominated by sky-created polarized light, and the maximum band of polarized light lies in the

zenith direction; 2) light levels are low during crepuscular periods (hence restricted to near the water surface) and the waves were relatively small during these measurements (~ 30-50 cm peak to trough amplitude).

The spectral sensitivity results suggest that polarization sensitivity may be achieved by the ON response of the UV and long wavelength mechanisms alone (Fig. 2.14C). These two mechanisms exhibit opposite polarization sensitivity in rainbow trout and goldfish (Hawryshyn & McFarland, 1987; Parkyn & Hawryshyn, 1993), and may give rise, through neuronal interactions, to the "W"-shaped curve under white light background conditions. Figure 2.14C also shows the importance of the middle and long wavelength mechanisms to the OFF response under crepuscular times. Interestingly, single unit recordings from the Torus semicircularis of rainbow trout report biphasic polarization units with ON responses in the UV part of the spectrum, and OFF in the long wavelength part, giving rise to a "W" function (Coughlin & Hawryshyn, 1995).

There is only one study, using the green sunfish, *Lepomis cyanellus*, that reports polarization sensitivity in the long wavelength part of the spectrum alone (Cameron & Pugh, 1991). Our light measurements show that the use of long wavelengths alone for polarization sensitivity is realistic, provided the green sunfish is at least as sensitive as rainbow trout (UV polarization levels are generally slightly higher than corresponding long wavelength ones). A biophysical

polarization sensitivity model for fishes possessing a UV cone and showing the characteristic photoreceptor opponent curves of rainbow trout is yet to be formulated. However, such a model will have to consider the input of UV cones to the polarization response, as behavioral experiments suggest that rainbow trout does not orient in experimental tanks without UV light in the stimulus (Hawryshyn & Bolger, 1990), and large trout (having lost most of the UV cones, Beaudet et al., 1993) also fail to orient (Hawryshyn & Bolger, 1990).

The conclusion that fish underwater polarization sensitivity should be possible only during crepuscular time periods may not be restricted to meso-eutrophic waters (waters with medium to high productivity, see Table 2.2). In blue oligotrophic waters, where smaller-radii particles would create higher Rayleigh-type scattering, maximum % light polarizations nearing only 60% (usually in the mid to low 50's though) have been reported for daylight hours (Ivanoff & Waterman, 1958; Waterman & Westell, 1956). Unless fish species living in such waters are more sensitive to polarized light than rainbow trout, the conclusion reached in this study should be general. Our polarization sensitivity experiments with open ocean and oligotrophic lake-dwelling temperate species (also living in clear water environments), support the conclusions in this study.

Although the hypotheses are hard to evaluate, it is interesting to speculate on the ecological advantages that

sensitivity to polarized light may confer animals in nature. For both terrestrial and aquatic invertebrates, it has been shown that natural polarized light cues can play an important role in orientation (Wehner, 1983; Goddard & Forward, 1991). Similarly, but under laboratory settings, rainbow trout can orient to the E-vector of polarized light (Hawryshyn et al., 1990; Hawryshyn & Bolger, 1990). There are nonetheless two problems that fish are faced with when using this sensory capability in nature: 1) their low sensitivity to percent polarized light (as compared to the invertebrates; Labhart, 1996), and, 2) atmospheric and water factors (e.g. clouds, waves) that readily disrupt any E-vector patterns by concentrating most of the light vertically. Given this combination of impediments, the potential use of E-vector patterns by fish to orient and navigate in nature is likely restricted to ideal crepuscular light conditions. A less complicated means to orient using polarized light would involve extracting information by responding to the most intense polarized light band alone. Anatomically, this would only require one photoreceptor type sensitive to polarized light coupled to a luminance detector. Observing the position and rotation of this band during clear crepuscular times could give the fish valuable position and time cues during migration. Such a behaviour would nevertheless require the fish to have prior knowledge of the zenith angle of this band at different times and locations in the lake/ocean. But this

could potentially be learned by the animal during its early life displacements.

Yet another possible use for polarization sensitivity in fish is contrast enhancement of underwater targets (Lythgoe & Hemmings, 1967; Tyo et al., 1996). In particular, the strongly polarized downwelling and sidewelling backgrounds during crepuscular periods may be disrupted by swimming zooplankton, which fish could then easily detect. Furthermore, even under open-ocean waves (which mainly enhance the size of Snell's window (Plass et al., 1975), and may focus the light in highly restricted bands (McFarland & Lowe, 1983)), this capability could remain useful.

One remaining possibility is the use of polarized light to recognize substrates, plants and/or other animals underwater. The source of polarization in this case would arise from reflection off targets, and this polarization need not be restricted to crepuscular periods provided the targets polarize light to levels above the fish's detection threshold. Object recognition by analysis of reflected polarized light has many engineering applications (Wolff, 1987, 1994b). For instance, the range of materials from dielectrics to perfect conductors can be classified with reflected polarization cues (Wolff, 1994b). Dielectrics usually exhibit radiance(E-max)/radiance(E-min)>3 for high polarizing angles, which translates into % polarizations > 50%. These high values suggest that surface recognition by fish of some underwater

dielectric-like targets (e.g. kelp blades, coral mixtures) may be possible through the analysis of reflected polarized light. Such a function could potentially be useful to select territories with optimal substrate composition for the animal's needs.

Whether fish use polarization sensitivity to enhance their foraging, for object recognition, for orientation and/or as a means of reflective communication still awaits discovery.

Appendix 1

Consider Figure 2.16 in which:

O: particle doing the scattering (the observer, or spectroradiometer sensor looks towards O along the line OP_{max})

S: a point in the refracted ray's direction of propagation, a source

P_{max}: target point, point in space being observed with highest polarization (according to Rayleigh approximation, angle ∠SOPmax = 90°)

Z: a point in the Zenith direction; on the normal to a flat surface and intercepting O; therefore ∠SZO and ∠OZP_{max} are right angles

Triangle SZP_{max} is in the xy plane (see Fig. 2)

φ: azimuth angle, ∠SZP_{max}

θ: zenith angle, ∠ZOP_{max}

r: refraction angle (corresponds to the zenith angle of the underwater source)

From this figure, we can write:

$$SP_{max}^2 = SZ^2 + ZP_{max}^2 - 2(SZ)(ZP_{max})\cos\varphi \quad (1)$$

$$OP_{max}^2 = ZP_{max}^2 + ZO^2 \quad (2)$$

$$SO^2 = ZO^2 + SZ^2 \quad (3)$$

$$SP_{max}^2 = SO^2 + OP_{max}^2 \quad (4)$$

$$ZP_{max} = (ZO)\tan\theta, \text{ and } SZ = (ZO)\tan(r) \quad (5)$$

Substituting, (2) and (3) into (4), and (4) and (5) into the left and right sides of (1) respectively, we obtain:

$$ZO^2 + SZ^2 + ZP_{max}^2 + ZO^2 = SZ^2 + ZP_{max}2 - 2(ZO)^2\tan\theta\tan(r)\cos\varphi,$$

$$\rightarrow 2ZO^2 = -2(ZO)^2\tan\theta\tan(r)\cos\varphi$$

$$\rightarrow \tan\theta = -1/((\tan(r))\cos\varphi) \rightarrow \mathbf{\tan\theta = -\cot an(r)/\cos\varphi}$$

Fig. 2.16

Figure for Appendix 1

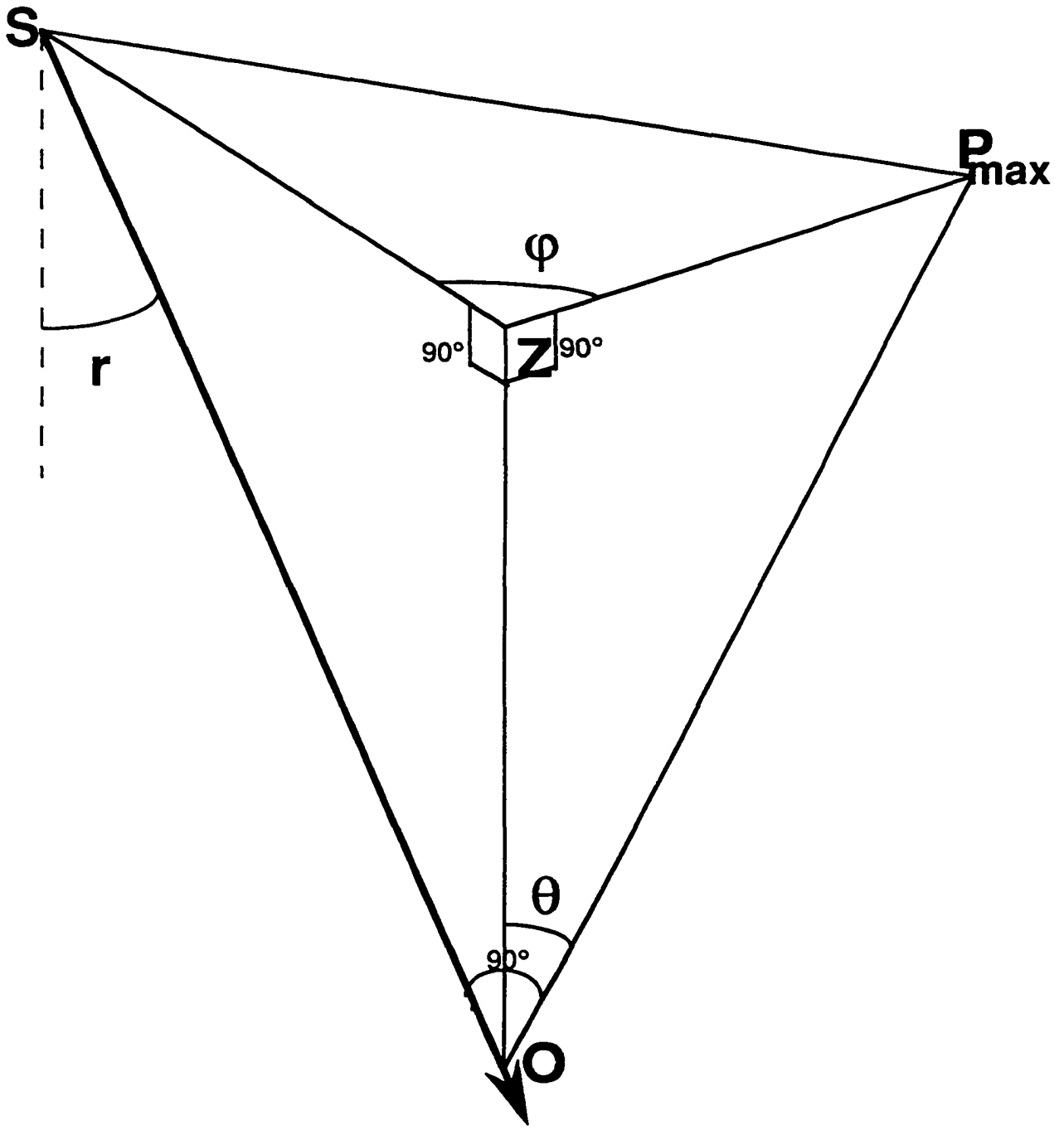

Chapter 3: Lack of polarization sensitivity in freshwater sunfish, a group of fishes with twin cone mosaics devoid of accessory UV cones.

3.1 Introduction

In contrast to the well-established microvillar dichroism mediating invertebrate sensitivity to polarized light (Goldsmith & Wehner, 1977; Labhart, 1980, 1988; Wehner, 1983; Nilsson et al., 1987), a general biophysical mechanism underlying polarization sensitivity among lower vertebrates has yet to be established. Sensitivity to the direction of the electric field of polarized light has been reported for a variety of fish species using electrophysiological and behavioral techniques (Groot, 1965; Dill, 1971; Hawryshyn & McFarland, 1987; Cameron & Pugh, 1991; Parkyn & Hawryshyn, 1993; Coughlin & Hawryshyn, 1995). Two major results have emerged from these studies. First, fishes with single ultraviolet-sensitive cones as well as with double cones (i.e. cone pairs with principal and accessory members maximally sensitive to middle (green) and long (red) wavelength radiation, Hárosi & MacNichol, 1974; Bowmaker & Kunz, 1987; Hawryshyn & Hárosi, 1994) exhibit opposite polarization sensitivity functions for these two cone receptor mechanisms (see Chapter 1; Hawryshyn & McFarland, 1987; Parkyn & Hawryshyn, 1993; Coughlin & Hawryshyn, 1995). When both cone mechanisms are active (i.e. under white light backgrounds of

moderate intensity), the total response can be a "W-shaped" function characterized by three local sensitivity maxima (Parkyn & Hawryshyn, 1993; Coughlin & Hawryshyn, 1995). Second, one study using the green sunfish (*Lepomis cyanellus*) has postulated a novel polarization detection system based on the action of a single cone mechanism with orthogonal channels, that of the "twin" cone (chapter 1; Cameron & Pugh, 1991). Unlike double cones, twin cones are morphologically identical and they usually possess the same visual pigment in both outer segments. The response to polarized light for wavelengths greater than 540 nm in this fish species has been reported to show 90° periodicity in sensitivity (Cameron & Pugh, 1991). This evidence has been used to formulate a mathematical model to explain vertebrate polarization sensitivity based on waveguide properties of paired cones in general (Rowe et al., 1994). However, this model cannot explain polarization sensitivity results from UV-sensitive fish species (e.g. salmonids and cyprinids).

The apparent discrepancies in polarization sensitivities between salmonids and cyprinids, on the one hand, and centrarchids, on the other, led me to investigate polarization sensitivity in the locally-available pumpkinseed sunfish (*Lepomis gibbosus*). Both pumpkinseed and green sunfish are morphologically similar, they exhibit identical retinal mosaics (personal observation), and they hybridize in nature giving rise to viable progeny (Scott & Crossman, 1973). The

goal of this study was to confirm the presence of two distinct neural polarization detection mechanisms present in fishes (Cameron & Pugh, 1991; Parkyn & Hawryshyn, 1993; Coughlin & Hawryshyn, 1995). However, the results obtained for pumpkinseed were found to be contradictory to those reported in the literature for the green sunfish (Cameron & Pugh, 1991). I then performed the same experiments on green sunfish only to obtain the same results as those from pumpkinseed.

3.2 Materials and Methods

Electrophysiological recordings from the optic nerve of sunfish were performed as previously described in chapter 2 for rainbow trout. Spectral sensitivity curves were obtained under two light backgrounds (white and long wavelength only), which isolated the long and middle cone mechanisms of sunfish respectively. Following the obtention of spectral sensitivity curves, polarization sensitivity curves were generated for specific wavelengths across the visual spectrum.

In the mathematical treatment of data, I used MSP-derived absorbance maxima from green sunfish to compute the absorbance polynomials according to Bernard's (1987) template. Absorbance maxima occur at 530 nm (single cone photopigment) and 621 nm (twin cone photopigment) in green sunfish (Dearry & Barlow, 1987).

3.3 Results

The spectral sensitivity responses of pumpkinseed and green sunfish were very similar (Fig. 3.1). Both species exhibited a predominant long wavelength cone mechanism under white light conditions (Figs. 3.1A,C), with a middle wavelength mechanism dominant under the long wavelength background (Figs. 3.1B,D). The ON and OFF responses followed similar trends; spectral sensitivity maxima occurred around 620 nm for the long wavelength mechanism, and around 530 nm for the middle wavelength mechanism.

Under the spectral backgrounds above, neither species of sunfish showed significant variation in the response to different E-vector orientations (Fig. 3.2; ANOVA model: raw sensitivity = E-vector angle, $P>0.05$). For any particular experiment, the mean modulation depth of the polarization sensitivity curve was less than 0.2 log units.

3.4 Discussion

In contrast to previous findings (Cameron & Pugh, 1991), neither of the two *Lepomis* species showed polarization sensitivity (Fig. 3.2). This surprising result led me to re-evaluate the equipment and methodology. I thus proceeded with three separate tests of the equipment and technique. First, I tested a parr rainbow trout using the same technique. Under white light conditions of moderate intensity, the spectral sensitivity ON response was dominated by the ultraviolet and

Figure 3.1 Spectral sensitivity curves from pumpkinseed under white light adaptation **(A)**, and long wavelength adaptation **(B)**, and from the green sunfish under white light adaptation **(C)** and long wavelength adaptation **(D)**. N=5 fish per species; average weights and total lengths were: 10.1 (±4.07) g and 8.67 (± 1.13) cm for pumpkinseed, and 28 (± 11.7) g and 12.07 (± 1.65) cm for green sunfish. Relative sensitivity values were calculated by normalizing all sensitivity values with respect to the smallest value for each of the ON and OFF responses independently, and inverting the result (Bernard, 1987; G.D. Bernard, personal communication); a value of one was then added to the normalized ON responses for clarity. Real values refer to the electrophysiological data, model values were generated by the Simplex algorithm as best approximations to the real data. The best fit parameters generated by Simplex were as follows: **(A)** ON response: K_m = 0.059, K_l = 1.061, p = 1.536, ss (sum of squares between real and predicted points) = 0.304; OFF response: K_m = 0.027, K_l = 0.937, p = 1.513, ss = 0.326, **(B)** ON response: K_m = 0.755, K_l = 0, p = 59.4, ss = 0.081; OFF response: K_m = 3.67, K_l = 0.002, p = 28.4, ss = 0.138, **(C)** ON response: K_m = 0.041, K_l = 0.844, p = 1.48, ss = 0.349; OFF response: K_m = 0.043, K_l = 0.821, p = 1.68, ss = 0.311, **(D)** ON response: K_m = 5.31, K_l = 0, p = 43.04, ss = 0.079; OFF response: K_m = 1.145, K_l = 0, p = 64.92, ss = 0.218. For purposes of computing the original sensitivities, we give the maximum sensitivity values

(smallest numerically) and the wavelength in nm at which they appear between parentheses for the various cone mechanisms: **(A)** Long-ON (620): -12.41; Long-OFF (620): -12.28; **(B)** Middle-ON (540): -12.56; Middle-OFF (540): -12.5; **(C)** Long-ON (620): -12.45; Long-OFF (620): -12.37; **(D)** Middle-ON (540): -12.61; Middle-OFF (540): -12.78. These values are in log (cm^2*sec/photons). No sensitivity was found below 390 nm probably as a result of lens transmission cut-off.

Fig. 3.1

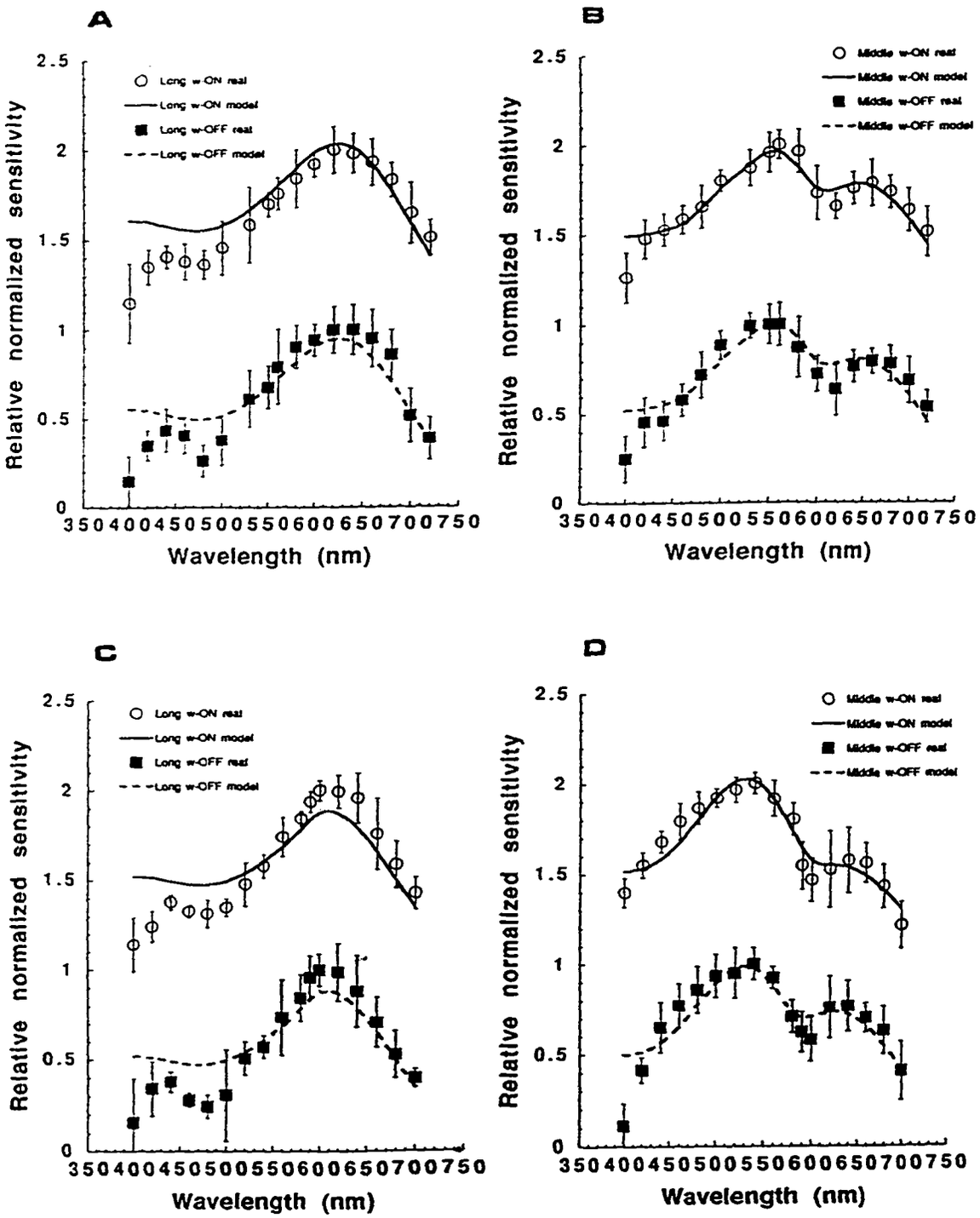
A
B
C
D
Relative normalized sensitivity
Wavelength (nm)
Long w-ON real
Long w-ON model
Long w-OFF real
Long w-OFF model
Middle w-ON real
Middle w-ON model
Middle w-OFF real
Middle w-OFF model
0
0.5
1
1.5
2
2.5
350 400 450 500 550 600 650 700 750

Figure 3.2 Polarization sensitivity responses from pumpkinseed under white light adaptation **(A)** and long wavelength adaptation **(B)**, and from green sunfish under white light adaptation **(C)** and long wavelength adaptation **(D)**. The curves were derived following the spectral sensitivity results presented in Figure 2 (n=5). In each graph, a value of 0.25 was added to subsequent relative curves for clarity. Bars are standard errors of the means.

Fig. 3.2

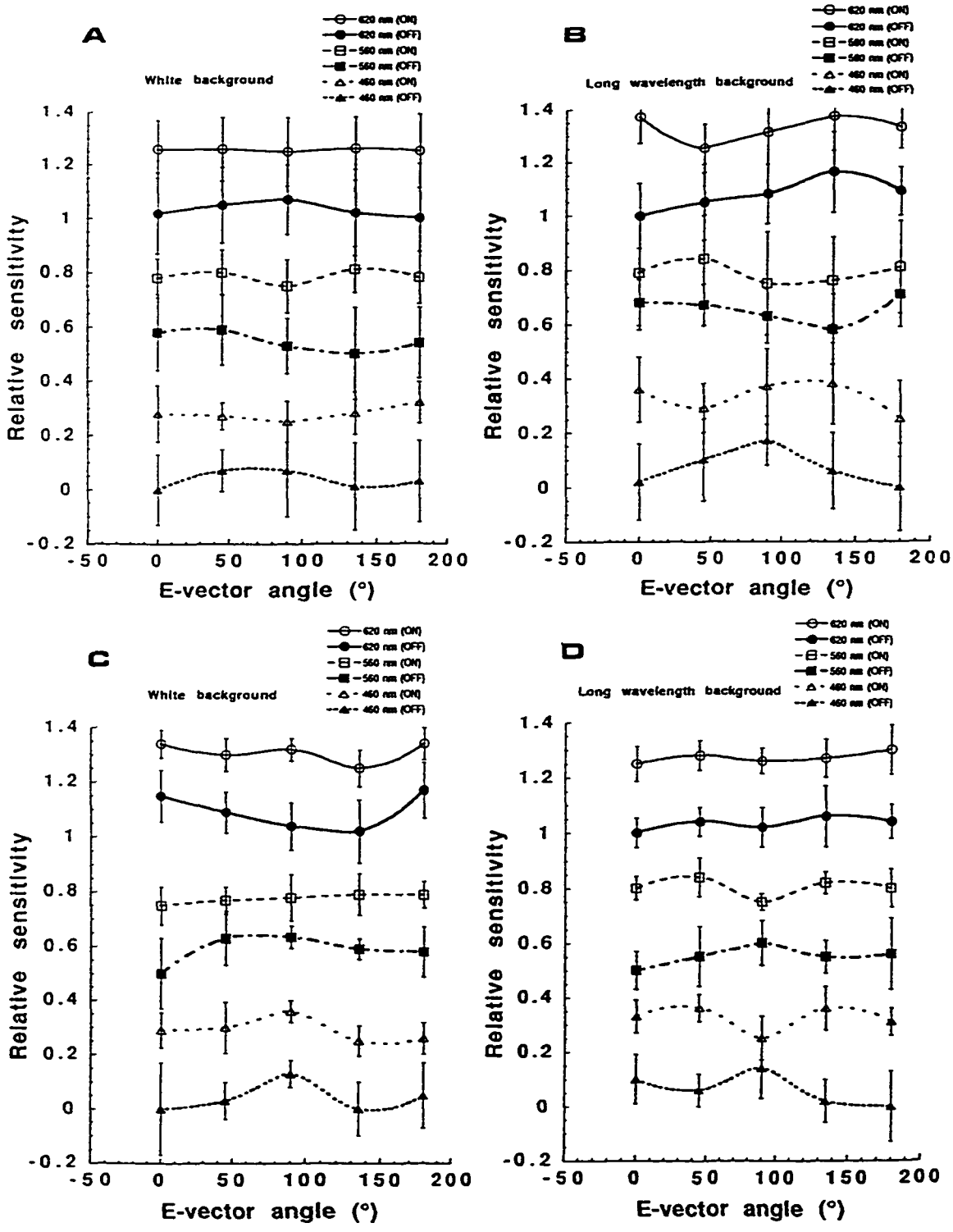
A
White background
620 nm (ON)
620 nm (OFF)
560 nm (ON)
560 nm (OFF)
460 nm (ON)
460 nm (OFF)
Relative sensitivity
E-vector angle (°)
B
Long wavelength background
C
White background
D
Long wavelength background

Figure 3.3 (A) Spectral sensitivity curve for a parr rainbow trout (5.1 g and 8.2 cm) under the previous dim white background. A Simplex model fit using published maximum absorbance values for the four cone mechanisms present in parr rainbow trout (UV, short (blue), middle (green) and long (red), Hawryshyn & Hárosi, 1994) gave the parameters: ON response: K_{uv} = 0.427, K_s = 0.018, K_m = 0.008, K_l = 0.894, p = 1.036 and ss = 0.137; OFF response: K_{uv} = 0.0002, K_s = 0.277, K_m = 0.643, K_l = 0.413, p = 1.27 and ss = 0.043. The maximum sensitivities (and the wavelengths at which they appeared) were: ON (600): -12.62; OFF (500): -13.19. **(B)** polarization sensitivity response for the ON component.

Fig. 3.3

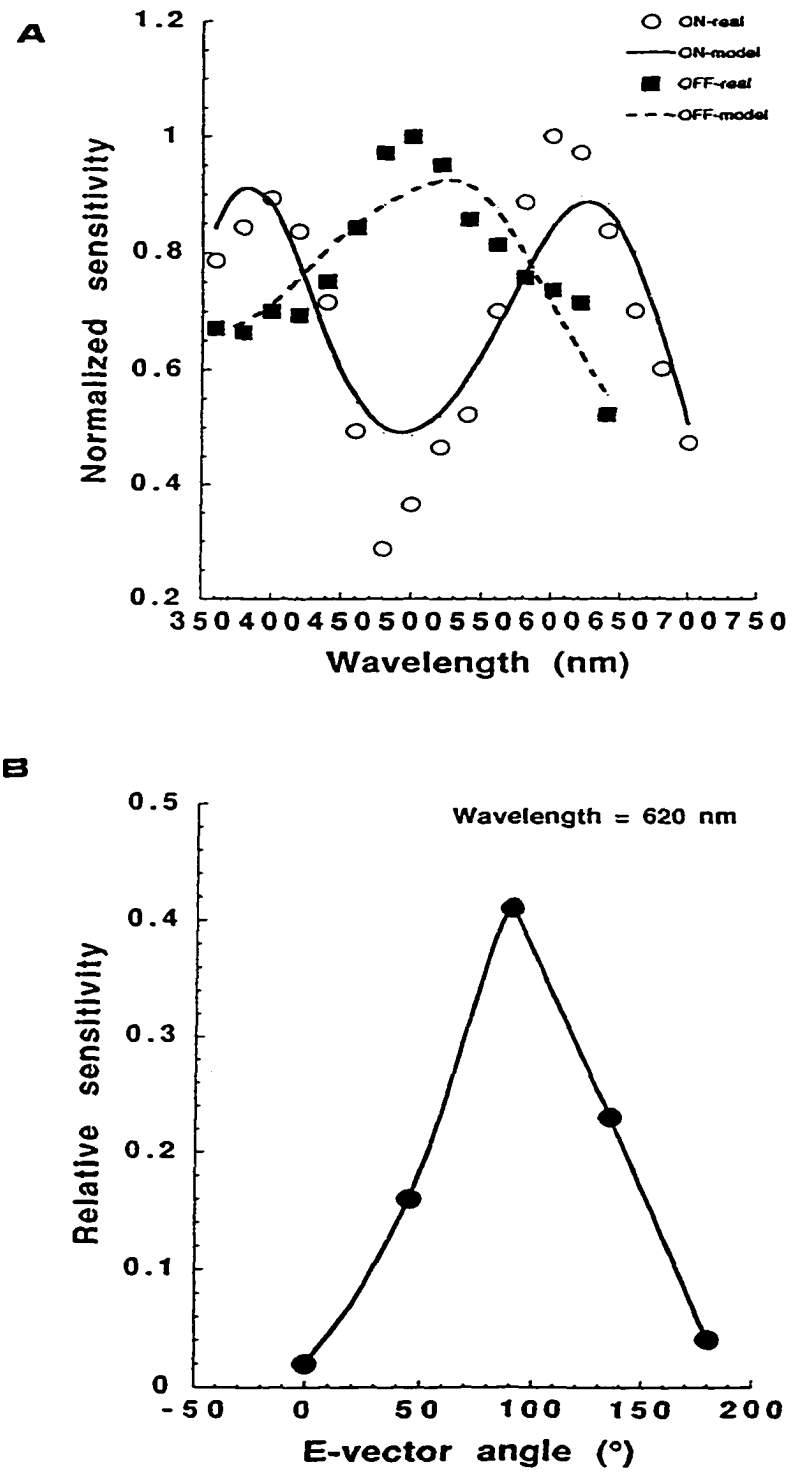
A
ON-real
ON-model
OFF-real
OFF-model
Normalized sensitivity
1.2
1
0.8
0.6
0.4
0.2
350 400 450 500 550 600 650 700 750
Wavelength (nm)
B
Wavelength = 620 nm
Relative sensitivity
0.5
0.4
0.3
0.2
0.1
0
-50 0 50 100 150 200
E-vector angle (°)

long wavelength cone mechanisms (Fig. 3.3A). The polarization sensitivity response for λ = 620 nm was 180° periodic as previously reported in the literature (Fig. 3.3B, Parkyn & Hawryshyn, 1993; Coughlin & Hawryshyn, 1995). Second, I inspected the polarizer and re-calibrated the entire electrophysiology system *de novo;* the results did not change. Third, I invited another investigator to carry out polarization sensitivity experiments using his own rainbow trout; following adaptation to a dim white background, a "W-shape" curve similar to that in the literature (Parkyn & Hawryshyn, 1993; Coughlin & Hawryshyn, 1995) was obtained with a 380 nm stimulus (D. Parkyn, personal communication).

It is worth noting that the electrophysiology procedure in this study was different from the classical conditioning technique used in the previous green sunfish study (Cameron & Pugh, 1991). It is conceivable that, if only a small population of optic nerve fibres carry polarization information, I may have failed to record from them with this technique. However, such a situation is unlikely for at least three reasons: 1) the same technique has been used to obtain polarization sensitivity in specimens from other species with a similar optic nerve projection to the brain (Parkyn & Hawryshyn, 1993; Coughlin & Hawryshyn, 1995; Novales Flamarique & Hawryshyn, 1996), 2) both techniques have been used to obtain similar spectral sensitivity results in previous studies (Browman & Hawryshyn, 1992; Beaudet et al.,

1993), and 3) the large diameter of the electrode used in this study would likely have intercepted most of the optic nerve fibres, especially in the case of the small pumpkinseed tested.

One may also argue that the polarization signal may have been swamped by a stronger (more numerous) input from non-polarization sensitive fibres, or that polarization sensitive fibres separate from the optic nerve bundle and project elsewhere before reaching the entrance to the brain in sunfishes. Once again, these ideas contrast with anatomical observations and our ability to show polarization sensitivity for specimens from other species using the present technique (Parkyn & Hawryshyn, 1993; Coughlin & Hawryshyn, 1995, Novales Flamarique & Hawryshyn, 1996). One possibility does exist, however, for amplification of minute signal differences at higher processing centres, like the optic tectum. Such differences, undetectable by the CAP technique at the level of the optic nerve, could be subtracted to form the basis of a polarization-detection system at the level of the brain. The technique of subtraction to increase the amplitude of the polarization signal has been long proposed for invertebrate visual systems (Wehner, 1983; Labhart, 1988), and lately applied to machine visual systems as a mechanism to improve target detection (Tyo et al., 1996; see Lythgoe & Hemmings, 1967 for original underwater observations). However, in fishes, to date, polarization responses observed in the brain

have also been detected at the level of the optic nerve (Parkyn & Hawryshyn, 1993; Coughlin & Hawryshyn, 1995), so it is doubtful that signal amplification to detectable levels would not be present in the optic nerve if the animal was indeed polarization-sensitive. I therefore conclude, based on the electrophysiological evidence obtained, that juveniles and young adults of these two species of sunfish are not sensitive to the direction of the electric field of polarized light.

Besides this apparent disagreement with the previous sunfish study (Cameron & Pugh, 1991), other results from that study also appear difficult to reconcile. For instance, in Cameron and Pugh (1991), a polarizer and a quarter wave retardation plate were used in series to test for fish responses to partially polarized light (partially polarized light in this set up is actually elliptically polarized light defined by the angle that the polarizer makes with the slow axis of the retardation plate, see birefringence discussion in chapter 1). Figure 4b of that study shows a progressively decreasing response as the horizontal component of polarized light is reduced from 100% to about 20%. Yet, if orthogonal ellipsoids are acting as waveguides and interacting linearly as postulated by the authors, one would expect a flat or single saddle point response. This would be so because one cone ellipsoid will transmit more light than the other as the horizontal component of light is reduced (and therefore the vertical enhanced!) while the intensity remains constant.

Hence, in order to be consistent with the polarization sensitivity results presented (Cameron & Pugh, 1991), the combined action of orthogonally-oriented twin cones in this experiment should have resulted in the absence of polarization sensitivity, or a single-peak sensitivity response to partially polarized light. As well, the neural circuitry proposed in a later study to reconcile corrected anatomical observations with operant conditioning results (Cameron & Easter, 1993) is also difficult to imagine. The reason being that neuron D in Figure 7 of Cameron and Easter (1993) is unknown. Neurons respond to the summed potentials from inhibitory and excitatory synapses; a neuron that takes the absolute value of the resultant potential (as postulated for neuron D) has yet to be discovered. I believe that a differential temporal integration of spikes from each input would have to take place at neuron D to obtain the postulated "absolute value" characteristic. But I have not heard from such a neuron to date.

The lack of polarization sensitivity in sunfish from optic nerve recordings suggests some difference, at the retinal level, between this group of fishes and the salmonids. From the work on invertebrates, two factors appear to be the major determinants for the presence/absence of polarization sensitivity. These are: 1) anisotropic structures within photoreceptors that render them polarization sensitive (Wehner, 1983; Nilsson et al., 1987), and 2) distribution of

photoreceptors in precise patterns exhibiting different polarization sensitivity maxima (Labhart, 1980; Wehner, 1983, see chapter 1). If we assume that polarization detection is a property of photoreceptors in vertebrates also, then two major differences are apparent between salmonids and goldfish, and sunfish. One is the presence of double cones in salmonids (Beaudet et al., 1993; Novales Flamarique & Hawryshyn, 1996) and goldfish (Stell & Hárosi, 1976) vs. twin cones in sunfish (Cameron & Easter, 1993), the other is the presence of multiple mosaic types (row to square) in salmonids and goldfish (Novales Flamarique & Hawryshyn, 1996; Stell & Hárosi, 1976) vs. the predominant square mosaic in sunfish (Cameron & Pugh, 1991; Cameron & Easter, 1993). It would thus appear that differences in the structure and arrangement of double cones vs. twin cones are responsible for polarization sensitivity in salmonids and cyprinids and lack thereof in freshwater sunfish. We will examine this possibility in the following chapter.

Chapter 4: Double cone internal reflection as a mechanism to detect polarized light in fish.

4.1. Introduction

Except for anchovies (Fineran & Nicol, 1976, 1978; see later chapter 6), vertebrate retinas have no apparent intrinsic or structural dichroism axially, with which to discriminate polarized from unpolarized light. This is so because rods and cones point with their axes of symmetry towards the centre of the pupil, and because the light-absorbing visual pigment molecules are confined to transverse lipid membranes where they undergo rapid rotational and translational diffusion (see chapter 1; Cone, 1972; Liebman & Entine, 1974). Thus, linearly polarized light entering the pupil should be equally effective in causing light stimulation irrespective of electric field orientation. Nonetheless, some fish species seem capable of discriminating polarized light (Hawryshyn & McFarland, 1987; Coughlin & Hawryshyn, 1995) and it is generally believed that their retinas must possess some subtle optical anisotropy and organizational asymmetry with respect to the direction of polarization of physiological light stimuli. In particular, paired cones, arranged in orderly mosaics in the retinas of teleost fishes (Engström, 1963), have been proposed to serve this purpose (Cameron & Pugh, 1991; Rowe et al., 1994).

Paired cones are composed of two photoreceptor cells that

are closely apposed along the length of their inner segment, sharing a wide and flat double membrane partition (chapter 1; Engström, 1963; van der Meer, 1992). If the two photoreceptor cells are identical in morphology and, usually, visual pigment content (Dearry & Barlow, 1987), the paired cone is termed a twin cone; however, if the two members are morphologically different (Stell & Hárosi, 1976; Bowmaker & Kunz, 1987; Hawryshyn & Hárosi, 1994; Stenkamp et al., 1996), the paired cone is a double cone. In cross section, the inner segments of paired cones appear as two semicircles squeezed together so that the overall contour approaches that of an ellipse (Engström, 1963; van der Meer, 1992). Given this geometry, it was proposed in a recent model that paired cones functioned as elliptical waveguides (Rowe et al., 1994). According to this hypothesis, the twin cones of the green sunfish could detect polarized light by virtue of differences in refractive index gradients along the major and minor axes of the elliptical cross-section. The main prediction of this model was a contrast or difference in light power transmission between fluxes of light polarized along the major and minor axes, with higher power transmission for light polarized along the major axis (Rowe et al., 1994).

To investigate the biophysical basis for polarization detection in fish with paired cones, I set out to look for optical manifestations of anisotropies observable by the use of polarized light. I thus carried out measurements of

birefringence and linear dichroism through end-on (axially oriented) cones of pumpkinseed sunfish (*Lepomis gibbosus*), green sunfish (*L. cyanellus*) and rainbow trout (*Oncorhynchus mykiss*) using two types of polarized light microscopes.

4.2. Materials and methods

4.2.1. Animals

Pumpkinseed were caught in ponds around Woods Hole (Mass., USA) while the green sunfish were obtained from a supplier in Texas. Parr rainbow trout were obtained from a local supplier near Woods Hole. The animals were acclimated in tanks for at least one week before use. The body mass and total length (average ± SD) of the animals used for optical measurements were: *L. gibbosus*: 71.56 (± 14.12g), 15.27 (± 0.87cm); *L. cyanellus*: 40.52 (± 2.52g), 13.64 (± 0.41cm); *O. mykiss*: 19.44 (± 5.02g), 12.35 (± 2.14cm).

All animal handling and experimentation followed protocols approved by the MBL veterinarian and/or the University of Victoria Animal Care Committee.

4.2.2. Optical measurements

Fish were dark-adapted overnight and decapitated under dim light conditions the next morning before use. Following eye removal, the retina was extracted, separated from the retinal pigment epithelium, and transferred into a container with Ringer solution (127mM NaCl, 4.8mM KCl, 1.2mM $MgSO_4 \cdot 7H_2O$, 1.5mM

$CaCl_2$, 3.3 mM $NaH_2PO_4 \cdot H_2O$, 3.7mM $NaHCO_3$, 5.6mM D-glucose, 20 mM HEPES, pH: 7.3). The retina was then cut into various pieces, and the centro-temporal ones selected for analysis. To remove rod outer segments, selected pieces were lightly shaken for 1-2 minutes. Then, some Ringer was removed to expose the upper part of the retina, and a piece of millipore filter paper (0.45μm pore size) was held over the retina so that its lower surface just made contact with the outer segments of photoreceptors. This piece was then raised gently away from the retina, effectively removing some cone outer segments. Only cones that were oriented axially, as judged by focusing up and down the length of the inner segment, were chosen for measurements. I determined axial birefringence and linear dichroism through cone inner segments with two laboratory-built instruments: the NPS and the D-AMSP.

The New Pol-Scope (NPS) (Oldenbourg & Mei, 1995) is an automated polarizing microscope that utilizes liquid crystal variable retarders and video image processing. Specimen illumination in the NPS is quasimonochromatic achieved by a narrow-band interference filter (10 nm FWHM centred at 546 nm). The Diode-Array Microspectrophotometer (D-AMSP) is built around a modified Axiovert 10 (Zeiss) microscope coupled to a spectrograph and an intensified diode-array detector system. This instrument uses a broad-band (Xenon) light source, rotatable prism polarizer (Glan-Thompson type), and a stationary linear polarizer as analyzer. Both instruments were

used in linear birefringence and dichroism determinations on similar retina preparations; results from the two instruments were in very close agreement.

The retina preparation was affixed onto a sliding, rotatable stage. Using a 0.45 NA condensor (which approximated physiological illumination; Charman & Tucker, 1973), the measuring light beam with rectangular cross section of dimensions 2.5-5 X 2.5-5 μm was focused at the centre of a cone ellipsoid. For a given cone (and fixed polarizer position), I rotated the specimen stage and collected the transmitted light through a glycerin immersion type objective (100/1.2 Ultrafluar, Zeiss) which was optically coupled to the spectrograph. Care was taken to contain the beam within the cone cross-section for all the cone orientations. Differences in transmission due to inherent irregularities of the optical elements were corrected for by subtraction of background recordings. To compare transmission of light fluxes for different cone orientations, I computed contrast as follows:

$$\text{Percent contrast} = 200(I_{min}-I_x)/(I_{min}+I_x),$$

where I_{min} was the flux transmitted when the polarization was parallel with the partition (0° orientation), and I_x was the flux for another direction of polarization: 45° or 90° with respect to the partition. In the case of birefringence measurements, the preparation was between crossed polarizers. The amount of light that traversed the analyzer was a function of sample birefringence (which is expressed as retardance

between light polarized along the fast and slow axis of the birefringent structure; see chapter 1, Inoué, 1989). To estimate cone birefringence, the light fluxes through cones were compared with those through known quartz standards. Similar determinations carried out with the NPS further indicated the orientation of the slow and fast optical axes for any position within the cones examined (Oldenbourg & Mei, 1995).

4.2.3. Histology

The eyes of 3 fish from each species were used for anatomical observations. After careful extraction of the lens and some eye fluid, each eyecup was immersed and left overnight in primary fixative (2.5% glutaraldehyde, 1% paraformaldehyde in 0.06 mol/l phosphate buffer, pH 7.2 at 4°C; Ali & Anctil, 1976). The retinas were then removed from the eyecups, and the centro-temporal area cut into various pieces. These were post-fixed in osmium tetroxide for one hour, dehydrated through an increasing series of percent ethanol solutions and embedded in Epon plastic (Ali & Anctil, 1976).

The embedded blocks were cut for light and electron microscopy. Transverse sections showed the structure of the mosaic, while radial sections revealed the morphology of photoreceptors along their lengths.

4.3 Results and Discussion

4.3.1 Paired cones exhibit small birefringence

I found with both instruments that paired cone inner segments have less than 2 nm axial retardance (Figs. 4.1A,B). Significant birefringence occurs only along partitions and cell contours; elsewhere, the optical cross section do not show any systematic anisotropy pattern (Fig. 4.1B). When using the formula: retardance = $(n_e-n_o)d$, where d is the pathlength of light through the birefringent structure, and n_e and n_o are the refractive indices for the extraordinary and the ordinary rays, respectively, the limiting value of 2 nm retardance gives $(n_e-n_o)=2nm/d$ [Note: the principal indices for a positive uniaxial crystal, such as quartz, would be larger for n_e (slow axis), smaller for n_o (fast axis) and would yield a positive retardance]. If the positive retardance is interpreted in terms of inner segment length, say 20μm, $(n_e-n_o)=2nm/20\mu m=0.0001$, which is a very small value. However, if interpreted in terms of cell membrane properties, the following may be suggested. Artificial lecithin films have been investigated for their optical properties (Cherry & Chapman, 1969) [Note: lecithin, or phosphotydilcholine, is one of the most abundant phospholipids in higher plants and animals, and it is a major component of most animal cell membranes; Lehninger, 1975]. Lecithin films were found to behave as positive uniaxial crystals with the slow axis perpendicular to the film's surface, with $n_e=1.486$, and the fast axis parallel to the

FIGS. 4.1A,B. (A) Retardance counts for a twin cone at various cone orientations using the D-AMSP; top trace was obtained with a 2 nm quartz standard. **(B)** NPS birefringence image of green sunfish twin cone mosaic (similar images were obtained with pumpkinseed). The arrow indicates the slow axis of propagation at the twin cone partition; retardance scale goes from 0 nm (black) to 2 nm (white).

Fig. 4.1

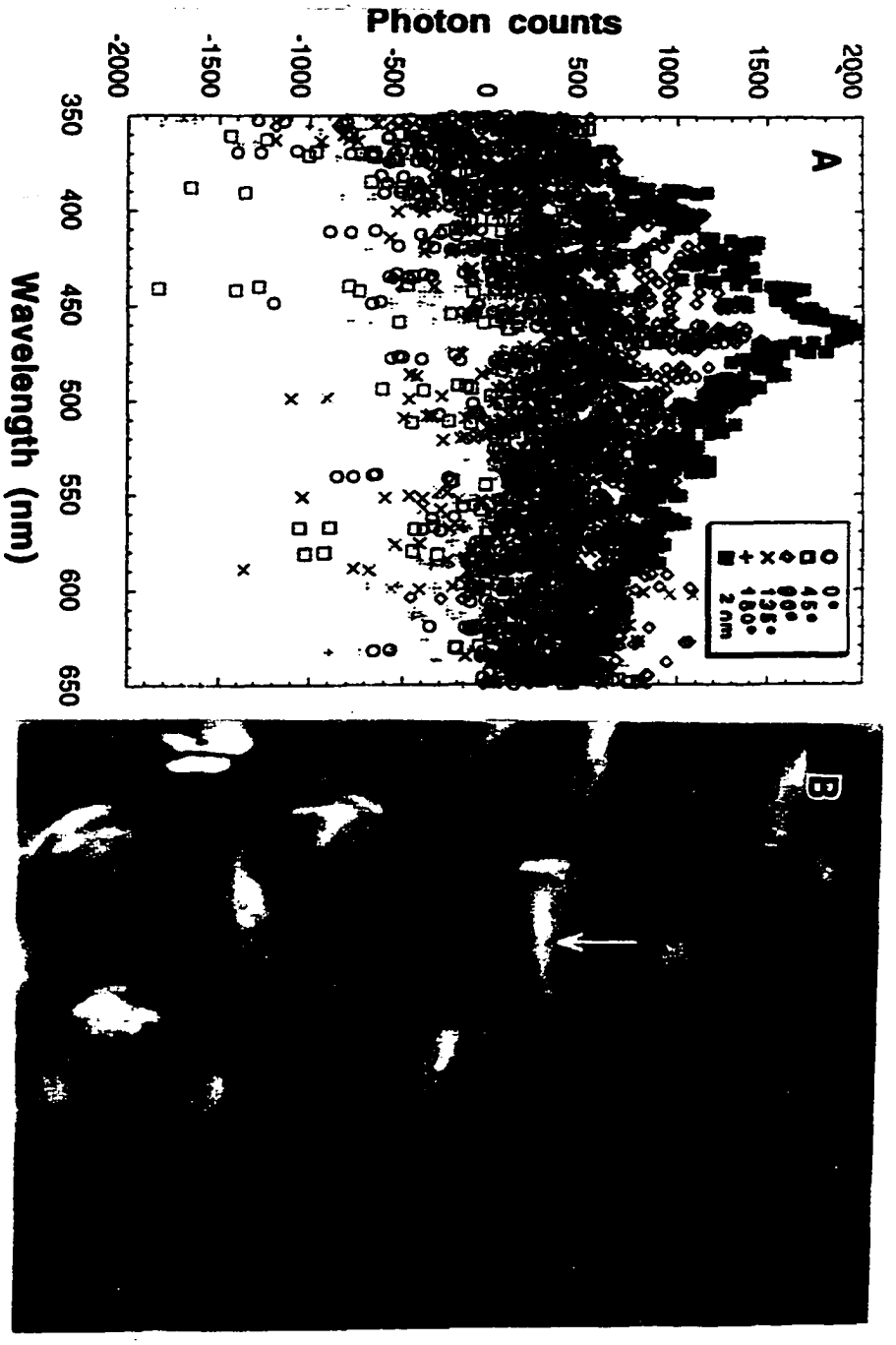
Photon counts
-2000
-1500
-1000
-500
0
500
1000
1500
2000
Wavelength (nm)
350
400
450
500
550
600
650
A
0°
45°
90°
135°
180°
2 nm
B

surface, with n_o=1.464 (Cherry & Chapman, 1969). By using the above formula and the 2 nm retardance, the effective pathlength can be calculated to be d=2nm/0.022=91nm. Therefore, if paired cone partitions behaved like lecithin films, a pathlength of less than 0.1μm would yield a retardance of 2 nm. By further assuming the average angle of incidence to be the median at 14° (the median angle is the inclination of the median ray in a homogeneous cone of rays for the case: NA=0.45 and medium refractive index of 1.334), the geometry with the foregoing figures would yield 22 nm for partition thickness. I consider this to be a realistic estimate of the actual value.

Although these birefringence measurements do not rule out graded refractive index variations within cone ellipsoids, they indicate the absence of internal discontinuities other than the birefringence at the dividing partitions, which appear ascribable to phospholipid-based membranes. As the most prominent optical feature in paired cone ellipsoids, dividing partitions cannot be ignored for mathematical convenience without running the risk of drastically altering the problem at hand. In my view, the negligence of the partition in the paired cone description is a major flaw of the elliptical waveguide hypothesis (Rowe et al., 1994).

4.3.2 Paired cone inner segments show axial dichroism

The axial transmittances of paired cone inner segments are

anisotropic, i.e. light polarized parallel to a dividing partition is transferred more effectively than light with perpendicular polarization (Table 4.1). Irrespective of type, single cones' ellipsoids are isotropic.

Based on these results and the birefringence findings reported above, I propose the ellipsoid partitions of paired cones to be the crucial elements in providing axial anisotropy in the fish retina. I further hypothesize these partitions to act as partial dielectric mirrors upon which reflection, refraction and scattering occur in a polarization-dependent manner, transducing incident polarization into a pattern of intensity variation across the cones's outer segments. Although the resulting modulation is only a few percent "contrast" (see Table 4.1), it can constitute a biophysical basis for the detection of polarization.

4.3.3 Anatomical features are consistent with the presence of reflecting partitions

Histological preparations from the retina of trout and sunfish show paired cone partitions in orientation and distribution that appear to form orthogonal sets of reflectors (Fig. 4.2, 4.3). These partitions also stain darker than the surrounding lumen suggesting higher lipid and protein content and therefore a larger refractive index (Sidman, 1957; Barer & Joseph, 1954). Given their greater refractive index and planar morphology (Berger, 1967), the partitions have the

Table 4.1. Percent contrast (± SD), calculated from transmitted polarized light fluxes averaged over the various spectral intervals shown; variables were: species of fish, cone type [numbers in brackets] and cone orientation angle (measured with respect to the direction of polarization of the incident beam at 0°). The wavelength intervals were chosen to encompass the peaks in maximum absorbance for the various cone types in the three species (Dearry & Barlow, 1987; Hawryshyn & Hárosi, 1994). The *L. cyanellus* data is the result of experiments in which green sunfish cones were immersed in a 50% Ringer-glycerol solution, a mixture that approximated the average refractive index of cone ellipsoids (1.39; Sidman, 1957). Average total % contrasts (390-620nm interval) for paired cones varied between 1.66 and 2.22, while those for single cones fluctuated around zero. Percent contrast averages for twin cones were in between those for single and double cones, and the large standard deviations associated with these averages may suggest mounting artifacts (such as overall tilt) in addition to polarization-dependent scattering. Rainbow trout double cones, however, gave positive contrasts consistently, a result which is likely due to anisotropic reflection and scattering from the inner segment partition.

Species	cone type	Angle(°)	390-430	480-520	580-620	390-620
L.gibbosus	twin[10]	45	1.43(1.6)	1.77(1.58)	1.91(2.41)	1.82(2.04)
		90	1.74(2.81)	1.51(2.56)	1.95(2.32)	1.66(2.29)
	single[3]	90	-0.08(0.54)	0.38(0.39)	-0.1(0.62)	-0.002(0.19)
L.cyanellus	twin[6]	90	1.75(2.72)	1.77(2.35)	1.99(2.58)	1.80(1.91)
	single[3]	90	0.12(1.21)	-0.06(0.69)	-0.17(1.22)	0.044(0.62)
O.mykiss	double[5]	90	1.31(0.86)	2.58(0.98)	2.52(0.92)	2.22(0.82)
	[1]	135	1.065	1.388	1.179	1.331
	single(S)[5]	90	0.084(0.54)	-0.27(0.71)	0.13(1.01)	-0.079(0.4)
	single(UV)[5]	90	0.11(0.73)	-0.4(0.58)	-0.41(0.58)	-0.21(0.39)

Figures 4.2A-D Photoreceptor micrographs from the centro-temporal retina of light-adapted parr rainbow trout (weight: 12.2g, total length: 11.1cm) near the optic nerve. **(A)** transverse section of retinal mosaic in which double cone (DC) inner segments and their partitions (arrowhead) were cut perpendicular to their long dimensions; the partitions, which show up here as two orthogonal sets of lines, lie approximately parallel to the vertical and horizontal planes in the fish eye in this region of the retina. Centre cones (CC) are located at partition intersections and define the centres of the unit mosaic. Accessory corner cones (ACs) form the corners of the mosaic and face the DC partitions. **(B)** Closer to the retinal pigment epithelium, the row mosaic in Figure 4.2A turns into a square mosaic with DCs defining the sides of the unit square. This alteration is accompanied by a change in the shape of the DC and a tilt in the partition (up to 30° from the normal to the outer segment), but the partition does not rotate significantly. The partition also becomes concave at this level. **(C)** Tangential-oblique section at the nuclear level showing differential staining of DC nuclei, the pattern for which alternates around the unit square mosaic. **(D)** Radial section showing partition tilt at the ellipsoid level of DCs. This tilt is accompanied by bigger mitochondria that commonly stain darker (see also (A)) in one of the DC members, as compared to the smaller mitochondria in the other member. DCs outer segments (*) also stain

differently for each member, further attesting to their unequalness (Bowmaker & Kunz, 1987; Hawryshyn & Hárosi, 1994). Adjacent to the DCs, the outer segments of ACs expand the lengths of neighbouring ellipsoids. The two white dotted lines indicate the approximate levels for the tangential cuts in (A) (shorter inter-spaced line) and (B) (longer inter-spaced line). In Figures (A)-(D), the large arrowhead points to the partition membrane; magnification bars are as follows: (A) 7.2 μm, (B) 4 μm, (C) 2.95 μm, (D) 5.6 μm.

Fig. 4.2

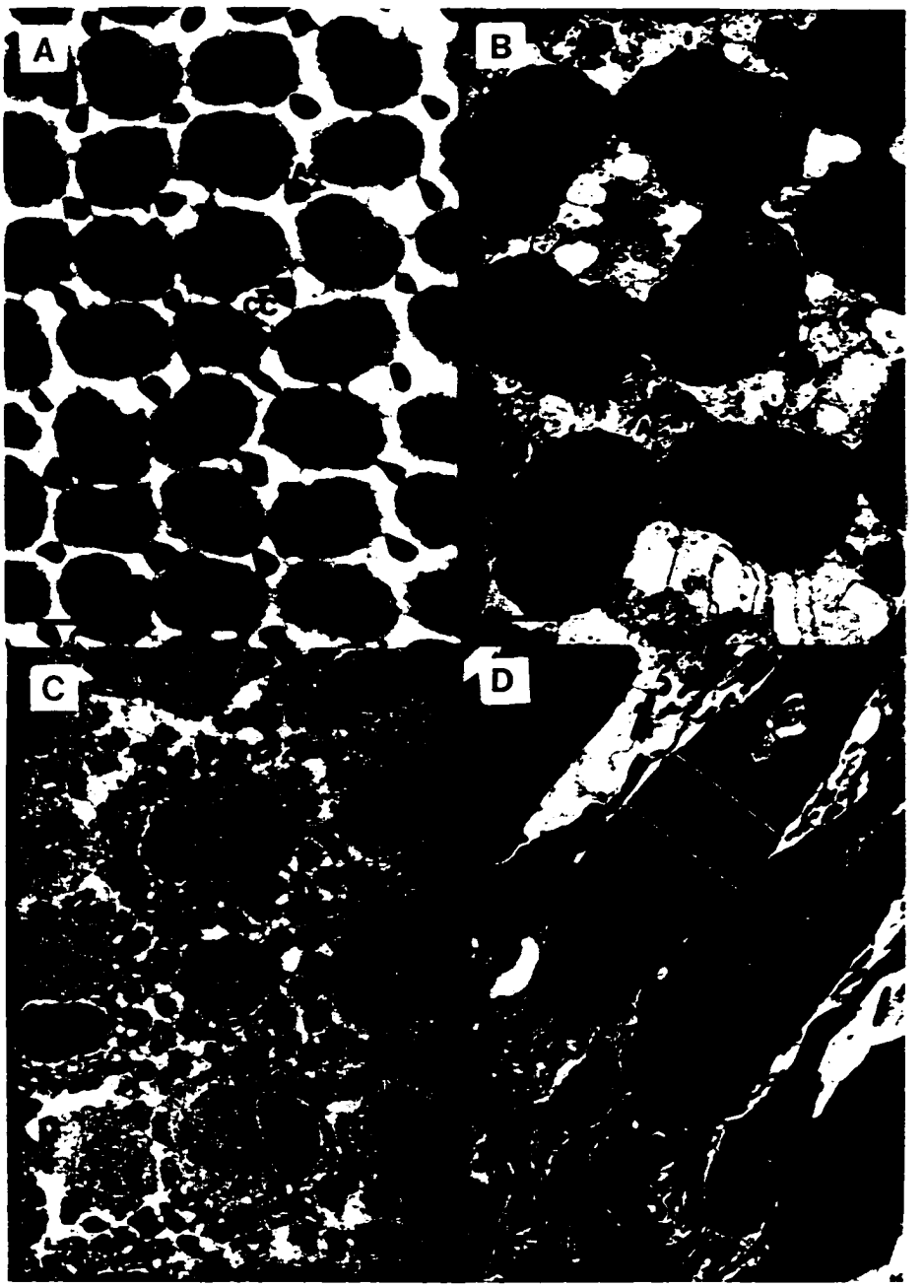

Figures 4.3 A-D Morphology of the centro-temporal retina in young pumpkinseed (weight: 9.8g, total length: 8.5cm). **(A)** Transverse section showing twin cones (TCs) surrounding centre cones (CCs) in the mosaic. TCs are oriented approximately 45° and 135° with respect to the vertical in situ (Cameron & Easter, 1993). **(B)** Tangential electron micrograph near the outer segment suggesting higher mitochondrial packing within a ring approximately 1.5 μm in radius centred at the intersection between major and minor axes of the ellipsoid. This distribution resembles that of CCs which are round and exhibit a similar ring of centrally packed mitochondria. **(C)** Radial section through the photoreceptor layer showing a nearly straight partition separating TC members; stars (*) label the identical outer segments. **(D)** Higher magnification of the TC labelled in (C) showing a nearly straight partition near the outer segments. The white dotted line in (C) and (D) indicates the level of tangential cut for Figures (A) and (B). In Figures (A)-(D), the arrowhead points to the partition membrane; magnification bars are as follows: 5) 6.43 μm, 6) 2.1 μm, 7) 3.75 μm, 8) 5.6 μm.

Fig. 4.3

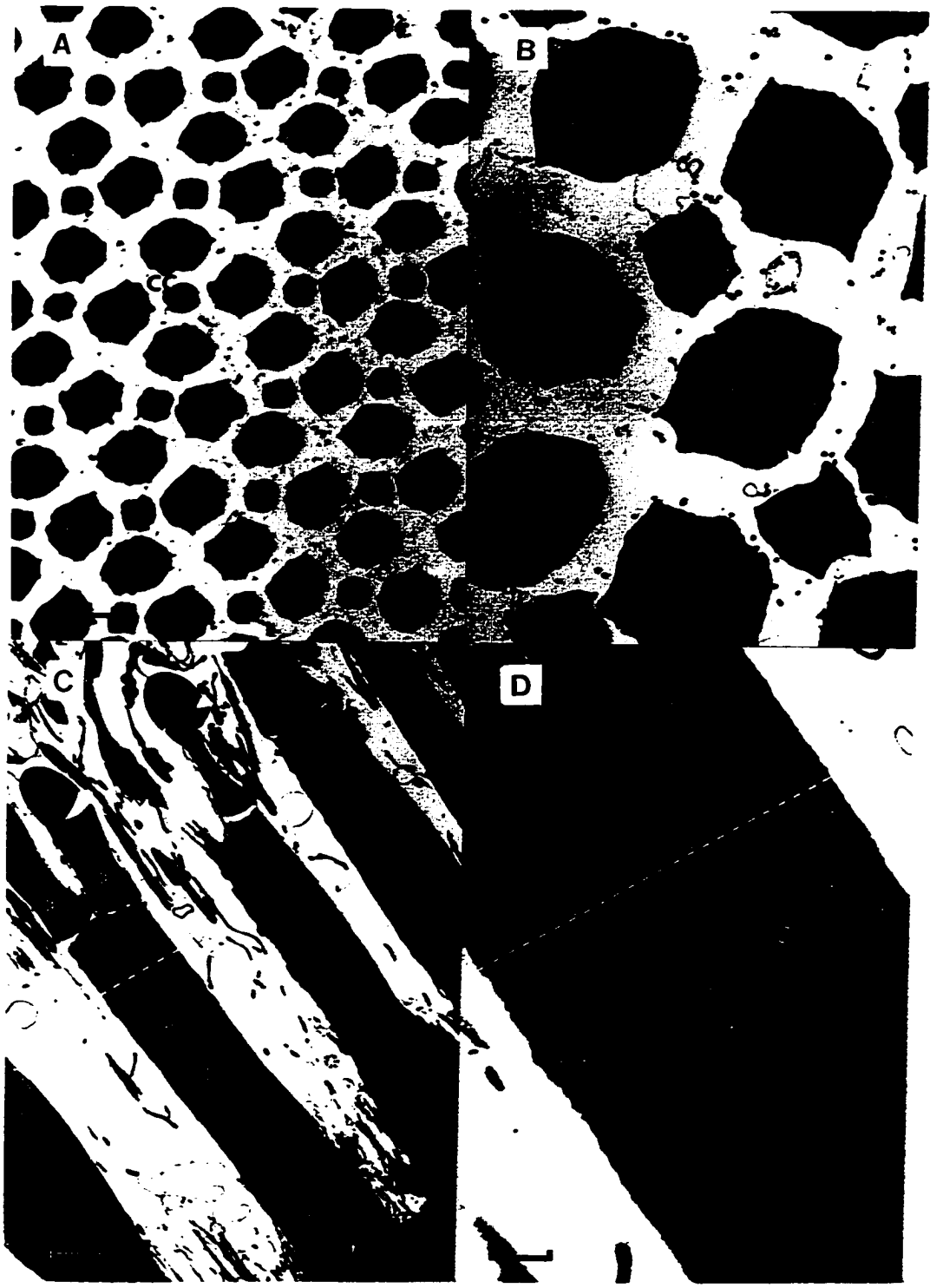

physical attributes for serving as dielectric mirrors (Behroozi & Luzader, 1987). In trout, the partition is tilted so that illumination of the two outer segments is asymmetric (Fig. 4.2D). In sunfish, however, the partition appears straight and the two outer segments of twin cones would be expected to receive symmetrical illumination (Fig. 4.3C,D); such a system would be polarization-insensitive, unless the cones were tilted off-axis as a whole. Lack of polarization sensitivity from twin cones is consistent with the results presented in chapter 3.

4.3.4 Large-scale optical model and Fresnel's reflection formulas

In an attempt to demonstrate the feasibility of reflection to produce intensity variation from a homogeneous incident beam in which only the direction of linear polarization is varied, Dr. Hárosi built the optical model outlined in Figure 4.4A. The commonly available components were mounted on sliding carriers and assembled on an optical bench. The arrangement was intended to mimic the paired cone geometry and physiological illumination as closely as possible. Referring to Figure 4.4A, diode currents generated by D1 and D2 are proportional to the incident flux density (intensity) but not to polarization. This was verified for all rotational positions of the polarizer, while the partition was removed. When the partition was positioned axially (τ=0°), D1 and D2

detected near zero contrast upon polarizer rotation. However, similar rotations of the polarizer yielded increasing contrast with increasing partition tilts (clockwise or counterclockwise) up to a certain angle commensurate with the geometry. When refractive indices for glass and air were used and the tilt angles substituted into Fresnel's formulas (Born & Wolf, 1975), the observed contrasts could be accounted for (Fig. 4.4B). I then substituted biologically relevant refractive indices (Sidman, 1957; Liebman et al., 1974) into the formulas and computed contrast values that could be expected at tilt angles observed in photomicrographs of trout double cones (e.g. Fig. 4.2D). Results from these calculations indicated reasonable agreement with the contrasts determined experimentally from retinal preparations (Table 4.1, Fig. 4.4B).

4.3.5 Polarization sensitivity of ultraviolet cones can be explained with the reflection hypothesis

As stated above, I found single cone ellipsoids to be axially isotropic (Table 4.1). This is consistent with expected light propagation along a cylindrical, dielectric waveguide, with either homogeneous or radially-graded refractive index profile (e.g. Midwinter, 1979). However, the ultraviolet (UV) retinal mechanism in rainbow trout, which is mediated by UV-absorbing single cones, has been reported to be polarization sensitive (Hawryshyn & McFarland, 1987; Parkyn &

FIGS. 4.4A,B. (A) Schematic drawing of a large scale optical model to mimic anisotropic transmission of polarized light in paired cone inner segments. Photocurrents of D1 and D2 were recorded for various partition tilts for polarized light as determined by the position of the rotatable linear polarizer. Parallel and perpendicular polarizations are defined with respect to the plane of incidence. **(B)** Experimental and theoretical contrast (in percent) as a function of partition tilt angle, τ (for clockwise partition tilt). Negative contrasts could result, when D2 received more light than D1 (which occurred for perpendicular polarizations). The light intensity at each detector was a function of reflected and transmitted light and was computed, for a given polarization, using Fresnel's reflection formulas for a dielectric interface (Born & Wolf, 1975):

$T=1-R=1-\rho_{\parallel}(\varnothing)^2$ (parallel polarization)

$T=1-R=1-\rho_{\perp}(\varnothing)^2$ (perpendicular polarization),

where T=transmissivity, R=reflectivity, and the amplitude reflection coefficients are given by:

$$\rho_{\parallel}(\varnothing)=\{n_2^2\cos\varnothing-n_1[n_2^2-n_1^2\sin^2\varnothing]^{1/2}\}/\{n_2^2\cos\varnothing+n_1[n_2^2-n_1^2\sin^2\varnothing]^{1/2}\}$$

$$\rho_{\perp}(\varnothing)=\{n_1\cos\varnothing-[n_2^2-n_1^2\sin^2\varnothing]^{1/2}\}/\{n_1\cos\varnothing+[n_2^2-n_1^2\sin^2\varnothing]^{1/2}\}$$

The calculations were carried out for two light rays, incident on either side of the partition, representing the median angle ($\Phi=18°$ for the large scale optical model, and $\Phi=14°$ for physiological refractive indices) of the full cone illumination (this procedure was adapted to approximate

contrast produced by the entire cone of light with incident rays in the interval $-25° \leq \Phi \leq 25°$ and $-20° \leq \Phi \leq 20°$ respectively). The two optical media were assumed to have refractive indices n_1 for the surround and n_2 for the partition. These corresponded to air and glass for the optical model (Fig. 4.4A). Percent contrasts were also computed for physiological refractive index pairs; in these calculations n_2 was that of frog rod outer segment membrane (1.475; Liebman et al., 1974), and n_1 corresponded to either frog rod outer segment cytoplasm (1.365; Liebman et al., 1974), or an average value obtained from various cone ellipsoids (1.39; Sidman, 1957).

Fig. 4.4A

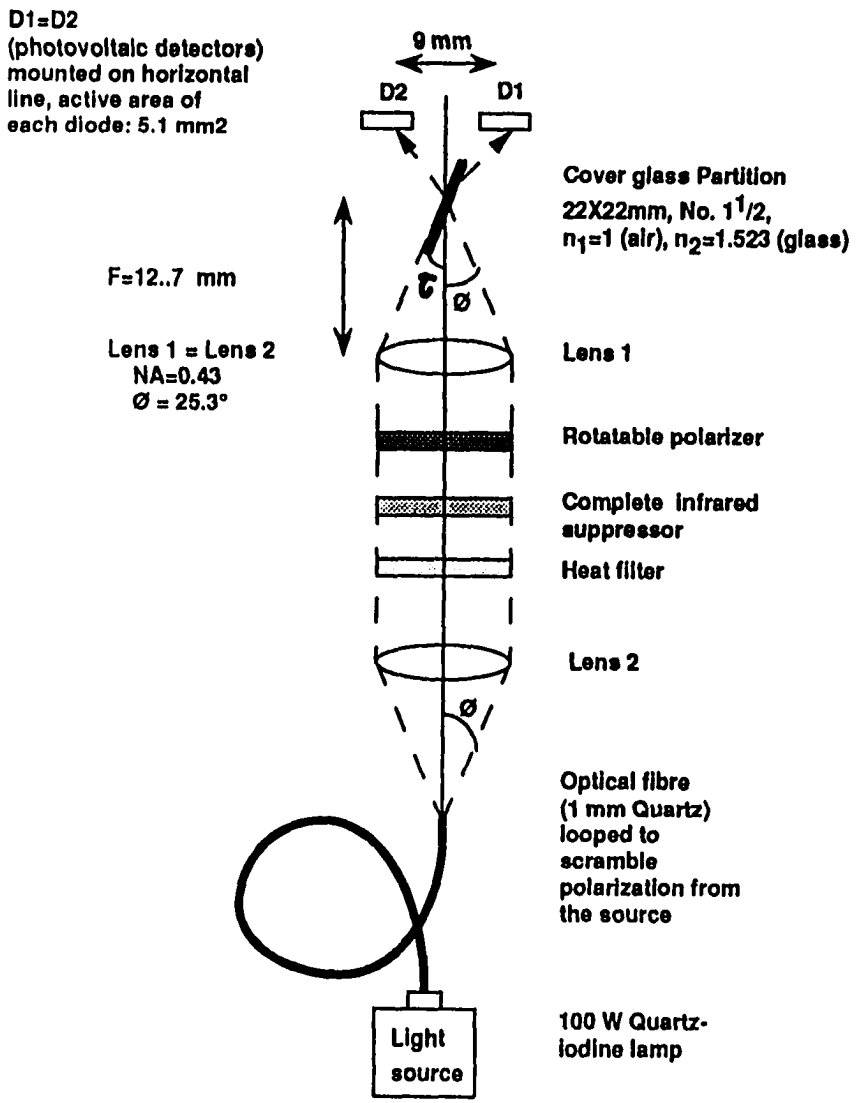

Fig. 4.4B

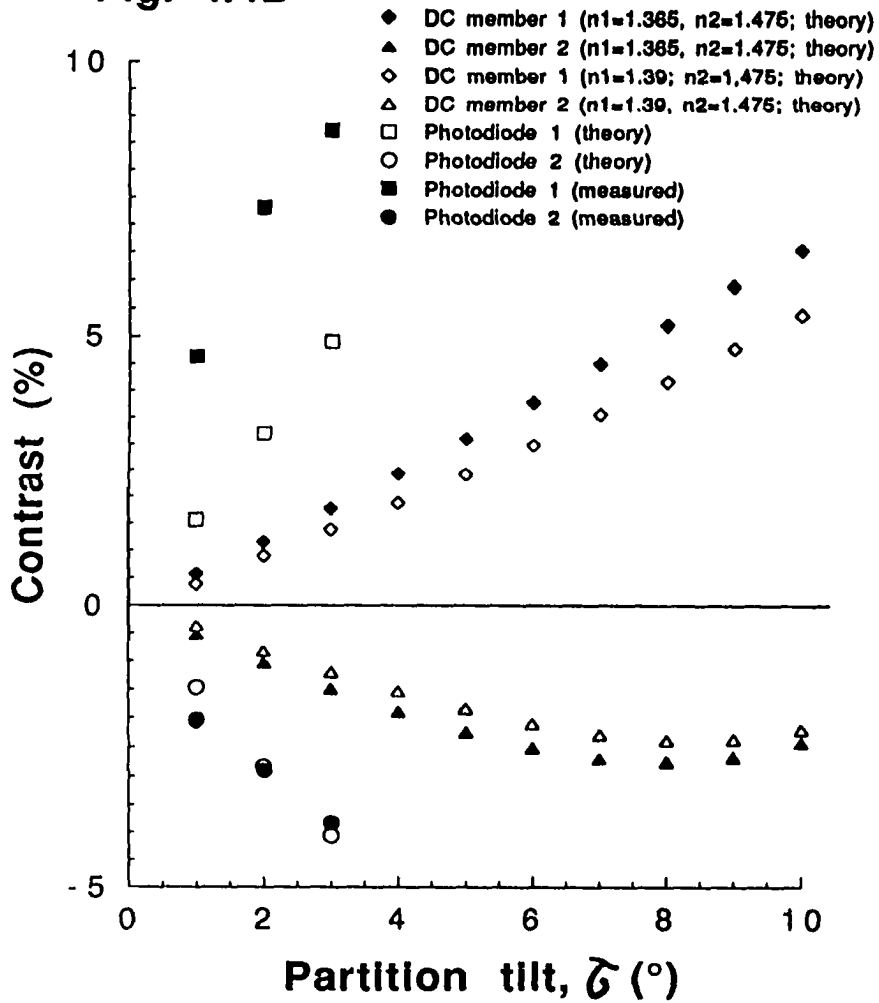

Hawryshyn, 1993; Coughlin & Hawryshyn, 1995). This polarization sensitivity cannot be explained with any previous model, including the graded-index model proposed for the elliptical waveguide hypothesis (Rowe et al., 1994).

The reflection hypothesis presented here provides a plausible explanation (Fig. 4.5A). Accordingly, polarization sensitivity of UV-absorbing single cones would come about by anisotropic reflection of light from tilted double cone partitions toward adjacent single cone outer segments. The relative displacement of single cones toward the vitreous appears to facilitate the capture of light by their outer segments as they face the partition bends of the nearby double cone inner segments (Fig. 4.2D). It is noteworthy that centrally located single cones do not face any partitions and hence should not receive reflected light (Figs. 4.5A). Thus, centre cones should be polarization-insensitive and hence mediate neural mechanisms that lack polarization sensitivity. The latter expectation is supported by electrophysiological determinations (Hawryshyn & McFarland, 1987; Parkyn & Hawryshyn, 1993; Coughlin & Hawryshyn, 1995).

4.3.6 Neural model for polarized light discrimination

In Figure 4.5B, I provide a simple scheme of neural circuitry which could reproduce the main features of polarization sensitivity in fish as currently known. Assumed in this scheme are primary cell loci that sum the outputs from

FIGS. 4.5A,B. (A) Schematic representation of anisotropic transfer of linearly polarized light assuming the partitions to act as dielectric mirrors. The spectral regions of peak absorption are indicated on the various cones composing the mosaics. Double arrows indicate the predominant polarization direction after reflection from the partition (see Table 4.1 for optical measurements). It is assumed that, during photopic conditions, light is focused at the ellipsoid level of paired cones since (1) photon capture is maximized by tight spacing between cones (Figs. 4.2A,C; 4.3A), and (2) pigment epithelium projections are almost absent at this level (Figs. 4.2A-D; 4.3B,C). Light reaching the paired cone partition is partially reflected because of its presumed higher refractive index with respect to the ellipsoid lumen. If the partition is tilted, as in rainbow trout, the two outer segments should receive different illumination (see Fig. 4.4). Furthermore, because of the one-sided pattern in partition tilt around the mosaic (Fig. 4.2A and micrographs not shown), each AC should receive reflected light polarized primarily in one direction (the minimum angle Φ for ray escapement from a DC towards an AC, in the worse case scenario of no partition tilt, can be calculated to be around 30°, see TC figure for measurements used; computed numerical apertures for trout (0.22-0.46) support a maximum angle of only 20° without partition tilt, but this angle can increase to more than 45° with tilt). If the partition is not tilted, as may be the case in sunfish,

each member of the twin cone should receive similar illumination irrespective of its orientation in the mosaic. Such a system would be insensitive to polarized light. In vivo, and possibly in some of the in vitro experiments (see sunfish results in Table 4.1), twin cones may occur with a slant, a condition which would render them anisotropic. **(B)** Neural model for the processing of polarized light (polarization sensitivity responses as a function of polarization direction are shown next to relevant loci; v=vertical, h=horizontal polarization; Hawryshyn & McFarland, 1987; Parkyn & Hawryshyn, 1993; Coughlin & Hawryshyn, 1995). The black and white synapses are excitatory and inhibitory respectively, other symbols are as in Fig. 4.5A. Following polarized light detection by DCs and ACs, the first series of cell loci sum the outputs from all the cone types that share the same polarization detection maxima. Then, another set of loci subtract the horizontal total from the vertical total for the L mechanism (L_h-L_v) and do the opposite for the UV mechanism (UV_v-UV_h). These two neural pathways result in the observed maxima to E_h for the L and M mechanisms (note that the same diagram as that for the Ls can be drawn connecting the Ms), and to E_v for the UV mechanism. The observed 90° periodic response under low white light intensities (Parkyn & Hawryshyn, 1993; Coughlin & Hawryshyn, 1995) can be explained by assuming a nonlinear inhibition of L and/or M cones on UV cones, and a summation of outputs from competing mechanisms.

The neural mechanism for this inhibition is not clear at present, but it may be due to nonlinear recruitment of the more numerous polarization signals from DCs as the E_h condition is approached, or to changes in retinal adaptation state.

Fig. 4.5

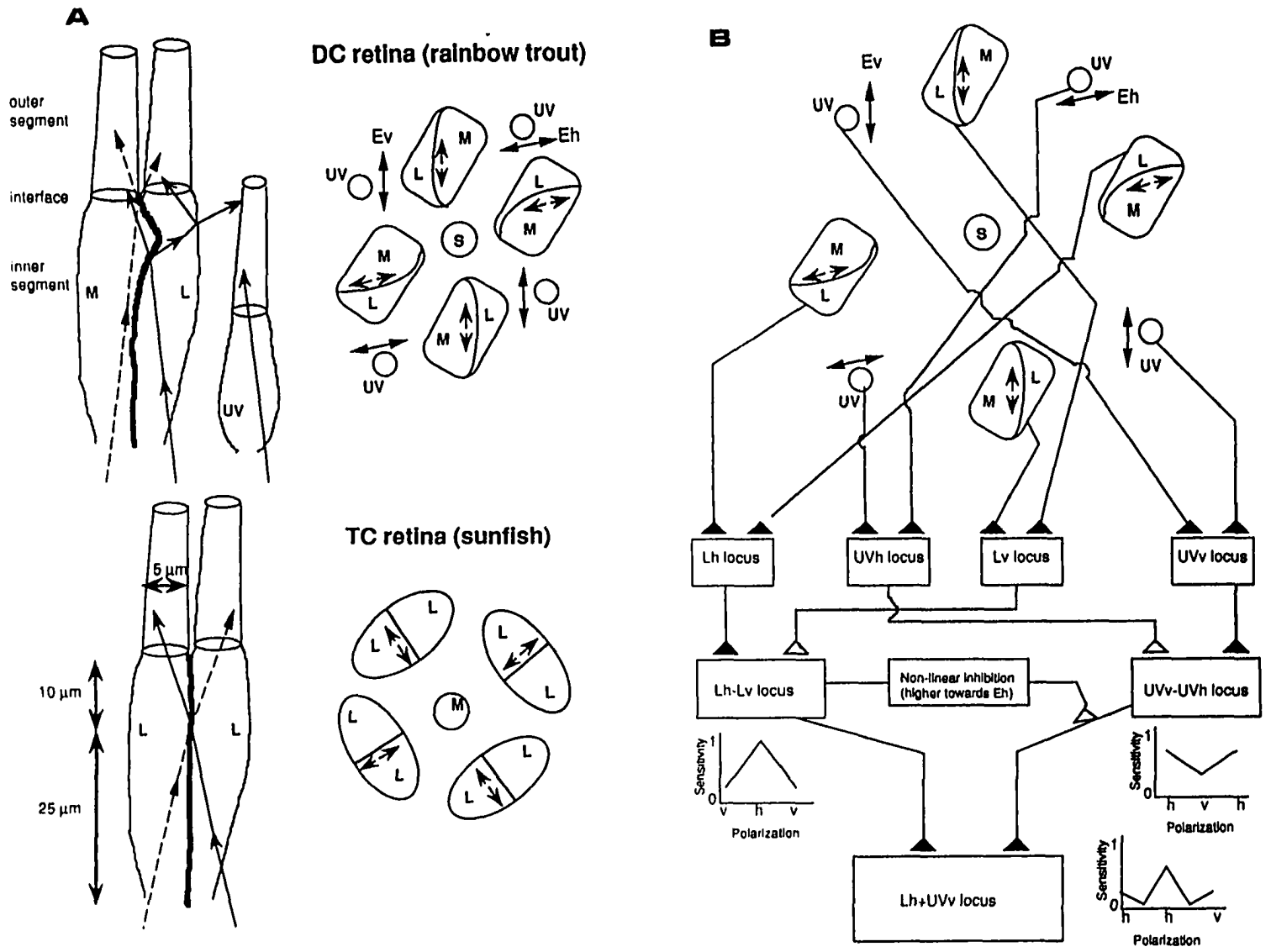
A
outer segment
interface
inner segment
M
L
UV
5 µm
10 µm
25 µm
DC retina (rainbow trout)
Ev
UV
Eh
S
TC retina (sunfish)
B
Photoreceptor layer
Horizontal cell layer to optic nerve
Lh locus
UVh locus
Lv locus
UVv locus
Lh-Lv locus
Non-linear inhibition (higher towards Eh)
UVv-UVh locus
Lh+UVv locus
Sensitivity
Polarization

each of the two polarization-type receptors, and secondary loci that compute differences between the total responses from peak horizontally-sensitive loci and those from peak vertically-sensitive loci (analogous neural processing is presumed to take place in the retinas of invertebrates; Shaw, 1969; Wehner, 1983; Labhart, 1988). The response curves generated resemble electrophysiological results obtained when the action of each cone mechanism is isolated (Hawryshyn & McFarland, 1987; Parkyn & Hawryshyn, 1993; Coughlin & Hawryshyn, 1995). Under illumination that favour interactions between L (or M) and UV mechanisms, the observed response curve (Parkyn & Hawryshyn, 1993; Coughlin & Hawryshyn, 1995) with three maxima could be produced through nonlinear inhibition on the UV mechanism by the L and/or M mechanisms. The latter interactions and subsequent summations would produce a curve with small modulation depth compared with those from isolated mechanisms (Fig. 4.5B), a feature which also agrees with electrophysiological data (Hawryshyn & McFarland, 1987; Parkyn & Hawryshyn, 1993; Coughlin & Hawryshyn, 1995).

4.4 Summary

In conclusion, I propose paired cone partitions to play a key role in the conversion of polarization directional information into patterns of intensity variation that the retinal cones can detect. Special importance is attributed in

this scheme to the large numerical aperture of fish eyes, which can refract incident rays into conical bundles that can thereby proceed to interact with the paired cone partitions in predominantly axial orientation. For these partitions to function as dielectric reflectors, the requirement is a refractive index greater than that of the adjacent cytoplasm, a condition that lipoprotein membranes can easily satisfy. Additional requirements for the partitions are that their orientations be tilted or otherwise asymmetric with respect to the optic axis of the eye, and that their surfaces in the retinal mosaic be arranged along different but ordered planes (in case of the rainbow trout, these are two sets of planes orthogonal to one another that correspond to the horizontal and vertical directions). The pattern of intensity variation caused by the partitions over the cone outer segments needs further interpretation for polarization discrimination. For the latter, I envision the existence of a dedicated neural network like the one outlined in Figure 4.5B.

Chapter 5: Lack of polarization sensitivity in the common white sucker, *Catostomus commersoni*, a fish with ultraviolet vision but random cone mosaic in the central retina.

5.1 Introduction

The biophysical mechanism proposed for polarization detection in the previous chapter relies entirely on the presence of double cones. Ultraviolet polarization sensitivity is explained as a consequence of double cone reflection, a hypothesis that is consistent with the lack of preferential transmission of particular electric field orientations through single cones (see Table 4.1 of chapter 4). Furthermore, according to the proposed mechanism, ultraviolet polarization detection requires the presence of an ordered double cone mosaic. Hence, all other neural processing being equal to that in trout, a prediction of the mechanism would be the lack of polarization sensitivity for fishes with random cone mosaics.

To test the hypothesis that an ordered mosaic in the central retina coincides with the phenomenon of polarization sensitivity among ultraviolet-sensitive fishes, I investigated the visual system of the common white sucker (*Catostomus commersoni*) and compared it to that of polarization-sensitive species. I chose the common white sucker for two reasons: 1) it is in the same order as the cyprinid family (Scott & Crossman, 1973), a group of fishes with ultraviolet vision

(Neumeyer, 1985; Hawryshyn & Beauchamp, 1985; Hawryshyn & Hárosi, 1991), and 2) preliminary observations have suggested a random cone mosaic in the retina of this fish (Ali & Anctil, 1976). If the common white sucker possessed a random cone mosaic in the central retina, then I predicted the absence of polarization sensitivity in this species. If, however, the mosaic was orderly, then I expected to observe polarization sensitivity.

5.2 Materials and Methods

5.2.1 Animals

Common white suckers were obtained by bottom trawl from Mouse Lake (Dorsey county, Ontario, Canada). The fish were housed in a closed re-circulating fresh water flow-through system at the University of Victoria for 1.5 months before the start of experiments. The animals were fed a daily diet of BioDiet Grower pellets (Bio-Products Inc., Warrengton, Oregon, USA) and were held under a 12h:12h L:D cycle. The light intensity was dim and comparable to the levels found at 15-20 meters in meso-eutrophic lakes (see Novales Flamarique et al., 1992).

Experiments were conducted on 24 fish, the majority of which were adults. The average weight and size ± SD were: 44.28 (± 19 g) and 17.11 (± 3.1 cm). All handling and experimental procedures complied with the guidelines set by the Canadian Council on Animal Care and the University of

Victoria Animal Care Committee.

5.2.2 Electrophysiological recordings

The same compound action potential recording technique as described in chapter 2 was used in this study. Spectral sensitivity and polarization curves were obtained under the various light backgrounds presented in Figure 5.1. The maximum absorbance values (used in the model to generate the pigment absorbance spectra from the template) were those of photopigments with λ_{max} at 380 nm (ultraviolet), 453 nm (short), 533 nm (middle) and 620 nm (long), as determined using MSP on carp cones (*Cyprinus carpio*) by Hárosi (1985) (see also Hawryshyn & Hárosi, 1991; MSP data are not available for the common white sucker).

5.2.3 Retinal histology

The eyes from two specimens were removed following electrophysiological recordings. Following extraction of the lens and some eye fluid, each eyecup was immersed and left overnight in primary fixative (see chapter 4 for recipe). The retinas were then removed from the eyecups and cut into eleven pieces corresponding to eleven distinct topographical locations across the retina (Fig. 5.2A). These pieces were post-fixed, dehydrated and embedded as described before (chapter 4).

The embedded blocks were cut for light and electron

Figure 5.1 Spectral backgrounds used during electrophysiology experiments. The white and late crepuscular backgrounds mimic light regimes at 3-6 meters underwater in a mesotrophic lake on a sunny day at 12:00 hrs and 21:30-22:00 hrs respectively (see Novales Flamarique et al., 1992). For clarity, 1.5 log units have been added to successive graphs starting with the short (blue) isolation, except for the late crepuscular background to which 2 units were added above the previous, white, background.

Figure 5.1

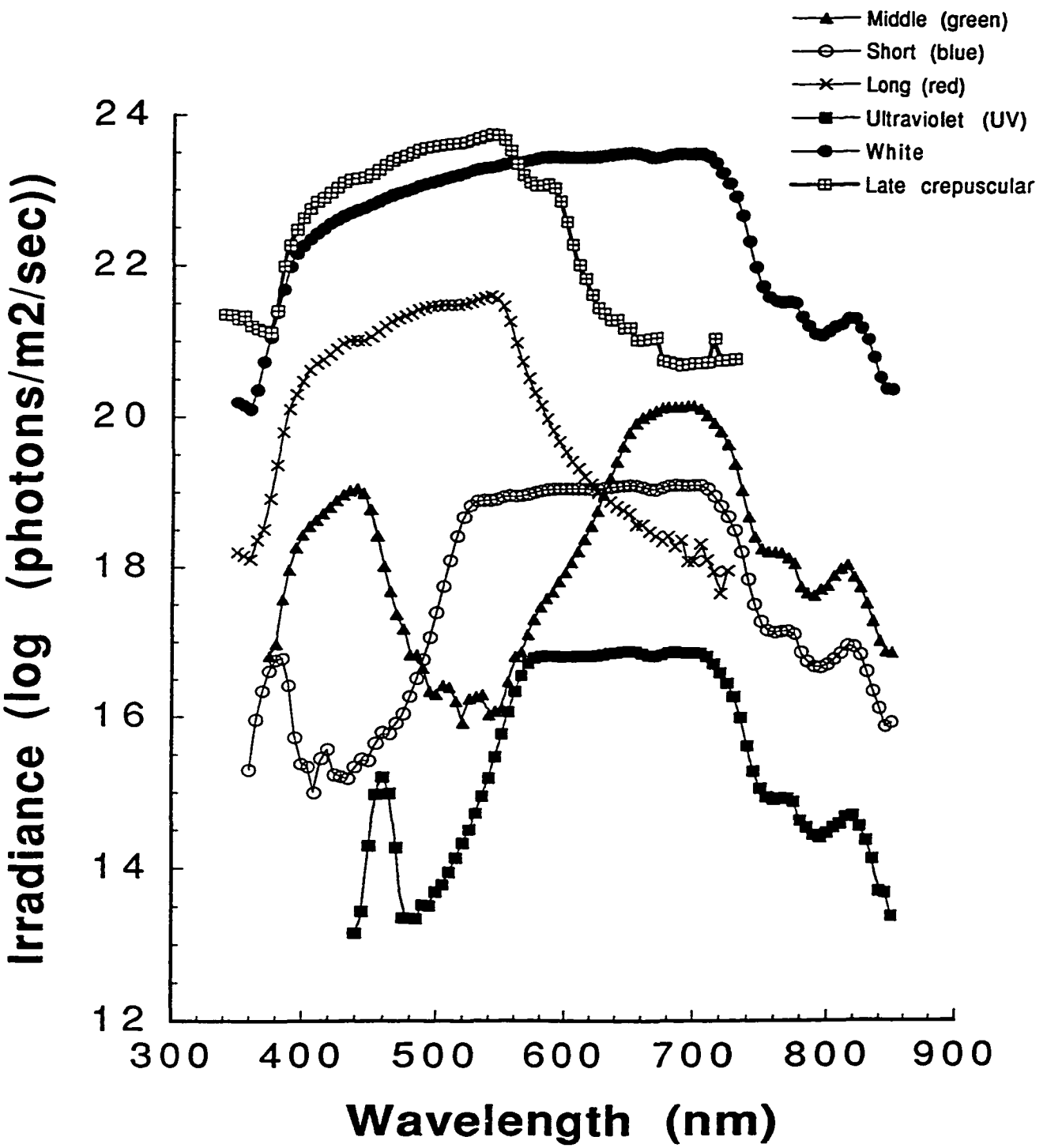
Middle (green)
Short (blue)
Long (red)
Ultraviolet (UV)
White
Late crepuscular
Irradiance (log (photons/m2/sec))
24
22
20
18
16
14
12
300
400
500
600
700
800
900
Wavelength (nm)

Figure 5.2 (A) Perimeter sketch of a common white sucker retina indicating double cone densities (± S.D.) per 0.03 mm^2 at the different topographical locations sampled (centres of each number; the areas used for mosaic identification were approximately 2.5 mm^2). Locations averaging 142 (±16) and 172 (±26) double cones were the centro-temporal and dorsal areas used for geometrical measurements. The shaded region marks the area of random cone mosaic; row mosaics were found in the remaining parts of the retina. V = ventral, D = dorsal, N = nasal and T = temporal. **(B)** Sketch of two double cones illustrating the measurement technique and the angle groupings used in the statistical tests.

Fig. 5.2

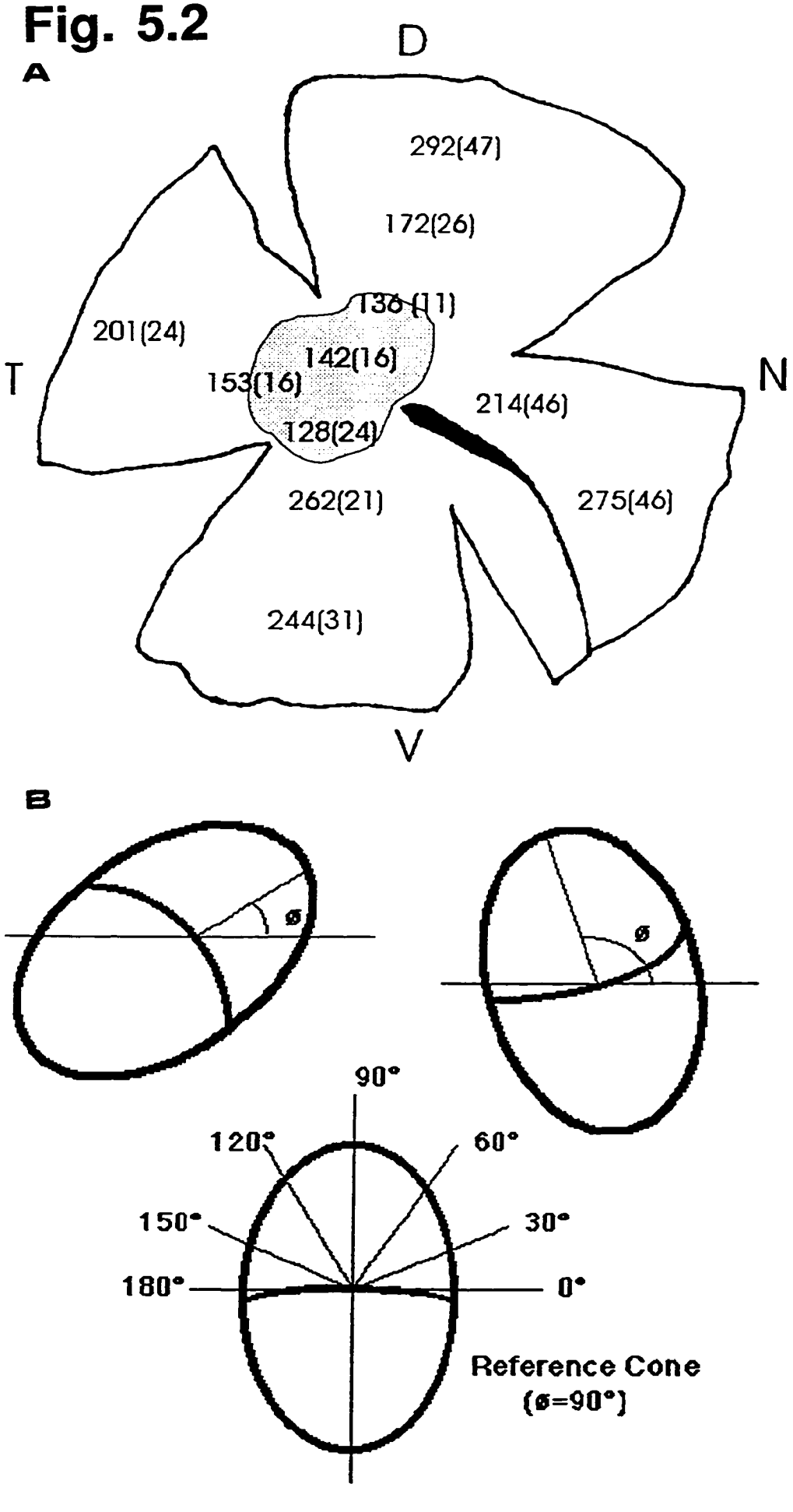
A
D
292(47)
172(26)
138(11)
201(24)
142(16)
T
153(16)
N
214(46)
128(24)
262(21)
275(46)
244(31)
V
B
ø
ø
90°
120°
60°
150°
30°
180°
0°
Reference Cone
(ø=90°)

microscopy. The type of retinal mosaic at each location was estimated from 1 μm thick tangential sections. Further to these observations, I determined the exact geometric distribution of double cones for two locations in the centro-temporal and dorsal parts of the retina (Fig. 5.2A). These areas were chosen because they were representative of the two mosaic types found in the study (see results). For each retina, I measured the angle that the perpendicular to the partition of each double cone at its centre made with the horizontal 0-180° reference line, in a 30000 μ^2 grid (Fig. 5.2B). The angles were then grouped in 45° increments, pooled together for the two sections, and compared to a uniform random distribution (for centro-temporal sections) or fitted to a normal distribution in the case of dorsal sections. In addition, to test whether double cone density differed with mosaic type, I counted the number of double cones within the 30000 μ^2 grid for all the retinal locations sampled. Thin sections (75 nm) were also cut to observe photoreceptor ultrastructural detail.

5.3 Results

5.3.1 Electrophysiology

The common white sucker exhibits four cone mechanisms with maximum absorbances for the ON component of the response in the ultraviolet (λ_{max} = 380 nm), short (blue, λ_{max} = 460 nm), middle (green, λ_{max} = 540 nm) and the long wavelength (red, λ_{max}

= 640 nm) parts of the visual spectrum (Fig. 5.3, Table 5.1). During daylight conditions, the ON response exhibits inputs primarily from the short and long wavelength mechanisms, but during the late evening (crepuscular conditions), it is the ultraviolet and long cone mechanisms that dominate the response (Fig. 5.3, Table 5.1). The OFF response under all adapting backgrounds was dominated by middle mechanism input ($\lambda_{max} \approx 520$ nm, Fig. 5.3, Table 5.1).

Polarization sensitivity experiments under the above mentioned adapting backgrounds did not reveal polarization sensitivity for any of the wavelengths selected across the spectrum (Fig. 5.4). The modulation depth for any curve was less than 0.25 log units and the responses to different orientations of the polarizer within a curve were not significantly different from each other ($P>0.05$ for all χ^2 tests comparing individual values per wavelength to the mean sensitivity for each curve).

5.3.2 Retinal histology

The retina of the common white sucker exhibits two kinds of mosaics: a random mosaic located in the centro-temporal retina and a row mosaic in the other locations (Table 5.2, Figs. 5.2,5.5A-D). In most areas, random mixtures of large and small single cones and thinner rods occupy extensive areas between double cones (Figs. 5.5A-D, 5.6A,B). This patterning is very different from that observed in other fishes where the single

Figure 5.3 Spectral sensitivity ON and OFF responses of the common white sucker under backgrounds that isolate: **(A)** the ultraviolet (UV) cone mechanism, **(B)** the short (blue), **(C)** the middle (green), and **(D)** the long (red) cone mechanism; **(E)** and **(F)** correspond to spectral sensitivity responses under midday and crepuscular light conditions respectively (see Fig. 5.1). The real values are the experimental data points (± S.E.), the model curve is the best fit generated with the simplex algorithm. Relative sensitivity values were calculated by normalizing all sensitivity values with respect to the smallest value for each of the ON and OFF responses independently, and inverting the result (Bernard, 1987; Palacios et al., 1996). For clarity a value of 1 unit was added to the real and model values of ON relative sensitivity to separate them from the OFF values. The bars in the graphs are the raw standard errors of the sensitivity averages (N=5 fish per mechanism). For purpose of computing the original sensitivities, we give the highest sensitivity values (and the wavelength in nm at which they appear between parentheses) for the various mechanisms: UV-ON (380): -12.39; UV-OFF (520): -12.41; Short-ON (460): -12.13; Short-OFF (500): -13.17; Middle-ON (540): -13.21; Middle-OFF (520): -12.98; Long-ON (640): -13.38; Long-OFF (520): -14.52; White-ON (430): -12.68; White-OFF (500): -14.28; Crep-ON (640): -13.17; Crep-OFF (540): -13.71. These values are in log (cm^2*sec/photons).

Fig. 5.3

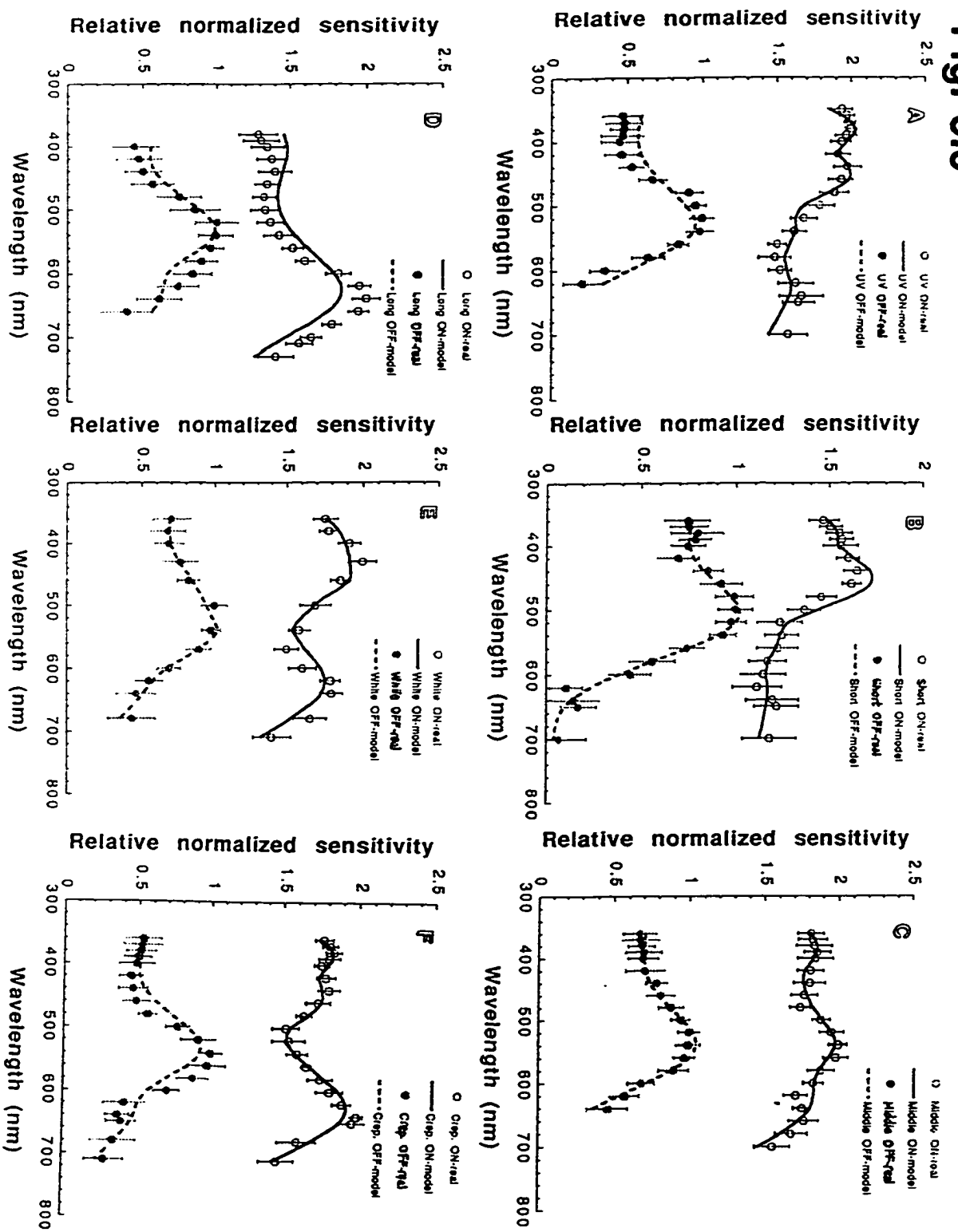
A
B
C
D
E
F
Relative normalized sensitivity
Wavelength (nm)
UV ON-real
UV ON-model
UV OFF-real
UV OFF-model
Short ON-real
Short ON-model
Short OFF-real
Short OFF-model
Middle ON-real
Middle ON-model
Middle OFF-real
Middle OFF-model
Long ON-real
Long ON-model
Long OFF-real
Long OFF-model
White ON-real
White ON-model
White OFF-real
White OFF-model
Crsp. ON-real
Crsp. ON-model
Crsp. OFF-real
Crsp. OFF-model

Table 5.1 Simplex-derived coefficients and least sum of squares (SS) statistic for the ON and OFF responses of the four cone mechanisms of the common white sucker. SS refers to the sum of squares residual derived from the sum of the differences between mean spectral sensitivity points and those predicted by the Simplex model. "M. response" is the mechanism response, "UV" is ultraviolet, "White" refers to the white midday background and "Crep" to the crepuscular background, other symbols are explained in the text.

M. response	k_1 (UV)	k_2 (short)	k_3 (middle)	k_4 (long)	p	SS
UV-ON	1.025	0.997	0.12	0.103	4.42	0.19
UV-OFF	0.015	0.122	0.884	0.07	1.25	0.13
Short-ON	0.005	0.075	0.00001	0	8.22	0.14
Short-OFF	0.021	0.146	0.711	0.123	0.009	0.04
Middle-ON	0.351	0.192	0.781	0.601	2.56	0.05
Middle-OFF	0.0003	0.043	0.608	0.357	0.031	0.07
Long-ON	0.001	0.002	0.001	0.727	1.84	0.33
Long-OFF	0.027	0.009	0.927	0.19	3.51	0.12
White-ON	0.272	0.661	0.004	0.621	1.72	0.07
White-OFF	0.075	0.312	0.998	0.185	2.49	0.02
Crep-ON	0.369	0.293	0.0001	0.752	4.08	0.04
Crep-OFF	0.018	0.01	0.786	0.108	3.02	0.15

Figure 5.4 Polarization sensitivity responses of the common white sucker for various wavelengths under the same background conditions described in Figure 5.3 (N=3). **(A)** ultraviolet mechanism isolation, **(B)** short (blue), **(C)** middle (green) and **(D)** long (red) cone mechanism isolation; **(E)** responses under midday lighting conditions, and **(F)** under crepuscular conditions. The values within a curve are not significantly different.

Fig. 5.4

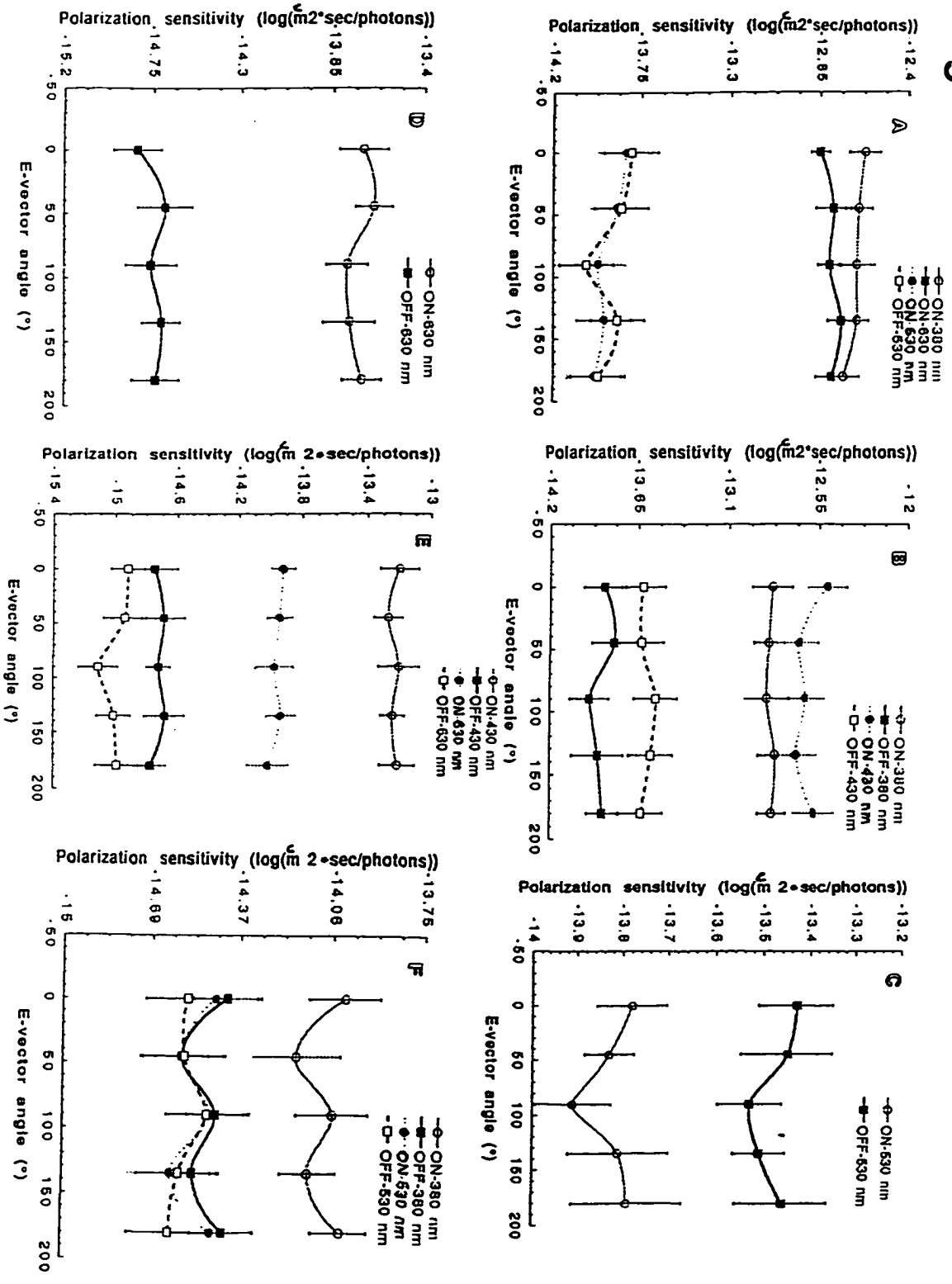
A
Polarization sensitivity (log(m2*sec/photons))
E-vector angle (°)
ON-380 nm
ON-630 nm
ON-530 nm
OFF-530 nm
B
Polarization sensitivity (log(m2*sec/photons))
E-vector angle (°)
ON-380 nm
OFF-380 nm
ON-430 nm
OFF-430 nm
C
Polarization sensitivity (log(m 2*sec/photons))
E-vector angle (°)
ON-530 nm
OFF-530 nm
D
Polarization sensitivity (log(m2*sec/photons))
E-vector angle (°)
ON-630 nm
OFF-630 nm
E
Polarization sensitivity (log(m 2*sec/photons))
E-vector angle (°)
ON-430 nm
OFF-430 nm
ON-630 nm
OFF-630 nm
F
Polarization sensitivity (log(m 2*sec/photons))
E-vector angle (°)
ON-380 nm
OFF-380 nm
ON-530 nm
OFF-530 nm

Table 5.2 Distribution of cones according to the angle made by the perpendicular to the partition at its centre with the horizontal 0-180° line (see Fig. 5.2B). The total number of cones counted for both areas was 286 (CT) and 359 (D). The centro-temporal (CT) distribution is not significantly different from a uniform distribution of 47.67 cones (286/6) (χ^2 = 6.4476, 5 df, P = 0.2651). This uniform distribution is also random as the double cones appear clustered in small randomly-oriented groups, with cones in each group sharing similar partition orientation (Fig. 5.5A). The dorsal (D) distribution is normally distributed around 87.79° (Kolmogorov-Smirnov normality subtest routine, $P<10^{-5}$), denoting a row mosaic in this direction.

Angle	0-30°	30-60°	60-90°	90-120°	120-150°	150-180°
# cones (CT)	54	58	40	46	50	38
# cones (D)	0	52	139	132	36	0

cones occupy well-defined intermittent spaces between double cones (Figs. 5.5E,F).

Double cone density was lowest in areas associated with random mosaic. The highest densities were found in the ventral and dorsal parts of the retina (Fig. 5.2).

Electron microscopy observations revealed the ultrastructure of two prominent cone types: double cones, with most member-pairs separating far (>7 μm) before the outer segment interface, and large single round cones that occupied about half the double cone tangential area at the ellipsoid level (Fig. 5.6C-F). In addition, small single cones with wider myoids were also observed among the rods (Figs. 5.6A-B; Fig. 5.6F shows the outer segment of one of these cones in tangential section). Each member of the double cone showed distinctive mitochondrial packing at the ellipsoid level, the larger member always staining darker than the accessory one (Figs. 5.6C-E, 5.7A). The overall morphology of double cones encountered in this study was different from that reported for other teleost fishes (Figs. 5.5E-F; Ali & Anctil, 1976).

Among the various cone types, single cones exhibited higher incidence of peculiar mitochondrial formations near the base of the outer segment (Fig. 5.7B-F). In many instances, neighbouring mitochondria near the outer segment showed continuity of cristae across boundaries, and the cristae were oriented approximately parallel to the photoreceptors's length (Fig. 5.7C).

Figure 5.5 Cone mosaics present in the common white sucker retina. Random mosaic shown in **(A)** bar, 19.6 μm, and **(B)** bar, 8 μm ; row mosaic of double cones in **(C)** bar, 19.6 μm, and **(D)** bar, 8 μm. For comparison, **(E)** and **(F)** are square mosaics from the centro-temporal retinas of the pumpkinseed (*Lepomis gibbosus*) and the rainbow trout (*Oncorhynchus mykiss*, parr stage) respectively; both bars, 8 μm. Notice the differences in overall morphology between the double cone ellipsoids in (E) and (F) and those of the common white sucker. AC, accessory corner cone (or ultraviolet cone); CC, centre cone, DC, double cone; LSC, long single cone; R, rod and SSC, short single cone.

Fig. 5.5

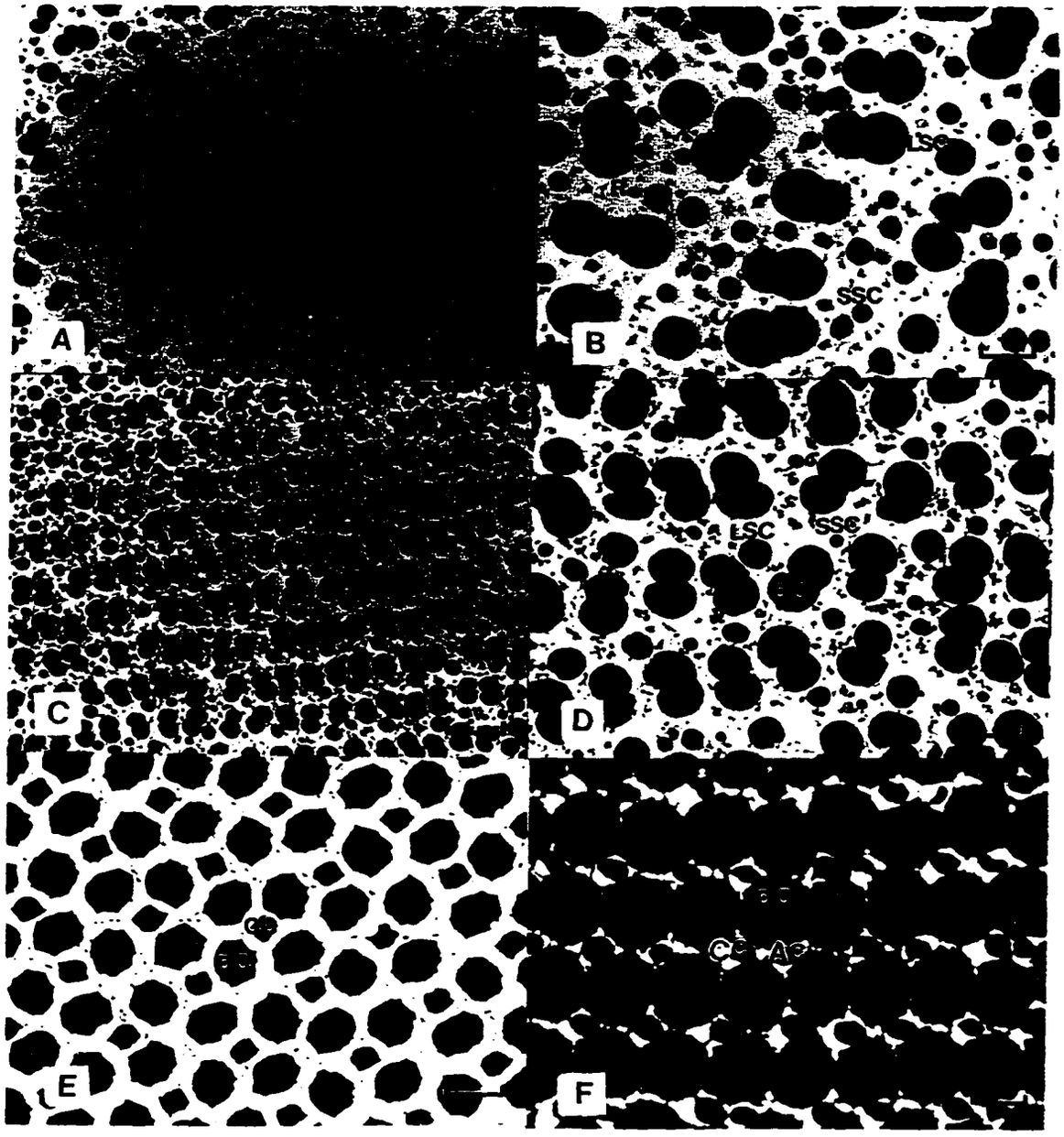

Figure 5.6 Radial section through the retina of the common white sucker shown in **(A)** bar, 20.7 μm, arrow head points to SSC and double arrow head points to LSC, and **(B)** bar, 8.32 μm. **(C)** Two members of a double cone showing different mitochondrial densities and/or mitochondria types near the outer segment; note also the difference with the rod mitochondria; bar, 2.05 μm. **(D)** double cone morphology at a more vitreal location; bar, 1.75 μm. **(E)** double cone with vanishing accessory member, and long single cone; bar, 1.54 μm. **(F)** Arrow heads point to double membranes separating interstitial region between a double cone pair (occasionally, triple cones were observed in radial section, this may be a triple cone), and short single cone outer segment; bar, 2.46 μm. RPE, retinal pigment epithelium; VCL, visual cell layer; ONL, outer nuclear layer; other symbols as in Figure 5.5.

Fig. 5.6

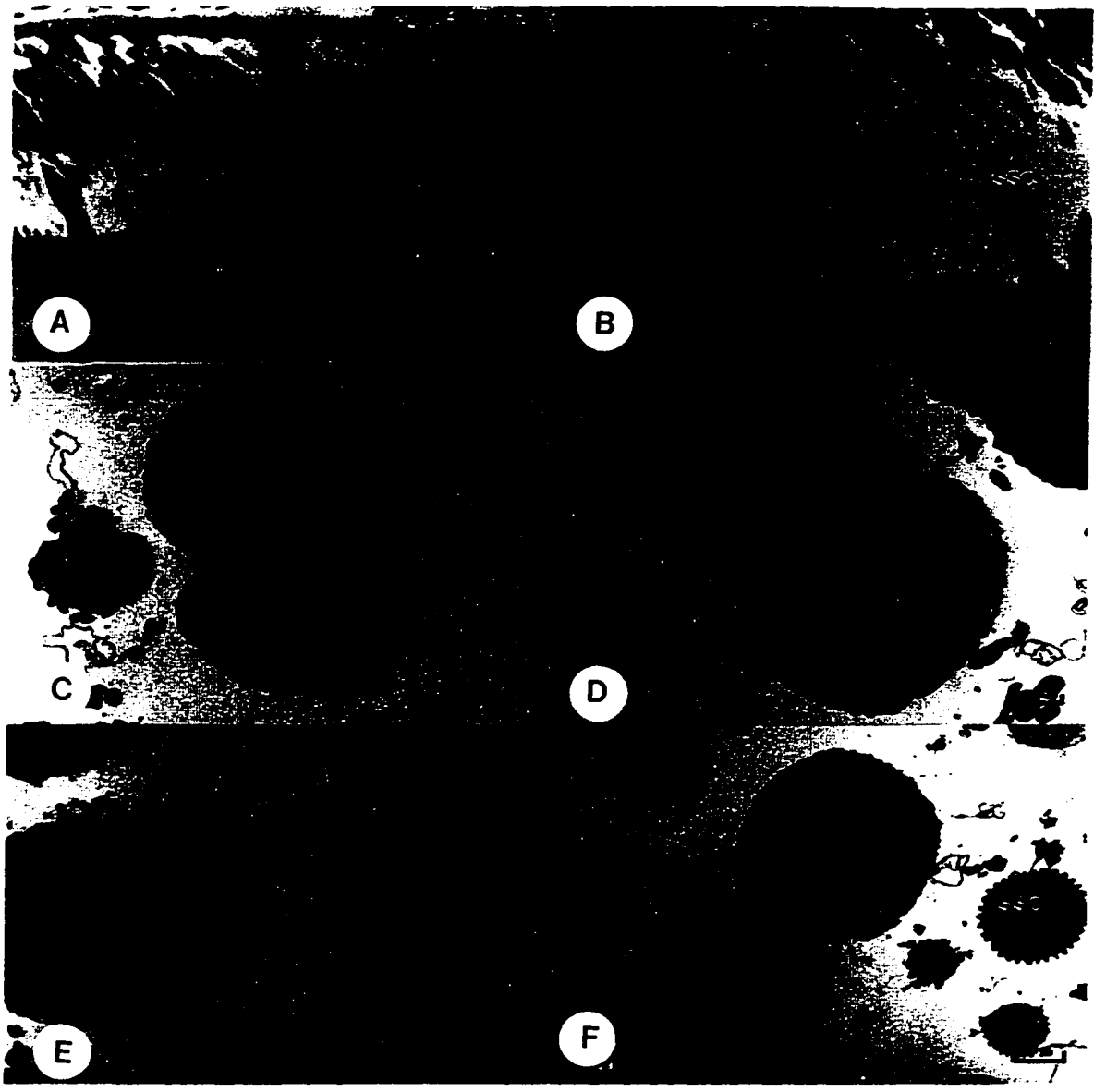

Figure 5.7 (A) Double cone in radial section, note the difference in mitochondrial density between members; bar, 3.08 μm. **(B)** Arrow head points to mitochondria cristae near the outer segment of a single cone, bar, 0.69 μm. **(C)** radial section through a single cone along its inner-outer segment division, note the continuity of cristae between neighbouring mitochondria; bar, 0.69 μm. **(D)** region of high single cone density, arrow heads point to inter-receptoral junctions between neighbouring cones; bar, 1.75 μm. **(E)** Single cone showing parallel array of mitochondria cristae; bar, 0.69 μm. **(F)** higher magnification of mitochondrial array in (E); bar, 0.31 μm. IS, inner segment; OS, outer segment and M, mitochondria; other symbols as in Figure 5.5.

Fig. 5.7

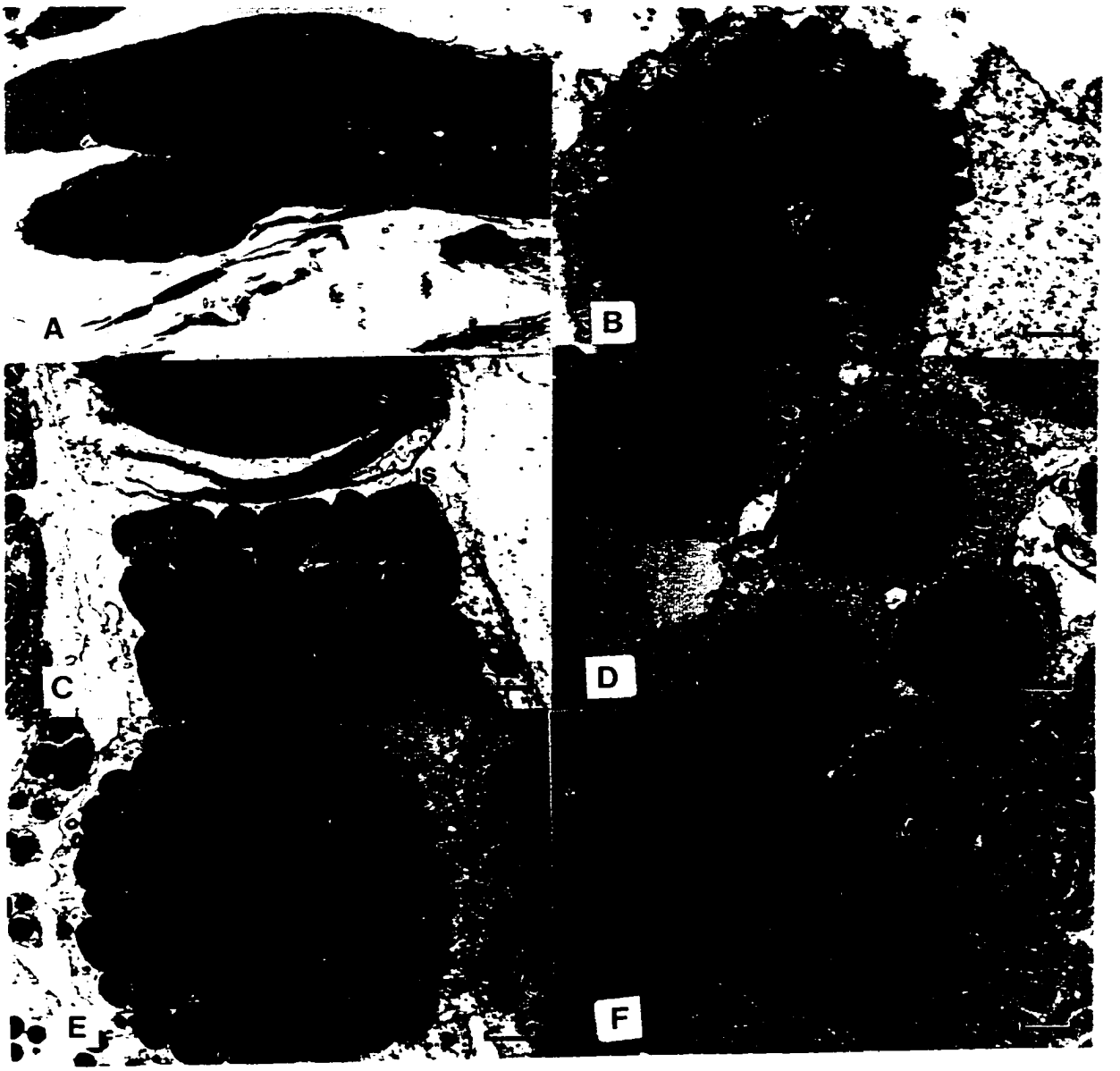

In areas of high single cone density, these cones would often make prominent inter-receptoral contacts (Fig. 5.7D). Figures 5.7E-F show one of these cones with large parallel arrays of cristae located close to the centre of the photoreceptor.

5.4 Discussion

This study presents the first evidence of a fish with four cone mechanisms that is not polarization sensitive. Unlike other species with tetrachromatic vision (Fratzer et al., 1994), the common white sucker, which has four cone mechanisms, is the first species to show a random cone mosaic in the centro-temporal retina. This suggests that it is the ordered arrangement of the cone mosaic in this area of the retina that is critical for polarization detection in the retinas of ultraviolet-sensitive fishes.

There are a number of possibilities that may explain the lack of polarization sensitivity observed. For instance, most double cones of the common white sucker may be insensitive to polarized light given their unique morphology (although peculiar double cones have also been observed in the goldfish, a polarization-sensitive species; Stell & Hárosi, 1976). If the incident light is focused at the ellipsoid level, many double cone members may be acting as single cones (although unlikely) due to their early separation, and hence be optically isotropic with regards to E-vector transmission.

Another possibility is that the common white sucker lacks polarization-sensitive receptors after a certain developmental stage, or that the neural pathways for polarization sensitivity disappear, as is the case for most ultraviolet-mediated sensitivity in salmonids (Beaudet et al., 1993; Parkyn & Hawryshyn, 1993). But this seems unlikely due to the presence of four cone mechanisms in the study animals, and the reported polarization sensitivity in adults of related species (Hawryshyn & McFarland, 1987). Instead, these observations and the lack of an ordered mosaic in the central retina suggest a more plausible explanation compatible with the detection mechanism and neural model in chapter 4. The lack of polarization sensitivity may simply result from an approximately equal number of polarization receptors hyperpolarizing maximally for any particular polarization orientation, given their random distribution across the central retina.

Besides the random cone mosaic in the centro-temporal retina and the peculiar morphology of the double cones, this study also shows peculiarities in mitochondrial formations. In particular, the mitochondria cristae found in some single photoreceptors resemble the arrays of cristae observed in single mitochondria of perch cones (Sjöstrand, 1959), lamprey (Ishikawa & Yamada, 1969) and toad rod-like photoreceptors (Ferrero et al., 1979). However, the observations presented in this study are novel in that the cristae often form continuous

arrays between mitochondria (Fig. 5.7C), whereas they are mostly confined to single mitochondria in other animals (Ishikawa & Yamada, 1969). Furthermore, the cristae often zig-zag in other animals (Ishikawa & Yamada, 1969), a situation not observed in the present study.

The presence of cristae arrays that are perpendicular to the inner-outer segment interface are interesting from a polarization-detection standpoint. This is because array structures of these dimensions can be highly birefringent and lead to form dichroism (Hárosi, 1981), an optical mechanism that may favour transmission of particular polarization orientations to the outer segment. Nonetheless, the sporadic and random orientation of photoreceptors with these cristae arrays, and the lack of polarization sensitivity observed during the study, suggests that these structures do not take part in a polarization detection system.

Continuity of cristae between mitochondria may also occur, although infrequently, in cells with high metabolic activity or in areas of rapidly-dividing mitochondria (Fawcett, 1966; Whittaker & Danks, 1978). This last situation, however, may not be the cause of formation in this case as active division and maturation of photoreceptor mitochondria usually follows a myoid to ellipsoid, periphery to centre gradient. Unusually large mitochondria similar in staining characteristics to those possessing cristae arrays in this study have been shown to give rise to oil droplets in fish retinas (Berger, 1966),

and such mitochondria may also be involved in the metabolic requirements of ellipsosomes (MacNichol et al., 1978; Nag, 1995). However, none of these organelles were observed in this study. Clearly, additional research is needed to understand the nature and function of these peculiar mitochondrial formations.

The common white sucker is a bottom-dwelling fish very common in mesoeutrophic lakes ranging depths up to 15-20 m during the day. In such environments with peak wavelength transmission in the green part of the spectrum (~ 520-560 nm, Novales Flamarique et al., 1992), the observed OFF response (Fig. 5.3) appears well suited, as in salmonids, for detection of shadows hovering above. In addition, the high double cone density in the ventral retina (Fig. 5.2) likely improves motion detection by increasing photon capture, as suggested for other fish species (Ahlbert 1969, 1975). Juveniles feed on zooplankton, and they are often observed foraging closer to the surface during the late evening-crepuscular time periods. These are the times of the day when the proportion of ultraviolet photons to that of the total spectrum is at a maximum (Novales Flamarique et al., 1992, chapter 2), and when these fish are likely using their ultraviolet cones to improve foraging by enhancing target contrast against an ultraviolet-veiling background (Loew et al., 1993; Browman et al., 1994; see also Cronin et al., 1994). In the early spring, adults congregate at the mouth of rivers to spawn. During these

periods, ultraviolet photoreception may serve some form of signalling as proposed for other silvery fish (Denton & Rowe, 1994), and shown for anoline lizards (Fleishman et al., 1993) and for mate choice in zebra finches (Bennett et al., 1996). In addition, ultraviolet reflection from the silvery backs of fish may help recognition of conspecifics or other fishes when foraging in muddy/algae-covered bottoms and in other turbid environments.

Chapter 6: Outer segment dichroism as a mechanism for polarization detection in the northern anchovy, *Engraulis mordax*.

6.1 Introduction

So far this thesis has provided evidence for double cone reflection as a mechanism for polarization detection among fish and, possibly, other vertebrates with similar retinal mosaics (Tovée, 1995). However, one must also keep in mind that polarization detection in vertebrates may arise from other optical anisotropies such as scattering by oil droplets (Young & Martin, 1984), and tilted cone outer segments (Haidinger's brush effect in humans, Bill, 1990; see also Kunz & Callaghan, 1989). Yet another possibility based on photopigment dichroism arose from the study of anchovy photoreceptors (Fineran & Nicol, 1976, 1978). In an extensive histological study, Fineran and Nicol (1978) showed that the cones of *Anchoa mitchilli* and *Anchoa Hepsetus* were arranged in "bifid" units. These "bifid" units consisted of long and short cones with outer segment lamellae perpendicular to each other, and parallel to the length axis of the cones. Such lamellar orientation (unique among vertebrates), was hypothesized to form a two channel analyzer for the detection of linearly polarized light (Fineran & Nicol 1978). However, no studies ensued to test this hypothesis.

Since only cursory histological observations have been made

on the retina of the northern anchovy, *Engraulis mordax* (Fineran & Nicol, 1978; O'Connell, 1981), and since there is no electrophysiology data available for any anchovy species, the goals of this study were as follows: 1) to describe the photoreceptors present in the northern anchovy retina, and 2) to determine the spectral and polarized light sensitivities of the animal. In addition, differential absorption as a physical mechanism for detection of polarized light by anchovy photoreceptors was also examined using light-adapted histological sections. Such observations are interesting in that they can further show structural differences between photoreceptor types, and/or suggest possible mechanisms for the detection of polarized light.

6.2 Materials and Methods

6.2.1 Animals

Schools of adult northern anchovy migrate to coastal waters of Grays Harbour (Washington State, USA) during the summer and early fall. Specimens were transported from Grays Harbour to Victoria and held in a flowing saltwater tank. The fish were held in the tank for one month prior to the start of experiments.

Ten fish were used for electrophysiology recordings and histological analysis. In addition, four fish were used for lamellar-absorption studies. Fish weights and total lengths were: 17.8 (± 3.2g) and 16.2 (± 2.5cm). All holding and

handling procedures carried throughout the study followed the guidelines set by the Canadian Council for Animal Care.

6.2.2 Electrophysiology experiments

The same optic nerve recording technique described in chapter 2 was used in this study. Spectral and polarization sensitivity recordings were obtained under the various cone-isolating backgrounds shown in Figure 5.1 of chapter 5.

The simplex algorithm (Caceci & Cacheris, 1984) was used to fit an eighth order polynomial template for vertebrate cone absorption with λ_{max} equal to 500 nm (Bernard, 1987). The value 500 nm was chosen because it approached the maximum sensitivity response of the fish under photopic conditions. This cone maximum lies near the maximum absorbance of retinal pigment extract from *Anchoa compressa* at 508 nm (Munz, 1958), an absorbance likely dominated by rods. Since only one cone mechanism was obvious from the electrophysiology recordings (see later, results section), Sirovich and Abramov's (1977) photopigment equation used in the fitting process reduces to $S = k_m A_m(\lambda)$. In this equation, S is the sensitivity, $A_m(\lambda)$ is the absorbance of the middle wavelength photopigment at wavelength λ (derived from Bernard's (1987) polynomial template), and k_m is the coupling constant obtained from the best fit of the model to the data.

6.2.3 Retinal histology

Following electrophysiological recordings, the fish was decerebrated and the eyes removed for light and transmission electron microscopy (LM and TEM). The cornea, lens and some fluid were removed before immersing the eye cup in primary fixative (see chapter 4 for chemical composition). The retina was removed a day later and post-fixed in Osmium Tetroxide. Thereafter the tissue was dehydrated through an increasing concentration of ethanol solutions and embedded in Epon plastic medium.

I examined regions from the central, dorsal and peripheral retina. Sections were cut radially (along the length axis of photoreceptors), or tangentially (widthwise across the photoreceptors). Table 6.1 shows a list of the abbreviations used in the micrographs.

6.2.4 Optical analysis of frozen retinae

The retinae from four fish were fixed in primary fixative for 15 to 30 minutes and quick frozen in a mixture (made of 30% sucrose in PBS buffer and 70% Tissue-Tech medium) using liquid nitrogen. These blocks were cut serially in 8 μm tangential sections and collected on a glass slide. Phosphate buffer saline solution was used as mounting medium.

The mounted thawed sections were viewed under a universal Zeiss microscope equipped with a rotatable polarizer and video camera (Fig. 6.1). Image acquisition and optical measurements

Table 6.1 Abbreviations used in histological sections

h	horizontal cell
INL	Inner nuclear layer
IPL	Inner plexiform layer
Lam	Lamella
Lcis	Long cone inner segment
Lcos	Long cone outer segment
LSis	Long single inner segment
LSos	Long single outer segment
mi	mitochondrion
ml	measurement line (transect)
Nu	nucleus
ONL	Outer nuclear layer
OPL	Outer plexiform layer
Pg	Pigment granule
Pl	Platelet
r	rod
Ris	Rod inner segment
RNu	Rod nucleus
Ros	Rod outer segment
SbNu	Short bilobed cone nucleus
Sbis	Short bilobed cone inner segment
Sbos	Short bilobed outer segment
TC	Tapetal crystal
VCL	Visual cell layer

Figure 6.1 Diagram of the microscope optics showing numerical apertures (NAs) of the objectives used. The polarizer could be rotated to accommodate incident E-vectors from 0° to 90° (corresponding to the plane perpendicular to the page, and the plane of the page).

Fig. 6.1

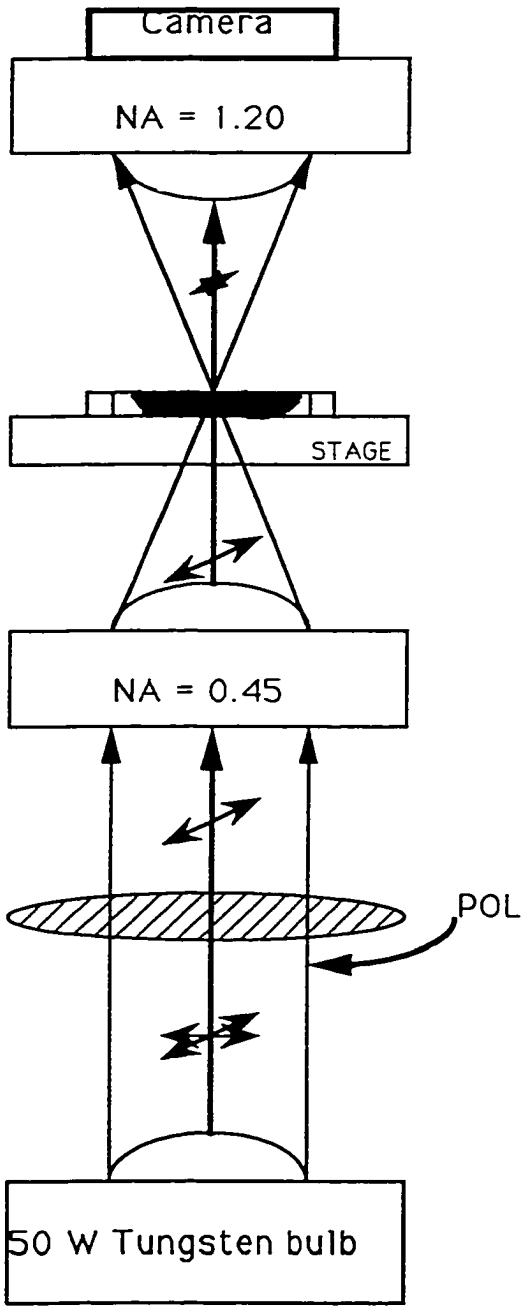

were conducted using Optimas (version 5, Optimas Corp.,Edmonds, Wa.). Using this software, the light transmitted through a given transect of pixels was measured. The output was expressed as relative transmission, measured from 0 (total absorbance) to 365 units (complete transmission), as a function of the distance along the transect (measurement line), which was arbitrarily divided into 65 equal segments. Maintaining the same transect for a given set of measurements, and re-acquiring the image at 3 different orientations of the polarizer (0°, 45° and 90°), I was able to measure the differences in light transmission with E-vector angle for specific cone orientations. Differences in light transmission due to optical inhomogeneities of the condensor lens and the polarizer were accounted for by measuring the light transmitted, for each polarizer orientation, in neighbouring areas of the preparation devoid of retinal tissue and multiplying the results by correction ratios (an identical procedure to that for MSP measurements in chapter 4). The three cone orientations were such that the 45° polarizer position made an actual angle of 90° with the lamellar length plane (see Fig. 6.6). These measurement positions covered the limits of the range possible due to a fixed microscope stage and restricted rotation of the polarizer to one quadrant of the trigonometric circle. Measurements were made on outer segment sections from 5 rods and 5 cones (long and short bilobed ones). If the extent of

absorption was a consequence of lamellar orientation, then I expected to see a difference in light transmitted with E-vector orientation in cones but not rods. The reason being that only cones show lamellae parallel to their long axis (see results section).

To verify the identity of photoreceptors during optical measurements, the remaining parts of frozen blocks (after cryosection) were thawed and prepared for TEM. Thin sections (70 μm thick) were obtained showing the photoreceptor types present in the last frozen sections.

6.3 Results

6.3.1 Electrophysiology

The northern anchovy exhibited a single peak spectral sensitivity ON response with maximum around 500 nm (Fig. 6.2A). The OFF response was similar in spectral range but showed lower amplitude. These results were constant (within error limits) for all adapting backgrounds used. No sensitivity was found below 400 or above 620 nm, the lower limit being a possible consequence of lens transmission cutoff.

Using a 500 nm light stimulus, the polarization sensitivity curve obtained for the ON response was unimodal and maximal at 90° E-vector angle (Fig. 6.2B). The maximum modulation depth in polarization sensitivity was approximately 0.41 log units.

Figure 6.2 (A) Spectral sensitivity function showing a one peak maximum at 500 nm under the previous photopic backgrounds (n=10). K_m values are: 1.037 (ON), and 0.918 (OFF), and sum of squares differences between model and real values are: 0.133 (ON) and 0.185 (OFF). Maximum threshold sensitivities are at 500 nm, with mean values: -12.82 (ON) and -13.1 (OFF). **(B)** Polarization sensitivity function for the ON component with maximum at 90° (horizontal E-vector) under the middle mechanism isolating background.

Fig. 6.2

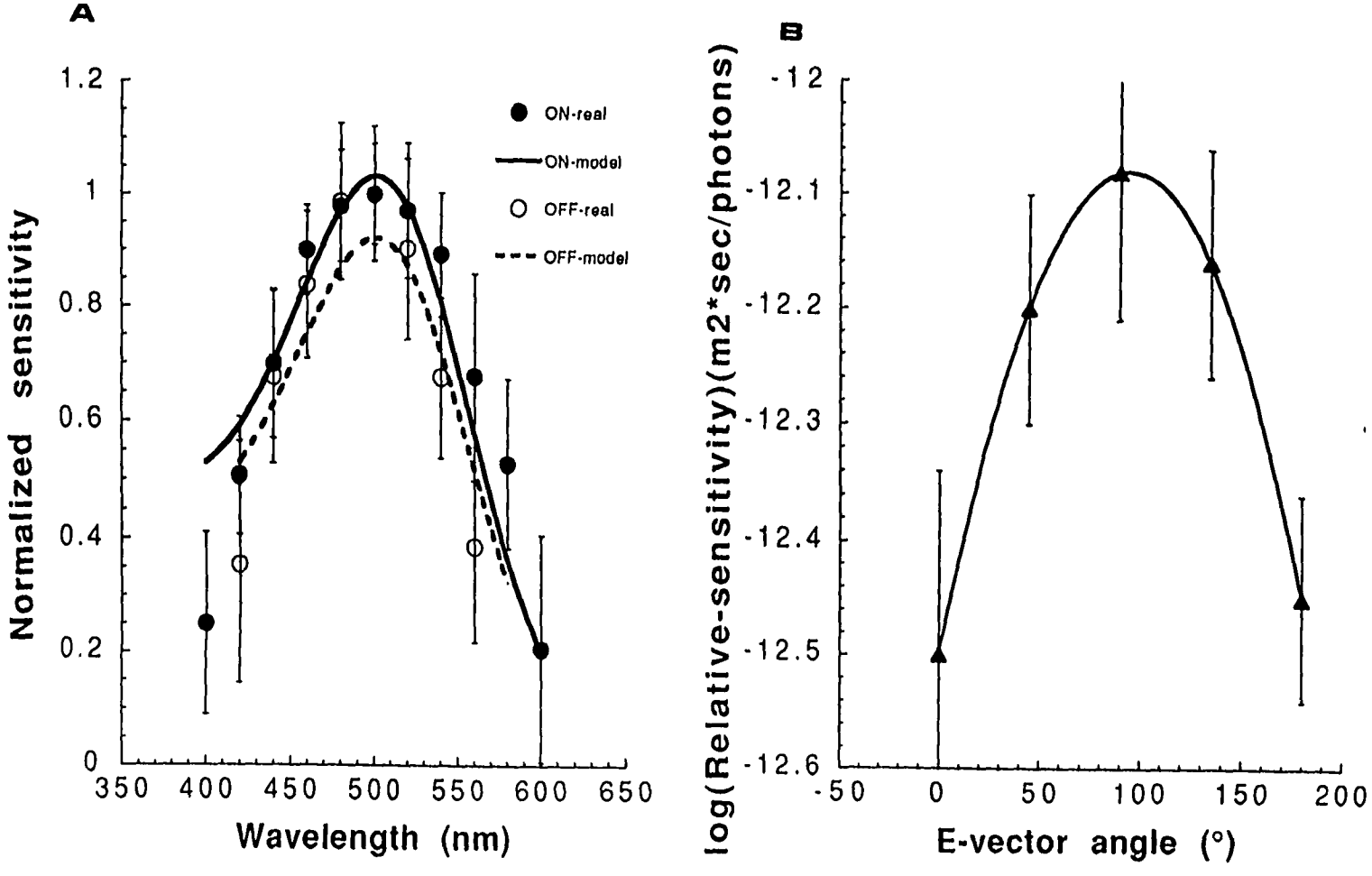
A
Normalized sensitivity
1.2
1
0.8
0.6
0.4
0.2
0
350 400 450 500 550 600 650
Wavelength (nm)
ON-real
ON-model
OFF-real
OFF-model
B
log(Relative-sensitivity)(m2*sec/photons)
-12
-12.1
-12.2
-12.3
-12.4
-12.5
-12.6
-50 0 50 100 150 200
E-vector angle (°)

6.3.2 Histology

The northern anchovy exhibits two types of cones in the central retina: long single and short bilobed ones (Figs. 6.3A-E). Given the overlap between the short bilobed and long cone outer segments (Fig. 6.3B and tangential sections not shown), over 90% of the light must pass through the lobed outer segments before reaching the long cone outer segment.

The lamellae of short and long cones are oriented parallel to the long axis of the cones (Figs. 6.3B,C). In tangential cross section, these lamellae are perpendicular to each other (see Fig. 6.4). The long cone's outer segment long axis (viewed tangentially) is directed naso-temporally in the retina, the opposite is true for the short cone's bilobed outer segment (Fig. 6.4). Rod lamellae are perpendicular to the rod's length axis, as is the case for all other vertebrates examined so far (Figs. 6.3B,D).

Near the pigment epithelium, rows of rods and long cones's outer segments alternate dorso-ventrally throughout the retina (Fig. 6.4A). Rows of rods are usually clusters of 2 to 5 rods widthwise, the cones's outer segments stand alone (Fig. 6.4B). More vitreously, the inner segment of long cones is visible along with the first signs of bilobed outer segments (Fig. 6.4C). As deeper sections are cut, photoreceptoral units comprising a small area of long cone inner segment and two bilobed outer segments appear (Fig. 6.4D). These units, link vitread form continuous rows (Fig. 6.4E), that run dorso-

Figure 6.3 (A) Radial LM section of an adult northern anchovy retina, bar = 10μm. **(B)** Oblique TEM section of a bifid cone showing the two half outer segment lobes protruding into the sides of the long cone inner segment, bar = 4μm. **(C)** Lamellae of long cone outer segment, and platelet stacks, running parallel to the long axis of the cone, bar = 1.5μm. **(D)** Radial section at the inner segment level of short bilobed cones. There is a progression of higher mitochondrial packing from the myoid to the ellipsoid. Also, as in other fishes's cones, mitochondrial development appears to follow this gradient. Long cones's mitochondria are more packed towards their outer segments; below the short cones's outer segments, long cones's inner segments show prominent smooth endoplasmic reticulum cisternae and filamentous networks. An electron-transparent body (perhaps a "connecting structure", see Fineran & Nichol, 1978) is indicated by the tailed arrow, bar = 4.5μm. **(E)** Detail of the membrane separation between cone types prior to the photoreceptor nuclei level (ONL). Notice the large numbers of microtubules (tailed arrow) at the base of the long cones, and between cone types, bar = 2.7μm.

Fig. 6.3

Figure 6.4 **(A)** Tangential section showing rows of long cone outer segments and rods, bar = 1.8μm. **(B)** Higher magnification of long cone outer segment, bar = 0.5μm. **(C)** Oblique section showing the disappearing base of the long cone outer segment in one "bifid" unit, and the surging bilobed outer segments of short cones in another "bifid" unit. Double arrows point in the directions of lamellar orientations; these are orthogonal between cone types. This section should be rotated 90° clockwise to be in the same orientation as (A) and (B), bar = 1μm. **(D)** Tangential section at the outer segment level of short cones, bar = 2μm. **(E)** Oblique section of cone rows. Triple arrow in lower row shows membrane apposition between inner segments of both cone types, bar = 1.5μm. **(F)** Alternating rows of cone and rod nuclei; long cone nuclei are located more sclerally and thus do not appear in this section, bar = 1.5μm.

Fig. 6.4

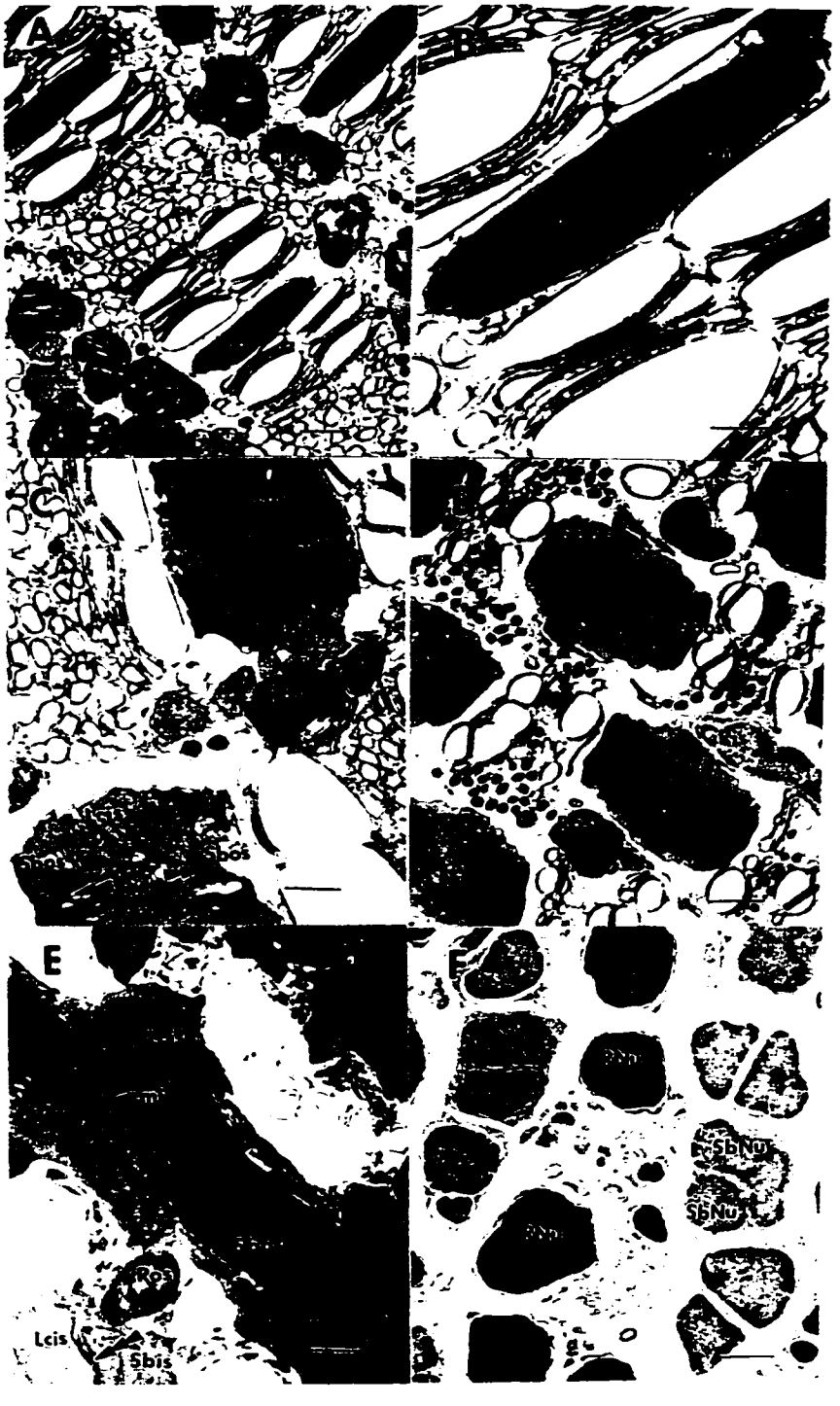

ventrally along the retina. The alternating cone-rod pattern is also visible at the nuclear cell layer (Fig. 6.4F).

In contrast to this regular cone pattern, some peripheral areas exhibit single long cones with lamellae perpendicular to the cone's length axis (Fig. 6.5). Short bilobed cones are also present in these areas. At this stage, it is interesting to note that only short bilobed cones were found to have lamellae oriented parallel to the cone's long axis in the black sea anchovy (*Engraulis encrasicholus*, Zueva, 1980). Unfortunately, there is no indication of the retinal locations sampled by this author in his report.

6.3.3 Optical analysis of frozen retinae

Transmission of light through cone outer segment lamellae varied with E-vector angle (Fig. 6.6). Transmission was highest when the E-vector of the incident light was perpendicular to the length plane of the lamellae (Fig. 6.6E). The ratio between highest and lowest transmittance varied between 1.03 and 1.15 for all the cone measurements pooled together. By comparison, no discernable variation was detected radially through rod outer segments with polarizer angle (Fig. 6.6C).

6.4 Discussion

6.4.1 Perception of polarized light and potential uses

The unequivocal detection of E-vector patterns in the

Figure 6.5 (A) Peripheral radial section showing long single cone with membrane perpendicular to its long axis, bar = 1.7μm. **(B)** Magnification of the long single cone outer segment in (A), bar = 0.6μm.

Fig. 6.5

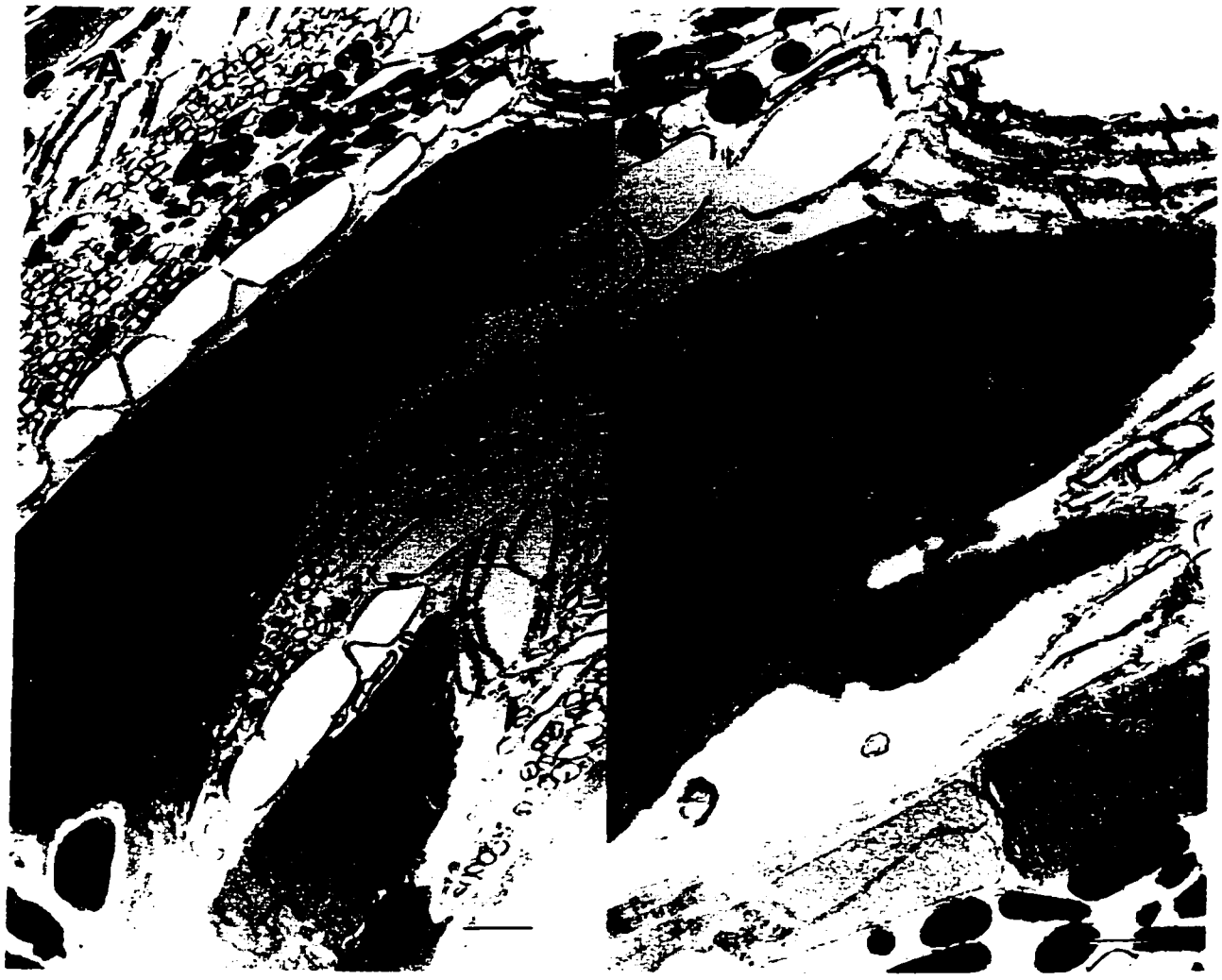

Figure 6.6 (A) Tangential LM of rod rows near the sclera, bar = 15μm. **(B)** TEM section of rod rows showing measurement line and E-vector orientations, bar = 1.5μm. **(C)** Measurements for two rods showing representative differences in relative transmittance for the three polarizer positions. No significant differences were ever detected. **(D)** Tangential LM of rods and long cone outer segments, bar = 15μm. **(E)** Measurement line and E-vector orientations for a long cone (Lc) outer segment (the cone orientations with respect to polarizer angle were the same for measurements involving short bilobed (Sb) cone outer segments), bar = 0.65μm. **(F)** Measurements for two short bilobed and two long cones showing representative differences in relative transmission for the three polarizer angles; relative transmission was highest for the 45° E-vector orientation. For clarity, different constants have been added to the various sets of photoreceptor measurements so the curves would not overlap.

Fig. 6.6

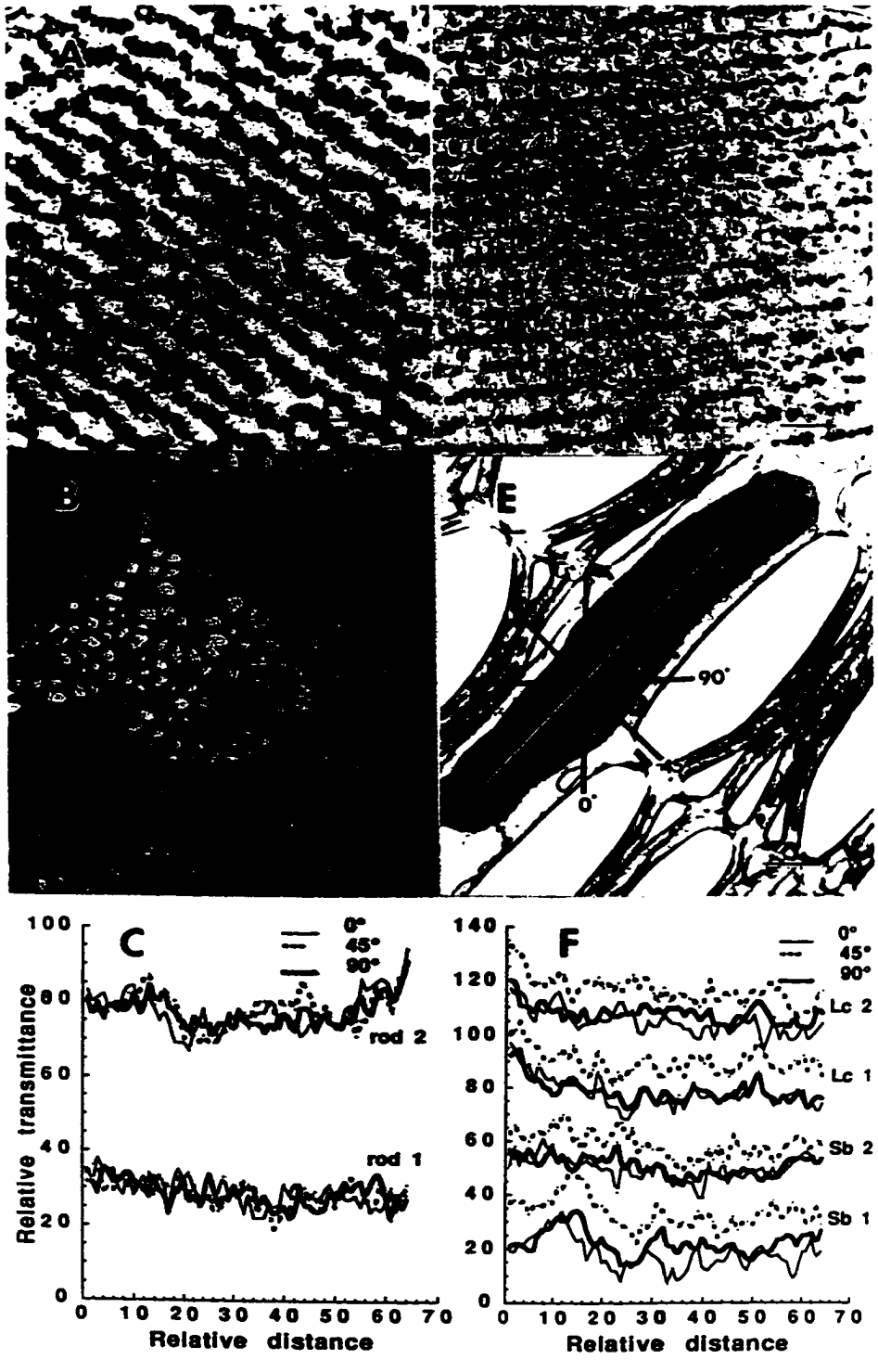
A
B
E
90°
0°
C
0°
45°
90°
rod 2
rod 1
Relative transmittance
Relative distance
F
0°
45°
90°
Lc 2
Lc 1
Sb 2
Sb 1
Relative distance

environment requires at least two distinct polarization detectors and a luminosity detector (i.e. a 3-dimensional system, Bernard & Wehner, 1977). Alternatively, a two-dimensional system could be used to detect percent polarization; but E-vector analysis would be difficult due to the presence of "confusion states" (Bernard & Wehner, 1977). The northern anchovy, having only one cone mechanism (Fig. 6.2A), exhibits a two dimensional system.

The fact that the anchovy may be limited in its perception of E-vector patterns suggests that it is perhaps the detection of percent polarization that is most important to the animal. This suggestion is supported by two observations: 1) E-vector patterns in the water column are seldom useful for orientation as they are easily disrupted by overcast and waves (chapter 2), and 2) the ventro-temporal orientation of cone rows throughout the anchovy retina appears to form a parallel scanning system optimally suited for the detection of percent polarized light in turbid waters, and during crepuscular periods. In this regard, one should note that stacks of orthogonal dichroic filters (like those in the anchovy retina) result in high photoreceptor polarization sensitivity even at low light intensities (Snyder, 1973b).

During clear-sky crepuscular periods, we have seen that over 60% of the downwelling light can be polarized in the horizontal direction (chapter 2). Upon Rayleigh scattering by particles in the water column, this light remains,

theoretically, with maximum polarization in the horizontal direction, 90° to the orientation of the scattering dipole (chapter 1). Hence, while swimming horizontally during crepuscular periods, the majority of cone rows in the anchovy retina are stimulated uniformly by highly polarized light. Detection of this polarized light, which matches in E-vector orientation the lamellar orientation of the long cones, is likely used by the anchovy to detect planktonic prey that diffuse the background polarization (Fineran & Nicol, 1978; Novales Flamarique & Hawryshyn, 1993; see also Jones & Fairney, 1989). Crepuscular periods are further favourable for polarized light detection because the intensity of downwelling incident light varies little with azimuth (chapter 2 and personal observations). This minimizes "confusion states" due to differences in background intensity (see Bernard & Wehner, 1977).

6.4.2 Enhancement of polarization signals

Although MSP measurements on dark adapted cells have yet to be made on anchovy cones, the evidence presented in this study suggests a functional similarity between the crustacean and cephalopod rhabdoms and the anchovy "bifid" cone unit (Figs. 6.4-6.6; Moody & Parriss, 1961; Snyder, 1973b; Bernard & Wehner, 1977). The stacked layers of orthogonal microvilli present in crustacean-like rhabdoms (Eguchi & Waterman, 1965) lead to E-vector filtering and enhanced polarization

sensitivity of the entire rhabdom (Shaw, 1969; Snyder, 1973b). The same filtering process by stacked cells with orthogonal microvilli leads to enhanced polarization sensitivity in flies and bees (e.g. in the fly, the polarization sensitivity of cell 8 is enhanced due to the filtering process of cell 7; Snyder, 1973b). Furthermore, theoretical and experimental results show that this enhancement mechanism is improved when both cells possess the same photopigment, and when the cells are not electrically coupled (Snyder, 1973b; chapter 1). In analogy with the crustacean system of orthogonal microvilli, the northern anchovy shows orthogonal disposition of cone lamellae between cone types. As well, our spectral sensitivity measurements indicate the presence of only one type of cone pigment in the retina of this animal. These observations suggest that the bilobed outer segments of "bifid" cones act to enhance the polarization sensitivity of the adjacent long cones. The single peak curve obtained during polarization sensitivity experiments supports this hypothesis as it shows a strong long cone contribution to the polarization sensitivity response (Fig. 6.2B; long cone lamellae are oriented horizontally in the anchovy eye). Nonetheless, this response may be the result of a subtractive interaction between outputs from both cone types, as postulated for orthogonal rhabdomeres in the POL area of terrestrial arthropods (Labhart 1980, 1988; Wehner 1983, 1989).

6.4.3 Maximization of photon capture

The northern anchovy possesses two major retinal adaptations to maximize photon capture. The first is a combination of photoreceptor packing into rows (Fig. 6.3), and uneven "vertical" placement of cone types (Fig. 6.4). The second is the stacked arrangement of platelets surrounding the cone outer segments (Fig. 6.3B; Fineran & Nicol, 1978), and the presence of tapetal crystals in the retinal pigment epithelium (RPE; Fineran & Nicol, 1978).

Cone packing into rows has been observed among fish living in low light environments, presumably to maximize photon capture (Boehlert, 1978; Lythgoe, 1979). As well, cone rows are apparent among schooling fish where quick motion detection of reflection flashes may keep the schools oriented (Blaxter & Pattie Jones, 1967; Denton & Rowe, 1994). Uneven superposition of cone types also enhances photon capture as most incident light must travel first through the bilobed outer segment before reaching the long cone outer segment.

Once the light has travelled through the cone layer, it may still regain the cones due to reflection by tapetal crystals, or platelet-mediated reflection (Fineran & Nichol, 1978). Platelet-mediated reflection is especially interesting because of the platelet stacking direction along the long cones's outer segments (Figs. 6.3C, 6.4A). According to Fresnel's theory, reflection of unpolarized light at a dielectric interface will result in partially polarized light with E-

vector perpendicular to the plane of incidence (chapters 1,4). At Brewster's angle (when $\theta_r + \theta_t = 90°$), the reflected light will be 100% polarized. Given the high angles of incidence which photons traversing short cones's outer segments make with the platelet surface, the stacks of platelets in the anchovy retina could thus act as "stack-of-plates" polarizers (Fig. 6.7). Two main absorption processes can ensue. If the reflected photons are incident directly on the sides of the long cone outer segment (i.e. normal to the lamellar surface), most will be absorbed as there is no preferred orientation for chromophoric absorption in this case. If, however, the photons travel towards the tapetal crystals (located above the platelet stacks), and reflect back to the outer segment, only photons with E-vectors mostly parallel to the lamellar plane will be absorbed. However, as can be seen in the diagram, the majority of photons are already polarized along this plane (Fig. 6.7). Finally, since there are few if any platelets between the long cone outer segment and the rods, reflection in this direction (which would lead to E-vectors transverse to the chromophore orientation) is minimal. These observations suggest that the total reflection mechanism enhances photon capture of the long cone, while optimizing the polarized light detection system.

6.4.4 Orthogonal dichroic polarizers in the anchovy retina

The differential absorption exhibited by cone but not rod

Figure 6.7 Reflection of light from the platelet stacks in the anchovy retina. Also shown in this diagram are the lamellar orientations for each outer segment, and the preferential absorption of photons with E-vectors along the long axis of the lamellar planes. Long cone outer segments lengths should be twice those drawn. φ_i is the angle of incidence, φ_r the reflection angle, and φ_t the transmission angle (or refraction angle).

Fig. 6.7

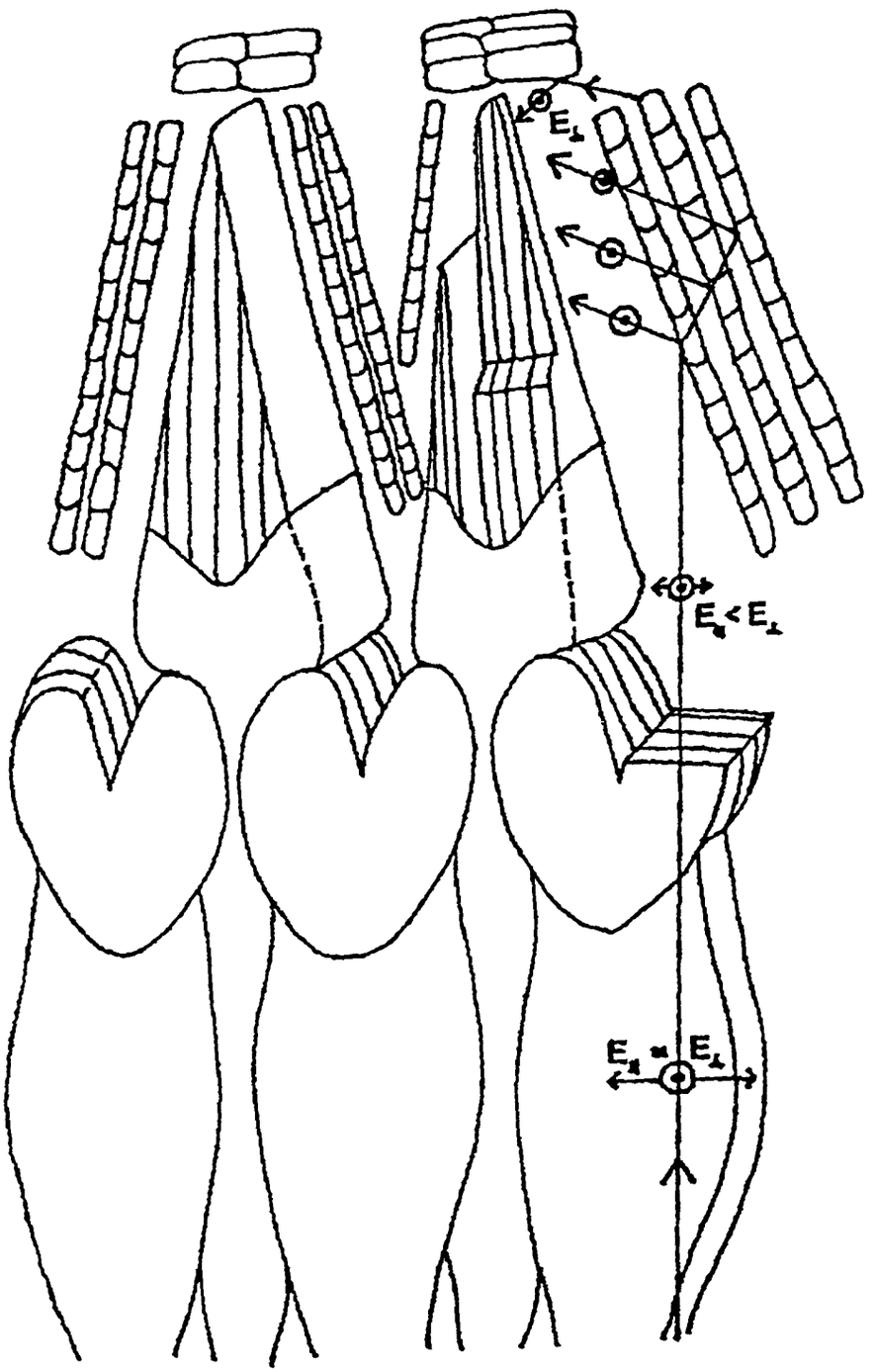

lamellae (Fig. 6.6) corroborates anatomical observations which show both photoreceptor types to be structurally different. In addition, these observations support the hypothesis that anchovy cones are dichroic due to either form (Hárosi, 1981), or dichroic absorbance of the photopigment molecules.

Measured dichroic ratios obtained using MSP for various fish and amphibian species range approximately from 1.5 to 4.5 (e.g. Hárosi, 1975; Hárosi & MacNichol, 1974). These ratios are calculated as the ratio of intensities transmitted when "typical" photoreceptor outer segments are illuminated from the side with E-vectors parallel and perpendicular to the lamellar surface. Such a procedure is in principle equivalent to our optical measurements since the anchovy's cone lamellae are parallel to the long axis of the cone. In evaluating our results however, it is important to emphasize that the measurements were made on light-adapted moderately-fixed retinae. Two main consequences result from this experimental protocol: 1) absorbance by pigment molecules is greatly diminished through bleaching (e.g. Wald et al., 1955), and 2) directional chromophoric absorption also decreases due to multiple detachments of chromophores from opsins during the bleaching process (Hargrave & McDowell, 1992). Nevertheless, because of spontaneous opsin-chromophore regeneration in the live retina, and the decreasing effectiveness of phototransduction as the active pigment concentration is reduced, 5-10% of the dark-adapted pigment concentration may

still remain in the isolated light-adapted retina (Rushton, 1961). These chromophore-opsin complexes, and those stopped prior to the Meta II transduction stage absorb photons with E-vectors in the direction of the chromophore axis preferentially (Chabre & Breton 1979; Chabre, 1985). And these chromophores are oriented parallel to the lamellar surface within, approximately, 11° (Chabre, 1985). It may therefore be that it is the structural properties of these attached chromophore complexes that are responsible for the small differences in absorbance observed.

In this regard, it is worth noting that MSP measurements on light-adapted carp retina exhibit dichroic ratios of 1.2 (Hawrsyshyn & Hárosi, 1991). Such a value is very close to the range of absorbance ratios obtained in this study, especially when considering that our 0° and 90° E-vector conditions were not parallel to the lamellar long axis (Fig. 6.6). If photopigment dichroism indeed underlies the results observed, the anchovy detection system for polarized light would be somewhat analogous to that of marine invertebrates except for having phospholipid lamellae in place of microvilli to restrict chromophoric orientation (Moody & Parriss, 1960; Goldsmith & Wehner, 1977; Wehner, 1983, 1989; Shashar & Cronin, 1996).

Chapter 7: General Discussion

This thesis has contributed to the field of vertebrate detection of polarized light in the following ways: 1) it has improved the characterization of the polarized light field underwater, and provided evidence suggesting that polarization sensitivity is primarily a crepuscular capability in fishes, 2) it has presented a general mechanism for polarization detection based on reflection from paired cone partitions, 3) it has presented a simple neural model that can reproduce polarization sensitivity results observed for vertebrates to date, 4) it has given a new role to the ordered cone mosaic in polarization detection, and 5) it has demonstrated polarization sensitivity in the northern anchovy and provided evidence for lamellar dichroism as the possible mechanism for polarization detection in this group of fishes.

The similarity in retinal structure between fish, other lower vertebrates and birds suggests that the reflection-based mechanism for polarization detection should be applicable to other animals with similar retinas. Such mechanism, in conjunction with another based on scattering of light by oil droplets (Young & Martin, 1984), gives a general framework to understand polarization detection in vertebrates (with special cases like the anchovies exempted, although the neural model can still be applied in this case). The lack of double cones in mammals and their general inability to detect polarized light are consistent with the detection mechanism and MSP

results (see chapter 4).

Even though polarization sensitivity has been observed in this and other studies (e.g. Parkyn & Hawryshyn, 1993; Coughlin & Hawryshyn, 1995), the contradictory results reported for some fish species (chapter 3) and migratory birds (Coemans et al., 1990; Vos Hzn et al., 1995) indicate that further experimentation is necessary. In trout, for instance, polarization sensitivity is not found in all animals, using the optic nerve recording technique in this thesis (chapter 2). Although this may be a consequence of electrode placement (i.e. compartmentalization of polarization-sensitive fibres in the optic nerve), and/or the less-likely possibility that only some animals are polarization-sensitive, other factors may influence the results obtained. For instance, incomplete retinal adaptation before the testing phase, changes in fish physiology during the experiment, and small, unpredicted changes, in background or stimulus intensities are all factors that may result in erroneous polarization sensitivity curves. This is especially a concern when the variation between data points is little beyond the error range of the technique used, as is the case here. In this thesis, I have discarded results that looked suspicious due to any of the above factors. Individual data points were repeated at least twice, and I made sure that the third order polynomial fit to each set of data points was precise ($R^2>0.98$, see electrophysiology technique, chapter 2). Other (behavioural) experiments used to

support the contention of polarization sensitivity in vertebrates suffer from small sample size and great variability in the results observed; one should therefore be prudent in drawing conclusions from such studies. Further research in vertebrate polarization systems should have different laboratories confirm the results obtained to date, especially as these results have only been obtained by a handful of researchers from only two laboratories primarily.

Much of the mystique behind polarization sensitivity in vertebrates would be overcome if someone were to report polarization sensitive cells using intracellular recording. Such cells have been found projecting from the cricket POL area (Labhart 1988, 1996). They exhibit 180° periodicity in their firing pattern and are insensitive to intensity modulations over a 2-3 log unit range. The results from this thesis suggest that such interneurons should be found in the centro-temporal retina of fish, if anywhere (chapters 2,4,5). Such an area may be the POL area of vertebrates with polarization detection capabilities.

In addition to these experiments, intracellular recordings should also be carried out for additional fish groups besides salmonids and cyprinids. The detection mechanism presented in this thesis predicts that fishes with square and/or row mosaics, with double cones similar to those in trout, should exhibit polarization sensitivity. Furthermore, this mechanism also predicts polarized light detection properties of single

cones (regardless of photopigment content) provided these face the partition membrane of paired cones and an anisotropy such as the partition tilt is present and is regularly distributed in the mosaic. Other anisotropies like oil droplets and differing concentrations of mitochondria between members of the double cone could also lead to the required reflection and/or scattering. For fishes with twin cone mosaics, the detection mechanism herein could explain future polarization sensitivity results based on polarized light created by reflection at the partition. However, if such fish exist that have polarization sensitivity, I predict that the cones will twist (e.g. Wahl, 1994), rendering orthogonal partitions parallel and perpendicular in orientation at the ellipsoid level, or that an area of the retina, different from the typical arrangement observed for green sunfish (Cameron & Easter, 1993), will show such disposition without twist. As it stands now, the controversial polarization sensitivity in sunfishes requires very complex processing by unidentified neurons, or for the fish to swim at 45° angles (to match the parallel and perpendicular polarizations, see chapter 3).

The predictions outlined above are all amenable to testing and I encourage future research to do so. Much as the evidence supports the detection mechanism and neural model presented in this thesis, the validity of these hypotheses and previous polarization sensitivity results relies in their confirmation and repeatability. Besides which, other mechanisms for

polarization detection may still await discovery.

Literature Cited

-Able, K.P. (1982). Skylight polarization patterns at dusk influence migratory orientations in birds. Nature, 299, 550-551.

-Adler, K. & Phillips, J.B. (1985). Orientation in a desert lizard (*Uma notata*): time-compensated compass movement and polarotaxis. Journal of Comparative Physiology A, 156, 547-552.

-Ahlbert, I.-B. (1969). The organization of the cone cells in the retinae of four teleosts with different feeding habits (*Perca viatilis* L., *Lucioperca lucioperca* L., *Acerina cernua* L. and *Coregonus albula* L.). Arkiv fur Zoologie, 22, 445-481.

-Ahlbert, I.-B. (1975). Organization of the cone cells in the retinae of Salmon (*Salmo salar*) and Trout (*Salmo trutta trutta*) in relation to their feeding habits. Acta zoologica (Stockholm), 57, 13-35.

-Ahnelt, P.K., Hokoç, J. N. & Röhlich, P. (1995). Photoreceptors in a primitive mammal, the South American opossum, *Didelphis marsupialis aurita*: Characterization with anti-opsin immunolabeling. Visual Neuroscience, 12, 793-804.

-Ali, M.A. & Anctil, M. (1976). The Retinas of Fishes: An Atlas. Berlin: Springer.

-Bandai, K., Arikawa, K. & Eguchi, E. (1992). Localization of spectral receptors in the omnatidium of the butterfly compound eye determined by polarization sensitivity. Journal of Comparative Physiology A, 171, 289-297.

-Barer, R. & Joseph, S. (1954). Refractometry of living cells. Part I. Basic Principles. Quarterly Journal of Microscopial Science, 95, 399-423 (1954).

-Beaudet, L., Browman, H.I. & Hawryshyn, C.W. (1993). Optic nerve response and retinal structure in rainbow trout of different sizes. Vision Research, 33, 1739-1746.

-Behroozi, F. & Luzader, S. (1987). On the reflection of polarized light at surfaces. American Journal of Physics, 55, 279-280.

-Bennett A.T.D., Cuthill I.C., Partridge J.C. & Maier E.J. (1996). Ultraviolet vision and mate choice in zebra finches. Nature 380: 433-435.

-Berger, E.R. (1967). Subsurface membranes in paired cone photoreceptor inner segments of adult and neonatal *Lebistes* retinae. Journal of Ultrastructure Research, 17, 220-232.

-Berger, E.R. (1966). On the mitochondrial origin of oil droplets in the retinal double cone inner segments. Journal of Ultrastructure Research, 14, 143-157.

-Bernard, G.D. (1987). Spectral characterization of butterfly L-receptors using extended Dartnall/McNichol template functions. Journal of the Optical Society of America A, (2) 4, 123.

-Bernard, G.D. (1975). Physiological optics of the fused rhabdom. *In* Photoreceptor Optics. *Edited* by A.W. Snyder and R. Menzel. Springer-Verlag, New York. pp. 78-97.

-Bernard, G.D. & Wehner, R. (1977). Functional similarities

between polarization vision and color vision. Vision Research, 17, 1019-1028.

-Biggs, W.W. (1984). Li-1800 underwater spectroradiometer instruction manual. Publication no. 8405-0037. LiCor-Inc.

-Bill, R. (1990). Haidinger's Brush. In: The Physics Teacher (Stony Brook, NY), 28: 598

-Born, M. & Wolf, E. (1975). Principles of optics. Pergamon Press, Oxford.

-Brines, M.L. & Gould, J.L. (1982). Skylight polarization patterns and animal orientation. Journal of Experimental Biology, 96, 69-91.

-Blaxter, J.H.S. & Pattie Jones, M. (1967). The development of the retina and retinomotor responses in the herring. Journal. Marine Biological Association of the UK, 47, 677-697.

-Boehlert, G.W. (1978). Intraspecific evidence for the function of single and double cones in the teleost retina. Science, 202, 309-311.

-Bowmaker, J.K. & Kunz, Y.W. (1987). Ultraviolet receptors, tetrachromatic colour vision and retinal mosaics in brown trout (*Salmo trutta*): Age dependent changes. Vision Research, 27, 2101-2108.

-Browman, H.I., Novales Flamarique, I. & Hawryshyn, C.W. (1994). Ultraviolet photoreception contributes to the foraging performance of two species of zooplanktivorous fishes. Journal of Experimental Biology, 186, 187-198.

-Browman, H.I. & Hawryshyn, C.W. (1992). Thyroxine induces a

precocial loss of ultraviolet photosensitivity in rainbow trout (*Oncorhynchus mykiss*). Vision Research, 32, 2303-2312.

-Caceci, M.S. & Cacheris, W.P. (1984). Fitting curves to data, the Simplex algorithm is the answer. Byte, 5, 340-360.

-Cameron, D.A & Easter, S.S.Jr. (1993). The cone photoreceptor mosaic of the green sunfish, *Lepomis cyanellus*. Visual Neuroscience, 10, 375-384.

-Cameron, D.A. & Pugh, E.N.Jr. (1991). Double cones as a basis for a new type of polarization vision in vertebrates. Nature, 353, 161-164.

-Chabre, M. (1985). Trigger and amplification mechanisms in visual phototransduction. Annual reviews in Biophysics and Chemistry, 14, 331-360.

-Chabre, M. & Breton, J. (1979). Orientation of aromatic residues in rhodopsin. Rotation of one Tryptophan upon the Meta I-Meta II transition after illumination. Photochemistry and Photobiology, 30, 295-299.

-Charman, W.N. & Tucker, J. (1973). The optical system of the goldfish eye. Vision Research, 13, 1-8.

-Chen, H. & Nagaraja Rao, C.R. (1968). Polarization of light on reflection by some natural surfaces. British Journal of Applied Physics, 2, 1191-1200.

-Cherry, R.J. & Chapman, D. (1969). Optical properties of black lecithin films. Journal of Molecular Biology, 40, 19-32.

-Coemans, M.A.J.M., Vos Hzn, J.J. & Nuboer, J.F.W. (1990). No

evidence for polarization sensitivity in the pigeon. Naturwissenschaften 77, 138-142.

-Cone, R.A. (1972). Rotational diffusion of rhodopsin in the visual receptor membrane. Nature. New Biology, 236, 39-43.

-Coughlin, D.J. & Hawryshyn, C.W. (1995). A cellular basis for polarized-light vision in rainbow trout. Journal of Comparative Physiology A, 176, 261-272.

-Craig, B. (1984). Polarization of skylight. Weatherwise, 37: 261-265.

-Craig, R.A. (1965). The Upper Atmosphere. Meteorology and Physics. pp. 412-422.

-Cronin, T.W., Marshall, N.J, Quinn, C. & King, C. (1994). Ultraviolet photoreception in mantis shrimp. Vision Research, 34, 1443-1452.

-Davitz, M.A. & MacKaye, K.R. (1978). Discrimination between horizontally and vertically polarized light by the cichlid fish *Pseudotropheus macrophthalmus*. Copeia, 2, 333-334.

-Dearry, A. & Barlow, R.B. (1987). Circadian rhythms in the green sunfish retina. Journal of General Physiology, 89, 745-770.

-Denton, E.J. & Rowe. D.M. (1994). Reflective communication between fish, with special reference to the greater sand eel, *Hyperoplus lanceolatus*. Philosophical Transactions of the Royal Society of London, 334, 221-237.

-De Smet, D.J. (1994). Brewster's angle and optical anisotropy. American Journal of Physics, 62, 246-248.

-Dill, P.A. (1971). Perception of polarized light by yearling sockeye salmon. Journal. Fisheries Research Board of Canada, 28, 1319-1332.

-Duelli, P. & Wehner, R. (1973). The spectral sensitivity of polarized light orientation in *Cataglyphis bicolor* (Formicidae, Hymenoptera). Journal of Comparative Physiology, 86, 37-53.

-Eguchi, E. & Waterman, T.H. (1968). Cellular basis for polarized light perception in the spider crab *Libinia*. Zitschrift fuer Zellforschung und Mikroskopische Anatomie, 84, 87-101.

-Engström, K. (1963). Cone types and cone arrangements in teleost retinae. Acta Zoologica, 44, 179-243.

-Enoch, J.M. (1961). Visualization of waveguide modes in retinal receptors. American Journal of Ophthalmology, 51, 1107-1118.

-Fawcett, D.W. (1966). An atlas of fine structure. The cell, its organelles and inclusions. London: W.B. Saunders Company. pp. 68-76.

-Fein, A. & Szuts, E.Z. (1982). Photoreceptors: their role in vision. Cambridge University Press, Cambridge. pp. 72-93.

-Ferrero, E., Anctil, M. & Ali, M.A. (1979). Ultrastructural correlates of retinomotor responses in inner segments of vertebrate photoreceptors. Révue Canadienne de Biologie, 38, 249-264.

-Fineran, B.A. & Nicol, J.J.A.C. (1978). Studies on the

photoreceptors of *Anchoa mitchilli* and *A. hepsetus* (*Engraulidae*) with particular references to the cones. Philosophical Transactions of the Royal Society of London B, 283, 25-60.

-Fineran, B.A. & Nicol, J.A.C. (1976). Novel cones in the retina of the anchovy (*Anchoa*). Journal of Ultrastructure Research, 54, 296-303.

-Fleishman, L.J., Loew, E.R. & Leal, M. (1993). Ultraviolet vision in lizards. Nature, 365, 397.

-Fortini, M.E. & Rubin, G.M. (1991). The optic lobe projection pattern of polarization-sensitive photoreceptor cells in *Drosophila melanogaster*. Cell and Tissue Research, 265, 185-191.

-Forward, R.B.Jr., Horch, K.W. & Waterman, T.H. (1972). Visual orientation at the water surface by the teleost *Zenarchopterus*. Biological Bulletin, 143, 112-126.

-Fratzer, C., Dörr, S. & Neumeyer, C. (1994). Wavelength discrimination of the goldfish in the ultraviolet spectral range. Vision Research, 34, 1515-1520.

-Goddard, S.M. & Forward, R.B. Jr. (1991). The role of the underwater polarized light pattern in sun compass navigation of the grass shrimp *Palaemonetes vulgaris*. Journal of Comparative Physiology A, 169, 479-491.

-Goldsmith, T.H. & Wehner, R. (1977). Restrictions on rotational and translational diffusion of pigment in the membranes of a rhabdomeric photoreceptor. Journal of General

Physiology, 70, 453-490.

-Govardovskii, V.I. (1976). Comments on the sensitivity hypothesis. Vision Research, 16, 1363-1364.

-Goyal, I.C., Kumar, A., Sharma, A. and Ghatak, A.K. (1977). Stiles-Crawford effect; an inhomogeneous waveguide model for human cone-receptor. Optik, 49, 39-49.

-Grant, I.S. and Phillips, W.R. (1984). Electromagnetism. John Wiley & Sons Ltd., New York, Toronto, 514 pp.

-Groot, C. (1965). On the orientation of sockeye salmon (*Oncorhynchus nerka*) during seaward migration out of lakes. Behaviour (Supplement), pp. 105-158.

-Hagins, W.A. and Liebman, P.A. (1963). The relationship between photochemical and electrical processes in living squid photoreceptors. Abstract of the Biophysical Society, 7th Annual Meeting, New York.

-Hamdorf, K., Schwemer, J. and Gogala, M. (1971). Insect visual pigment sensitive to ultraviolet light. Nature, 231, 458-459.

-Hargrave, P.A. and McDowell, J.H. 1992. Rhodopsin and phototransduction: a model system for G protein-linked receptors. FASEB, 6, 2323-2331.

-Hárosi, F.I. (1985). Ultraviolet- and violet-absorbing vertebrate visual pigments: Dichroic and bleaching properties. *In* The visual system. *Edited* by A. Fein and J.S. Levine. Liss, New York. pp. 41-45.

-Hárosi, F.I. (1981). Microspectrophotometry and optical

phenomena: birefringence, dichroism and anomalous dispersion. *In* Vertebrate Photoreceptor Optics. *Edited* by J.M. Enoch and F.L. Tobey. Springer Series in Optical Sciences, Springer-Verlag, Berlin. pp. 337-399.

-Hárosi, F.I. (1975). Absorption spectra and linear dichroism of some amphibian photoreceptors. Journal of General Physiology, 66, 357-382.

-Hárosi, F.I. & MacNichol, E.F.Jr. (1974). Visual pigments of goldfish cones. Spectral properties and dichroism. Journal of General Physiology, 63, 279-304.

-Hawryshyn, C.W. (1991). Light adaptation properties of the ultraviolet-sensitive cone mechanism in comparison to the other receptor mechanisms of goldfish. Visual Neuroscience, 6, 293-301.

-Hawryshyn, C.W. and Hárosi, F.I. (1994). Spectral characteristics of visual pigments in rainbow trout (*Oncorhynchus mykiss*). Vision Research, 34, 1385-1392.

-Hawryshyn, C.W. and Hárosi, F.I. (1991). Ultraviolet photoreception in carp: microspectrophotometry and behaviorally determined action spectra. Vision Research, 31, 567-576.

-Hawryshyn, C.W. & Bolger, A.E. (1990). Spatial orientation of trout to partially polarized light. Journal of Comparative Physiology A, 167, 691-697.

-Hawryshyn, C.W., Arnold, M.G., Bowering, E. & Cole, R.L. (1990). Spatial orientation of rainbow trout to plane-

polarized light: The ontogeny of E-vector discrimination and spectral sensitivity characteristics. Journal of Comparative Physiology A, 166, 565-574.

-Hawryshyn, C.W., Arnold, M.G., Chiasson, D. & Martin, P.C. (1989). The ontogeny of ultraviolet photosensitivity in rainbow trout (*Salmo gairdneri*). Visual Neuroscience, 2, 247-254.

-Hawryshyn, C.W. and McFarland, W.N. (1987). Cone photoreceptor mechanisms and the detection of polarized light in fish. Journal of Comparative Physiology A, 160, 459-465.

-Hawryshyn, C.W. and Beauchamp, R. (1985). Ultraviolet photosensitivity in goldfish: An independent U.V. retinal mechanism. Vision Research, 25, 11-20.

-Hecht, E. & Zajac, A. (1974). Optics. Reading, MA: Addison-Wesley Publishing Company, pp. 219-271.

-Horvàth, G. & Varjú, D. (1995). Underwater refraction-polarization patterns of skylight perceived by aquatic animals through Snell's window of the flat water surface. Vision Research, 35, 1651-1666.

-Inoué, S. (1989). Video Microscopy. Plenum Press, NY, London, pp. 477-510

-Ishikawa, T. & Yamada, E. (1969). Atypical mitochondria in the ellipsoid of the photoreceptor cells of vertebrate retinas. Investigative Ophthalmology, 8, 302-316.

-Ivanoff, A. (1974). Polarization measurements in the sea. *In* Optical Aspects of Oceanography. *Edited* by N. Jerlov and E.

Steeman Nielsen. Academic Press, New York. pp. 151-175.

-Ivanoff, A. & Waterman, T.H. (1958). Factors, mainly depth and wavelength, affecting the degree of underwater light polarization. Journal of Marine Research, 16, 283-307.

-Jeffrey, S.W. & Humphrey, G.F. (1975). New spectrophotometric equations for determining chlorophylls a, b, c^1 and c^2 in higher plants, algae and natural phytoplankton. Biochemie und Physiologie der Pflanzen, 167, 191-194.

-Jenkins, F.A. & White, H.A. (1976). Fundamentals of Optics. McGraw-Hill, New York, St. Louis, 746 pp.

-Johnson, W.E. & Groot, C. (1963). Observations on the migration of young sockeye salmon (*Oncorhynchus nerka*) through a large, complex lake system. Journal. Fisheries Research Board of Canada, 20, 919-934.

-Jones, B.F. & Fairney, P.T. (1989). Recognition of shiny dielectric objects by analysing the polarization of reflected light. Image and Visual Computation, 7, 253-258.

-Kawamura, G., Shibita, A. & Yonimori, T. (1981). Response of teleosts to the plane of polarized light as determined by heart rate. Bulletin. Japanese Society of Scientific Fisheries, 47, 727-729.

-Kirschfeld, K. (1973). Vision of polarized light. International Biophysical Congress, Moscow, 4, 289-296.

-Kirschfeld, K. (1969). Optics of the compound eye. *In* Processing of optical data by organisms and machines. Edited by Reichardt. Academic Press, New York, London. pp. 144-166.

-Kunz, Y. W. & Callaghan, E. (1989). Embryonic fissures in teleost eyes and their possible role in detection of polarized light. Transactions of the American Fisheries Society, 118, 195-202.

-Labhart, T. (1996). How polarization-sensitive interneurones of crickets perform at low degrees of polarization. Journal of Experimental Biology, 199, 1467-1475.

-Labhart, T. (1988). Polarization-opponent interneurons in the insect visual system. Nature, 331, 435-437.

-Labhart, T. J. (1980). Specialized photoreceptors at the dorsal rim of the honeybee's compound eye: polarizational and angular sensitivity. Journal of Comparative Physiology A, 141, 19-30.

-Land, M.F. (1987). On the reflection of polarized light at surfaces. American Journal of Physics, 55, 279-280.

-Lehninger, A.L. (1975). Biochemistry, 2nd ed., Worth Publishers Inc., New York.

-Liebman, P.A. & Entine, G. (1974). Lateral diffusion of visual pigment in photoreceptor disk membranes. Science, 185, 457-459.

-Liebman, P.A., Jagger, W.S., Kaplan, M.W. & Bargoot, F.G. (1974). Membrane structure changes in rod outer segments associated with rhodopsin bleaching. Nature, 251, 31-36.

-Loew, E.R., McFarland, W.N., Mills, E.L. & Hunter, D. (1993). A chromatic action spectrum for planktonic predation by juvenile yellow perch, *Perca flavescens*. Canadian Journal of

Zoology, 71, 384-386.

-Loew, E.R. & McFarland, W.N. (1990). The underwater visual environment. *In* Vision in Fishes. *Edited* by R. Douglas and M.B.A. Djamgoz. Chapman and Hall publishers, London. pp. 1-43.

-Lythgoe, J.N. 1979. Ecology of vision. Clarendon Press, Oxford. pp. 141-142.

-Lythgoe, J.N. & Hemmings, C.C. (1967). Polarized light and underwater vision. Nature, 213, 893-894.

-MacNichol, E.F.Jr., Kunz, Y.W., Levine, J.S., Hárosi, F.I. & Collins, B.A. (1978). Ellipsosomes: organelles containing a cytochrome-like pigment in the retinal cones of certain fishes. Science, 200, 549-552.

-Marshall, B.R. & Smith, R.C. (1990). Raman scattering and in-water ocean optical properties. Applied Optics, 29, 71-84.

-McFarland, W.N. & Lowe, E.R. (1983). Wave-produced changes in underwater light and their relations to vision. Environmental Biology of Fishes, 8, 173-184.

-McIntyre, P. & Snyder, A.W. (1978). Light propagation in twisted anisotropic media: application to photoreceptors. Journal of the Optical Society of America, 68, 149-157.

-Menzel, R. & Snyder, A.W. (1975). Introduction to photoreceptor optics-An overview. *In* Photoreceptor Optics. *Edited* by A.W. Snyder and R. Menzel. Springer-Verlag, New York. pp. 1-13.

-Midwinter, J.E. (1979). Optical fibers for transmission. John

Wiley & Sons, New York, Toronto, 410 p.

-Moody, M.F. & Parriss, J.R. (1961). The discrimination of polarized light by octopus: a behavioural and morphological study. Zeitschrift fuer Vergleichende Physiologie, 44, 268-291.

-Moore, F.R. (1987). Sunset and the orientation behaviour of migrating birds. Biological Review, 62, 65-86.

-Munz, F.W. (1958). The photosensitive retinal pigments of fishes from relatively turbid coastal waters. Journal of General Physiology, 42, 445-459.

-Nag, T.C. (1995). Ultrastructure of ellipsosomes in the retina of *Garra lamta*. Journal of Electron Microscopy, 44, 405-407.

-Neumeyer, C. (1985). An ultraviolet receptor as a fourth receptor type in goldfish colour vision. Naturwissenschaften, 72, 162-163.

-Nilsson, D-E, Labhart, T. & Meyer, E. (1987). Photoreceptor design and optical properties affecting polarization sensitivity in ants and crickets. Journal of Comparative Physiology A, 161, 645-658.

-Novales Flamarique, I. & Hawryshyn, C.W. (1996). Retinal development and visual sensitivity of young Pacific sockeye salmon (*Oncorhynchus nerka*). Journal of Experimental Biology, 199, 869-882.

-Novales Flamarique, I. (1993). Ultraviolet light in the salmonid environment. University of Victoria Masters Thesis,

188 pp.

-Novales Flamarique, I. and Hawryshyn, C.W. (1993). Spectral characteristics of salmonid migratory routes from southern Vancouver Island (BC, Canada). Canadian Journal of Fisheries and Aquatic Sciences, 50, 1706-1716.

-Novales Flamarique, I., Hendry, A. & Hawryshyn, C.W. (1992). The photic environment of a salmonid nursery lake. Journal of Experimental Biology, 169, 121-141.

-O'Connell, C.P. (1981). Development of organ systems in the northern anchovy *Engraulis mordax*, and other teleosts. American Zoologist, 21, 429-446.

-Oldenboug, R. & Mei, G. (1995). New polarized light microscope with precision universal compensator. Journal of Microscopy 180, 140-147.

-Palacios, A.G., Goldsmith, T.H. & Bernard, G.D. (1996). Sensitivity of cones from a cyprinid fish (*Danio aequipinnatus*) to UV and visible light. Visual Neuroscience, 13, 411-421.

-Parkyn, D.C. & Hawryshyn, C.W. (1993). Polarized light sensitivity in rainbow trout (*Oncorhynchus mykiss*): characterization from multiunit ganglion cell responses in the optic nerve fibres. Journal of Comparative Physiology A, 172, 493-500.

-Plass, G.N., Kattawar, G.W. & Guinn, J.A.Jr. (1975). Radiative transfer in the earth's atmosphere and ocean: influence of ocean waves. Applied Optics, 14, 1924-1937.

-Rayleigh, L. (1889). On the transmission of light through an atmosphere containing many small particles in suspension, and on the origin of the blue of the sky. Philosophical Magazine, 47, 375-384.

-Reali, G.C. (1992). Reflection, refraction, and transmission of plane electromagnetic waves from a lossless dielectric slab (molecular optics approach, noting Brewster angles). American Journal of Physics, 60, 532-536.

-Ribi, W.A. (1980). New aspects of polarized light detection in the bee in view of non-twisting rhabdomeric structures. Journal of Comparative Physiology, 137, 281-285.

-Rossel, S. & Wehner, R. (1986). Polarization vision in bees. Nature, 11, 128-131.

-Rowe, M.P., Engheta, N., Easter, S.S.Jr. & Pugh, E.N.Jr. (1994). Graded-index model of a fish double cone exhibits differential polarization sensitivity. Journal of the Optical Society of America A, 11, 55-70.

-Rushton, W.A.H. (1961). Dark adaptation and the regeneration of rhodopsin. Journal of Physiology (London), 156, 166-178.

-Scarsbrook, J.R., Miller, P.L., Hume, J.M. & McDonald, J. (1978). Purse seine catches of sockeye salmon (*Oncorhynchus nerka*) and other species of fish at Babine lake, British Columbia. Fisheries and Marine Service. Pacific Biological Station, Nanaimo, BC, Canada. Data report 69, 41 pp.

-Scott, W.B. & Crossman, E.J. (1973). Freshwater fishes of Canada. Fisheries Research Board of Canada, Bulletin 184,

538-543.

-Shashar, N. & Cronin, T.W. (1996). Polarization contrast vision in octopus. Journal of Experimental Biology, 199, 999-1004.

-Shaw, S.R. (1969). Sense-cell structure and interspecies comparisons of polarized-light absorption in arthropod compound eyes. Vision Research, 9, 1031-1040.

-Sidman, R.L. (1957). The structure and concentration of solids in photoreceptor cells studied by refractometry and interference microscopy. Journal of Biophysical and Biochemical Cytology, 3, 15-33.

-Sirovich, L. & Abramov, I. (1977). Photopigments and pseudo-pigments. Vision Research, 17, 5-16.

-Sjöstrand, F.S. (1959). Fine structure of cytoplasm: the organization of membranous layers. Reviews of Modern Physics, 31, 301-318.

-Smola, U. and Wunderer, H. (1981). Fly rhabdomeres twist in vivo. Journal of Comparative Physiology A, 142, 43-49.

-Snyder, A.W. (1973a). Optical properties of invertebrate photoreceptors. *In* The compound eye and vision of insects. *Edited* by G.A. Horridge. University Press, Oxford.

-Snyder, A.W. (1973b). Polarization sensitivity of individual retinula cells. Journal of Comparative Physiology, 83, 331-360.

-Snyder, A.W. & Pask, C. (1973). Spectral sensitivity of dipteran retinula cells. Journal of Comparative Physiology,

84, 59-76.

-Snyder, A.W., Menzel, R. & Laughlin, S.B. (1973). Structure and function of the fused rhabdom. Journal of Comparative Physiology, 87, 99-135.

-Stell, W.K. & Hárosi, F.I. (1976). Cone structure and visual pigment content in the retina of the goldfish. Vision Research, 16, 647-657.

-Stenkamp, D.L., Hisatomi, O., Barthell, L.K., Tokunaga, F. & Raymond, P. (1996). Temporal expression of rod and cone opsins in embryonic goldfish retina predicts the spatial organization of the cone mosaic. Investigative Ophthalmology and Visual Science, 37, 363-376.

-Stockhammer, K. (1956). Zur Wahrnehmug der Schwingungsrichtungdes linear polarisierten Lichtes bei Insekten. Zeitschrift fuer Vergleichende Physiologie, 38, 30-83.

-Tannenbaum, P.M. (1975). Spectral shaping and waveguide modes in retinal cones. Vision Research, 15, 591-593.

-Taylor, D.H. & Adler, K. (1973). Spatial orientation by salamanders using plane polarized light. Science, 181, 285-287.

-Timofeeva, V.A. (1974). Optics of turbid waters (results of laboratory studies). *In* Optical Aspects of Oceanography. *Edited* by N. Jerlov and E. Steeman Nielsen. Academic Press, New York. pp. 177-218.

-Timofeeva, V.A. (1969). Plane of vibrations of polarized

light in turbid media. Izvestiya Atmospheric and Oceanic Physics, 5, 603-607.

-Timofeeva, V.A. (1962). Spatial distribution of the degree of polarization of natural light in the sea. Izvestiya Geophysics Series, 12, 1843-1851.

-Timofeeva, V.A. (1961). On the problem of polarization of light in turbid media. Izvestiya Geophysics Series, 5, 766-774.

-Tomita, T. (1968). Electrical response of single photoreceptors. Proceedings. Institution of Electrical and Electronics Engineers, 56: 1015-1023.

-Tovée, M.J. (1995). Ultra-violet photoreceptors in the animal kingdom: their distribution and function. Trends in Ecology and Evolution, 10, 455-460.

-Tyo, J.S., Rowe, M.P., Pugh, E.N. & Engheta, N. (1996). Target detection in optically scattering media by polarization-difference imaging. Applied Optics, 35, 1855-1870.

-Van de Hulst, H.C. (1957). Light Scattering by small particles. Dover Publ. Inc. pp. 114-130.

-van der Meer, H.J. (1992). Constructional morphology of photoreceptor patterns in percomorph fish. Acta Biotheoretica, 40, 51-85.

-von Frisch, K. (1949). Die Polarisation des Himmelslichts als orienterender Faktor bei den Tanzen der Bienen. Experientia, 5, 142-148.

-Vos Hzn, J.J., Coemans, M.A.J.M. & Nuboer, J.F.W. (1995). No evidence for polarization sensitivity in the pigeon electroretinogram. Journal of Experimental Biology 198, 325-335.

-Wald, G., Brown, P.K. & Smith, P.H. (1955). Iodopsin. Journal of General Physiology, 38, 623-681.

-Wahl, C.M. (1994). Periodic cone cell twists in the walleye, *Stizosteidon vitreum*; a new type of retinomotor activity. Vision Research, 34, 11-18.

-Waterman, T.H. (1984). Natural polarized light and vision. *In* Photoreceptors and Vision in Invertebrates. *Edited* by M.A. Ali. Plenum Press, New York. pp. 63-114.

-Waterman, T.H. (1981). Polarization sensitivity. *In* Handbook of Sensory Physiology. *Edited* by H. Autrum. Springer-Verlag, Berlin, Heidelberg, New York, Vol VII/6B. pp. 281-469.

-Waterman, T.H. (1955). Polarization of scattered sunlight in deep water. In: Papers in Marine Biology and Oceanography, Pergamon Press Ltd., London, pp. 426-434.

-Waterman, T.H. (1954). Polarization patterns in submarine illumination. Science, 120, 927-932.

-Waterman, T.H. & Hashimoto, H. (1974). E-vector discrimination by goldfish optic tectum. Journal of Comparative Physiology, 95, 1-12.

-Waterman, T.H. & Aoki, K. (1974). E-vector sensitivity patterns in the goldfish optic tectum. Journal of Comparative Physiology, 95, 13-45.

-Waterman, T.H. & Forward, R.B.Jr. (1970). Field evidence for polarized light sensitivity in the fish *Zenarchopterus*. Nature, 288, 85-87.

-Waterman, T.H. & Westell, W.E. (1956). Quantitative effect of the sun's position on submarine light polarization. Journal of Marine Research, 15, 149-169.

-Wehner, R. (1994). The polarization-vision project: championing organismal biology. *In* Neural Basis of Behavioural Adaptations. *Edited* by K. Schildberger and N. Elsner. Gustav Fischer Verlag, Stuttgart, Jena, New York. pp. 103-143.

-Wehner, R. (1989). Neurobiology of polarization vision. Trends in Neuroscience, 12, 353-359.

-Wehner, R. (1983). The perception of polarized light. *In* The Biology of Photoreception. *Edited* by D.J. Cosens and D. Vince-Price. Society for Experimental Biology Symposium XXXVI. pp. 331-369.

-Wehner, R. (1982). The bee's celestial map. A simplified model of the outside world. *In* The Biology of Social Insects. *Edited* by M.D. Breed, C.D. Michener and H.E. Evans. Westview Press, Boulder (Colorado). pp. 331-369.

-Wehner, R., Bernard, G.D. & Geiger, E. (1975). Twisted and non-twisted rhabdoms and their significance for polarization detection in the bee. Journal of Comparative Physiology, 104, 225-245.

-Whittaker, P.A. & Danks, S.M. (1978). Mitochondria:

structure, function and assembly. London: Longman Group Limited. pp. 112-115.

-Wolff, L.B. (1994a). Diffuse reflectance model for smooth dielectric surfaces. Journal of the Optical Society of America A, 11, 2956-2968.

-Wolff, L.B. (1994b). Polarization camera for computer vision with a beam splitter. Journal of the Optical Society of America A, 11, 2935-2945.

-Wolff, L.B. (1987). Surface orientation from polarization images. In Svetkoff, D.J. (Ed.), *Optics, Illumination, and Image Sensing for Machine Vision II*. Proceedings. Society of Photo-Optical Instrumentation Engineers, 850, 110-121.

-Young, S.R. & Martin, G.R. (1984). Optics of retinal oil droplets: A model of light detection and polarization detection in the avian retina. Vision Research, 24, 129-137.

-Zaneveld, J.R.V., Roach, D.M. & Pak, H. (1974). The determination of the index of refraction of oceanic particulates. Journal of Geophysical Research, 79, 4091-4095.

-Zueva, L.V. (1980). Retinal cones of the black sea anchovy *Engraulis encrasicholus* - an analyzer of polarized light in vertebrates. Zhurnal Evolyutsionnoi Biokhimii i Fiziologii, 17, 602-605.